LINEAR WATER WAVE DAMPING BY A BOTTOM-MOUNTED POROUS STRUCTURE AND BY VERTICAL DUAL POROUS PLATES

by

Santu Das

DEPARTMENT OF MATHEMATICS

INDIAN INSTITUTE OF TECHNOLOGY GUWAHATI,

GUWAHATI-781039, INDIA

September, 2014

LINEAR WATER WAVE DAMPING BY A BOTTOM-MOUNTED POROUS STRUCTURE AND BY VERTICAL DUAL POROUS PLATES

A Thesis submitted

in partial fulfillment of the requirements

for the degree of

DOCTOR OF PHILOSOPHY

by

Santu Das

(Roll Number: 09612306)

to the

DEPARTMENT OF MATHEMATICS

INDIAN INSTITUTE OF TECHNOLOGY GUWAHATI

September, 2014

CERTIFICATE

It is certified that the work contained in the thesis titled **Linear water wave damping by a bottom-mounted porous structure and by vertical dual porous plates** by **Santu Das**, a student in the Department of Mathematics, Indian Institute of Technology Guwahati, for the award of the degree of Doctor of Philosophy has been carried out under my supervision and this work has not been submitted elsewhere for a degree.

September, 2014

Dr. Swaroop Nandan Bora
Professor
Department of Mathematics
Indian Institute of Technology Guwahati, India

Dedicated to

My mother Lipika Das

and

My father Mohan Chandra Das

Acknowledgement

The completion of this study required the help and goodwill of various individuals. Without them, I might not have met my objective in doing this study. I would like to express my gratitude to the following people for their invaluable help and support.

To The God Almighty, our Lord and Saviour, for giving the wisdom, strength, support and knowledge in exploring things; for the guidance in helping surpass all the trials that I encountered and for giving determination to pursue my study and to make it possible.

The research included in this dissertation could not have been achieved if not for the assistance, patience, and support of many individuals. I would like to extend my gratitude first and foremost to my thesis supervisor Prof. Swaroop Nandan Bora for mentoring me throughout my passage of time as a research scholar. He has helped me through extremely difficult times over the course of the analysis and the writing of the dissertation and for that I sincerely thank him for maintaining his confidence in me. I could not have imagined having a better supervisor and mentor for my Ph.D study.

Besides my supervisor, I would like to thank the Chairman of my doctoral committee Prof. Durga Charan Dalal and the members Prof. Natesan Srinivasan and Dr. Siddhartha P. Chakrabarty, for their encouragement, insightful comments, and hard questions without which the enrichment of my thesis would not have been possible.

I would also like to thank the Department of Mathematics, Indian Institute of Technology Guwahati, India for selecting me as a research scholar and providing me the necessary cooperation in order to complete my PhD successfully. I would like to take this opportunity to thank the non-technical and technical staff for helping me in official works and providing a useful laboratory.

I would also like to extend my appreciation to my close friends, hostel-mates and research scholar roommates for being with me for the last five years, both in my happy days to share quality time as well as in pensive days to cheer me up. I would like to thank Himadri, Niladri da, Kaushik da, Arnab, Kalyan, Barun, Murali, Purnendu da, Debopam, Sunanda and Neelam for their support throughout these years. I extend my gratitude towards Sutanu who despite being outside India, always spared time to talk to and encourage me. I would also take this opportunity to appreciate Sudipta, Rajesh, Koushik, Pranabesh, Joydip, Raj, Pinku da, Sankar da, Soumen da, Tukai da, Kartick da with whom I spent a lot of time back at home. The space here is too limited to mention the names of all the people who were part of my life during these years, but still the quality time I spent with them is something which is stored deep inside my heart and I will cherish the memory for the rest of my life. Last but not the least, I would like to thank Mrs. Swapnali Bora for her constant support and care all along these years.

This research would not have been possible without the financial support of the Council

of Scientific & Industrial Research (CSIR), India. I am sincerely grateful to CSIR for the continuation of the fellowship for my entire PhD tenure.

Finally I would like to extend my deepest gratitude to my parents without whose love, support and understanding I could never have completed this doctoral degree. I cannot describe my love, respect and appreciation towards them in words because I could never be the person I am today without them.

September, 2014

Santu Das

Department of Mathematics

Indian Institute of Technology Guwahati, India

Abstract

Breakwaters and wave absorbers are structures constructed in the coastal areas to protect harbours, inlets and beaches by attenuating incoming wave energy. Different types of breakwaters can be constructed such as caisson type breakwaters where the vertical side is backed up with vessels, rubble-mound breakwaters that consist of different layers of materials, preferably sand and gravels on the outermost layer, to absorb most of the energy and inner concrete layer in order to block water to transmit. Breakwaters may also consist of metallic foams formed from different types of metals and alloys.

This thesis mainly studies oblique water wave scattering by a vertical porous structure placed on (*i*) an elevated horizontal bottom and (*ii*) a multi-step impermeable bottom in the presence of a rigid vertical wall. Linear water wave theory is considered along with time harmonic motion. In both cases, governing equation, boundary conditions and dispersion relation for flow inside the porous structure are derived. For the horizontal bottom case, a linearized friction factor is calculated to damp the motion whereas the friction factor is taken as fixed for the multi-step bottom. In the later part of the thesis, oblique water wave scattering by two thin vertical (*i*) surface piercing and (*ii*) fully submerged porous plates of different heights and having different porous effect parameters in an infinite channel of finite depth is also considered. Boundary value problems consisting of the governing equation, boundary conditions and matching conditions in terms of the porous effect parameters are derived.

First, a rectangular shaped porous structure, attached to a rigid vertical wall, is placed on an elevated horizontal impermeable bottom. Oblique waves are incident on the porous structure. Some part of the waves gets reflected by the sea-ward face of the porous structure and the rest of them passes through the porous structure before getting reflected by the rigid vertical wall. Inside the porous structure, the reflected and transmitted waves are reflected back and forth. Boundary value problems are set up with the help of the governing equation along with the boundary conditions in both porous and water regions. In order to find the reflection coefficient, matching conditions along the vertical boundaries are used to deduce a system of equations which are solved by a matrix method. It is observed that the propagating mode controls the reflection phenomenon up to a certain wave number beyond which the evanescent modes start affecting reflection. The value of the reflection coefficient decreases with an increase in the height of bottom elevation as well as in the values of porosity. Moreover, minimum reflection is observed for a fixed range of angles of incidence. Further, the problem is extended by placing the porous structure at some distance from the rigid vertical wall. In this case, the transmitted waves coming out from the porous structure pass through the water region between the porous structure and the rigid vertical wall, and get reflected by the wall. Here the dimensionless amplitude of the transmitted wave is also calculated by using the

matching conditions along the vertical boundaries and subsequently, energy loss of the waves due to passing through the porous structure is obtained. Oscillation in the reflection coefficient is observed for a thin porous structure and for lower values of porosity. Energy loss due to the presence of porous structure is independent of the number of evanescent modes whereas higher values of porosity result in higher energy loss. We investigate two distinct cases by considering the wall to be nearer the structure and far away from it.

Secondly, a multi-step bottom under the vertical porous structure is considered to study the scattering of oblique ocean waves. The porous structure is divided into multiple regions according to the number of steps and in each region, a boundary value problem is set up along with the matching conditions along the common boundary of every two successive porous regions. In order to find the reflection and the dimensionless amplitude of the progressive transmitted wave, a matrix system is constructed with the help of matching conditions. Moreover, energy loss of the waves is also calculated. With an increase in the number of steps, oscillation in the reflection coefficient is observed. But the oscillation in the reflection coefficient for lower values of friction factor disappears with an increase in the number of steps. This problem is also extended first by placing the rigid wall at a distance from the porous structure; and later by removing the rigid wall and considering the water region to the rear side of the porous structure to be unbounded. Corresponding studies are analyzed. Minimum admissible width of the porous structure in order to be an effective wave absorber is justified from the steep portion of the graph of the reflection coefficient. In the case of the unbounded water region to the rear side of the porous structure, the reflection is very small compared to the case when the wall was present for a thin porous structure. Moreover, the oscillations in the reflection coefficient and energy loss do not exist when the rigid wall is absent.

In the last part of the thesis, two thin vertical parallel porous plates of different heights and porous effect parameters are considered in an infinite channel of finite depth. The fluid domain is divided into three regions and boundary value problems are formulated in each of the regions. The matching conditions across the porous plates are derived and with the help of least square method, a matrix system is constructed. The reflection and the transmission coefficients are obtained by solving the matrix system and the effects of various related parameters are studied graphically. Energy loss in the scattering process is also considered in the study. Lower reflection is observed by increasing the inertial effect of the porous plates but higher energy loss is obtained by reducing the inertial effect of the porous plates. Moreover, when the properties of the porous plates are fixed, the transmission coefficient is not affected by the interchange of the positions of the porous plates. This problem is also extended by considering the porous plates to be fully submerged in the water region.

Contents

List of Figures

List of Tables

Nomenclature

C_0 : dimensionless amplitude of the progressive transmitted wave in the bounded region

C_M : added-mass coefficient

η : free surface elevation

f : linearized friction factor (a real number)

g : acceleration due to gravity

γ : porosity

l : y-component of the incident wave number

ν : $(= \omega^2/g)$

ω : angular frequency of the incoming water waves

Φ : three-dimensional time dependent velocity potential

ϕ : velocity potential

R : $(= f - \mathrm{i}S)$: dimensionless impedance of the porous structure

R_0 : reflection coefficient

R_n : dimensionless amplitude of the evanescent modes

ρ : density of the fluid

S : inertial coefficient

t : time

T_0 : transmission coefficient

θ : angle of incidence of the wave train

Chapter 1

Introduction

1.1 Preamble

In modern science and engineering, fluid dynamics is a very important subject which deals with the motion of fluid (both liquid and gas) in various physical scenarios caused by its interaction with physical objects and forces present in nature. Aerodynamics, a part of fluid dynamics, deals with the motion of gas whereas the motion of liquid (mainly water) is studied in hydrodynamics. Some of the practical applications of fluid dynamics can be found in aviation industry for calculating force and moments in aircrafts, measuring petroleum flow rate in pipeline, forecasting weather and even in cosmology to predict the property of interstellar objects like Nebulae. Fluid dynamics problems are solved by calculating many physical properties of the fluid such as velocity, pressure, temperature, density etc.

The fundamental equations of fluid dynamics contain the *conservation laws* (conservation of mass, momentum and energy, for example). One of the key concepts in defining the fluid properties like density, volume, temperature, pressure etc. is the *continuum assumption*. According to this assumption, fluids are continuous matter instead of being made up with particles so that the fluid properties can be defined at infinitesimally small points and they vary continuously from one point to another.

Fluid flow can be categorized into different types in accordance with its various properties. If the density of a fluid changes significantly with changes in pressure and temperature, the flow is called *compressible fluid flow*; and if the change in density is negligible, it is called *incompressible fluid flow*. Specifically in aerodynamics, Mach number (the ratio of speed of an object moving through a fluid and the local speed of sound) of the flow is utilized in order to

determine compressible and incompressible flows. The flow is called *inviscid* if the viscosity (measure of resistance to gradual deformation) is negligible, otherwise it is called *viscous*. If the fluid properties do not change with respect to time, the flow is termed as *steady flow* but if the properties change in time, the flow becomes *unsteady*. Recirculation, swirl in the flow and randomness in the fluid make a flow *turbulent*. Fluid flow is called *laminar* if turbulence is not exhibited in the flow. Depending upon the mathematical relation between stress and strain, fluid is categorized into two types: *Newtonian fluid* (water, air etc.), which satisfies a very close linear relation between stress (internal force) and strain (normalized measure of deformation); *non-Newtonian* (blood, polymer, latex, honey etc.), which does not follow any linear relation between stress and strain. Fluid flow is also termed as *subsonic, transonic, supersonic* and *hypersonic* depending upon the velocity (Mach number) of the flow.

Motion of fluid is defined in the form of waves, a form of oscillation which propagates through space and time, transferring energy from one point to another. There are two types of waves, namely, mechanical wave (water wave, sound wave etc.) which requires a medium and electromagnetic wave (visible light, radio-wave, ultraviolet wave, X-ray etc.) which does not require a medium to traverse. Moreover, depending upon the direction of propagation, waves are also categorized into two different types as longitudinal wave (water wave) where disturbance creates oscillation perpendicular to the direction of propagation and transverse wave (sound wave) where oscillation is parallel to the direction of propagation.

In real life, a simple example of water waves is the one when we throw a stone into a pond and observe sinusoidal ripples around the point of impact and spreading in all directions. More instances are: when wind blows over water region (lake, ocean etc.) and creates ripples on the water surface; due to the motion of a ship in an ocean; flow over bottom undulation under the water region. These types of waves have small amplitudes of oscillation. But there also exist cases where the amplitude is not that much small but is significantly visible. Tidal waves, Rogue waves and Tsunami waves are such kind of waves where a huge amount of energy is carried through waves which may create destruction in coastal areas, structures in ocean (petroleum extraction machinery) and floating objects (ships, submarines). Due to this, the study of water waves of different kinds commands reasonable attention from a large number of researchers. The most effective way to protect the object of interest is to make barriers of porous material or a structure consisting of both porous and non-porous materials to dissipate the wave energy.

Water waves, based on wavelength, are categorized into two types. When the wavelength of water wave is larger than the depth of water, it is called *shallow water wave* (or *long wave*).

Tidal waves, Tsunami waves, long waves in shallow water fall into this category. Then there are waves whose wavelengths are smaller compared to the depth of water and they are termed as *deep water waves* (or *short waves*). Rogue wave is an example of such waves. There are also waves which are neither shallow water waves nor deep water waves and they are known as *intermediate depth water waves*. Moreover, if the amplitude of the wave is small compared to the wavelength, the theory related to it is called linearized water wave theory. In this theory, it is assumed that the velocity components along with their derivatives and the free surface elevation are small. In reality, ocean waves are non-linear but for problems related to marine and offshore engineering, it is found that consideration of linearized theory is sufficient in handling most of the problems and at the same time keeping most of the features intact. In this thesis, the linearized water wave theory is utilized to tackle all the problems taken up.

In order to formulate the physical problem mathematically, water is assumed to be contained in a region bounded by a free surface (in contact with the atmosphere) or a rigid surface or a porous surface or any other medium. Moreover, virtual boundaries are also incorporated for the sake of simplification. If an object is submerged or emerged in water, the surface of the object in contact with water is treated as the boundary. For damping and scattering problems, time harmonic waves are taken into account. Depending upon the physics of the problem, the wave motion inside the water region follows either Laplace's or Helmholtz equation along with boundary conditions of Dirichlet type (no derivative involved) or Neumann type (only derivative involved) or Robin type (mixture of derivative and non-derivative). Analogous theory is also applicable for water waves inside a porous structure.

We would like to discuss briefly about the development of water wave theory in general from the very beginning. The early chronological development on water wave theory is thoroughly penned down by Craik (2004). Based on his findings, we are going to highlight some of the very important early works. It all started in 1687 when Sir Issac Newton correctly deduced that the frequency of deep-water wave must be proportional to the inverse of the square root of the wavelength (which he termed as *breadth of the wave*) after an questionable analogy of oscillation in a U-tube in *Book II, Prop. XLV of Principia*. Many authors such as Wilhelm-Jacobs Gravesande and Charles Bossut supported the arguments given by Newton. Later, Leonhard Euler derived the equations of hydrodynamics during 1757-1761. In 1776, Pierre-Simon Laplace took the challenge to achieve the complete form of wave motion correctly but failed. However, his solution was correct for small amplitude plane waves in a channel of finite water depth. Later, Joseph-Louis Lagrange derived the linearized governing equations for small-amplitude waves, and obtained the solution in the limiting case of long plane waves in shallow water.

But he wrongly claimed that his shallow-water results should remain a good approximation for deep-water waves because most of the motion was confined near the surface. In 1802, a ground-breaking paper by Franz Joseph von Gerstner gave the first exact non-linear solution for waves of finite amplitude on deep water. But the method employed in the paper did not get practical importance due to the consideration of wave motion which was not irrotational. Later in 1863, independent work of W.J. Macquorn Rankine on the same topic put the interest back. Simeon D. Poisson gave a brief and correct derivation of the frequency of linear sinusoidal standing waves in finite depth in 1818, whereas Augustin-Louis Cauchy's work (he was awarded a prize in 1816 for this work which eventually appeared in 1827) was valid for infinite depth water only. But the Cauchy-Poisson analysis is now acknowledged as an important milestone in the mathematical theory of initial-value problems. In the meantime, Ernst Heinrich Weber and Wilhelm Eduard Weber published a book *Wellenlehre auf Experimente gegründet* in 1825 which described the laboratory experiments on plane periodic wave trains in a channel. It was also included with comments and extracts from the theoretical works available then. Few years later, in 1837, John Scott Russell provided a remarkable report on wave characteristics at sea, in river and canals. His experiments are now well-known for the discovery of non-linear solitary waves. He had distinguished four types of waves: waves of translation, including his newly found solitary waves, tides, and bores; oscillatory waves, or periodic wave trains; capillary waves; and corpuscular waves, which are compressive sound waves propagating through water. Next year, George Green gave an exemplary analysis of the effects of slow variations on the motion of waves in a variable canal of small depth and width, though limited to the long linear shallow water wave. Later, Philip Kelland investigated long waves of small amplitude in canals with triangular cross sections, and correctly derived the result of the wave speed. The representation of a solitary wave by discontinuous expressions was taken up by Samuel Earnshaw. He pointed out the conspicuous lack of success in obtaining general solutions to the equations of hydrodynamics, and he emphasized the need to limit theoretical studies to restricted classes of motions, based on hypotheses suggested by experiments. A non-linear theory attempted by him failed which George Gabriel Stokes developed later. Rayleigh derived the correct approximate solution, retaining both dispersion and non-linearity, and he further observed that Earnshaw's solution was not irrotational. George Biddell Airy's main focus of interest was tidal phenomena but he also wrote a substantial section on the"Theory of Waves in Canal" and an "Account of Experiments on Waves", both in 1841. He gave the now-standard linear theory for plane waves. Airy then focussed on small-amplitude (linear) waves in canals with slowly varying depth and cross-section. Airy's results for long waves agreed with the

earlier works done by Green and Kelland. The now-famous paper by Korteweg and deVries appeared much later in 1895.

One of the most important issues of modern oceanography is to protect the offshore bodies as well as coastal areas from the high energy of the water waves. In order to do so, the amplitude of the waves must be reduced by some means and hence the concept of breakwater comes into picture. The mathematical formulation is very much complicated even with the use of linearized water wave theory and it needs special effort to solve these types of problems.

When a train of incident surface waves interacts with a totally submerged or emerged porous or rigid obstacle, some part of the wave gets reflected back which is known as the *reflected wave* and some part of the wave gets transmitted over or below or through the structure which is known as the *transmitted wave*. This is known as the scattering of the water waves and in this process, damping of waves occurs which reduces the amplitude of the waves. Scattering process is characterized by two quantities: *reflection coefficient* which is the ratio of the amplitude of the reflected wave to that of the incident wave and *transmission coefficient* which is the ratio of the amplitude of the transmitted wave to that of the incident wave. Energy loss (in per cent) is calculated with the help of these two coefficients.

Scattering problems are of great interest for the modern day engineers and scientists. An array of problems from different configurations of breakwaters to the effects of an uneven ocean-bed near the beaches and coastal areas fall into the scattering process. This thesis is solely devoted to the problems related in attenuating wave energy for different types of porous structures by considering horizontal and multi-step bottoms.

In the following sections, a brief description of the basic equations in linearized water wave theory for the case of constant depth are presented followed by a general theory for flow inside a porous structure.

1.2 Basic equations in linearized water wave theory

In this section, we briefly discuss the equations of motion inside the fluid domain. With the help of linearized water wave theory, different boundary conditions are derived and discussed.

We consider the fluid to be homogeneous, incompressible and inviscid, and the motion irrotational. Density and pressure of the fluid are considered to be ρ and p, respectively. A Cartesian coordinate system (x, y, z) is considered with the positive z-axis vertically upwards and the xy-plane along the free surface. The uniform bottom free surface is considered as $z = -h$ where h is a positive real constant and the fluid domain is unbounded in both x-

and y-directions, i.e., $-\infty < x < \infty$; $-\infty < y < \infty$. Since the fluid motion is irrotational, a velocity potential $\Phi(x, y, z, t)$ exists in the fluid domain where t represents time dependency of the fluid motion. If the velocity of the fluid at any point in the domain is $\boldsymbol{q} = (u, v, w)$, then $\boldsymbol{q}$ can be expressed as

$$\boldsymbol{q} = \boldsymbol{\nabla}\Phi. \tag{1.1}$$

The equation of continuity and Euler's equation of motion are, respectively, expressed as

$$\boldsymbol{\nabla}\cdot\boldsymbol{q} = 0, \tag{1.2a}$$

$$\frac{\partial \boldsymbol{q}}{\partial t} + (\boldsymbol{q}\cdot\boldsymbol{\nabla})\boldsymbol{q} = \boldsymbol{g} - \frac{\boldsymbol{\nabla} p}{\rho}. \tag{1.2b}$$

Combining equations (1.1) and (1.2a), the equation of continuity inside the fluid region becomes

$$\boldsymbol{\nabla}^2\Phi = 0, \tag{1.3a}$$

or,

$$\frac{\partial^2\Phi}{\partial x^2} + \frac{\partial^2\Phi}{\partial y^2} + \frac{\partial^2\Phi}{\partial z^2} = 0. \tag{1.3b}$$

After integration, Euler's equation reduces to Bernoulli's equation:

$$\frac{\partial\Phi}{\partial t} + \frac{1}{2}[u^2 + v^2 + w^2] + \frac{p}{\rho} - gz = 0. \tag{1.4}$$

Since the atmospheric pressure is constant at the free surface and balances the pressure of the fluid, it may be taken as zero. Then Bernoulli's equation (1.4) reduces to the following dynamic free surface boundary condition:

$$\frac{\partial\Phi}{\partial t} + \frac{1}{2}[u^2 + v^2 + w^2] - g\eta = 0 \quad \text{on} \quad z = \eta(x, y, t), \tag{1.5}$$

where $z = \eta(x, y, t)$ defines the instantaneously varying free surface elevation and $z = 0$ is the mean free surface.

According to linearized water wave theory, second order velocity component terms can be neglected to obtain the linearized Bernoulli's equation as

$$\frac{\partial\Phi}{\partial t} = g\eta \quad \text{on} \quad z = \eta(x, y, t). \tag{1.6}$$

Moreover, using small amplitude assumption on Taylor's series expansion of $\partial\Phi/\partial t$ about $z = 0$ and hence neglecting the second and higher order terms, the linearized free surface dynamic condition can be written as

$$\frac{\partial \Phi}{\partial t} = g\eta \quad \text{on} \quad z = 0. \tag{1.7}$$

The free surface in this study is a material boundary for which a particle on the free surface always remains on the free surface and hence the total derivative of the free surface $z - \eta(x, y, t) = F(x, y, z, t)$ (say) is zero. Therefore, we get

$$\begin{aligned} & \frac{\partial F}{\partial t} + u\frac{\partial F}{\partial x} + v\frac{\partial F}{\partial y} + w\frac{\partial F}{\partial z} = 0, \\ \Rightarrow \quad & \frac{\partial \Phi}{\partial z} = \frac{\partial \eta}{\partial t} + \frac{\partial \eta}{\partial x}\frac{\partial \Phi}{\partial x} + \frac{\partial \eta}{\partial y}\frac{\partial \Phi}{\partial y} \quad \text{on} \quad z = \eta(x, y, t). \end{aligned} \tag{1.8}$$

The free surface elevation, along with their derivatives and the velocity components, are small quantities and hence their products and higher powers can be neglected by the assumptions of linear water wave theory. Hence equation (1.8) reduces to the following equation

$$\frac{\partial \Phi}{\partial z} = \frac{\partial \eta}{\partial t} \quad \text{on} \quad z = \eta(x, y, t). \tag{1.9}$$

Expanding $\partial\Phi/\partial z$ about $z = 0$ and neglecting the second and higher order terms as done earlier, the linearized kinematic free surface boundary condition can be written as

$$\frac{\partial \Phi}{\partial z} = \frac{\partial \eta}{\partial t} \quad \text{on} \quad z = 0. \tag{1.10}$$

Now eliminating η from equations (1.7) and (1.10), we get the linearized free surface boundary condition as

$$\frac{\partial^2 \Phi}{\partial t^2} - g\frac{\partial \Phi}{\partial z} = 0 \quad \text{on} \quad z = 0. \tag{1.11}$$

Using equation (1.7), free surface elevation can be obtained by the following form:

$$\eta = \frac{1}{g}\frac{\partial \Phi}{\partial t} \quad \text{on} \quad z = 0. \tag{1.12}$$

If B is a boundary of an obstacle through which the fluid cannot pass, we define an impermeable boundary condition

$$\frac{\partial \Phi}{\partial n} = 0 \quad \text{on} \quad B, \tag{1.13}$$

where n is the outward normal drawn at the boundary B and $\partial/\partial n$ is the normal derivative at any point on the boundary B. In the case of an impermeable bottom boundary at a constant depth $z = -h$, the above condition reduces to

$$\frac{\partial \Phi}{\partial z} = 0 \quad \text{on} \quad z = -h. \tag{1.14}$$

If the equations of motion follow the simple harmonic motion in time with angular frequency ω, the velocity potential can be written as

$$\Phi(x, y, z, t) = \mathbf{Re}[\phi(x, y, z) \exp(-\mathrm{i}\omega t)], \tag{1.15}$$

where **Re** is the real part and $\phi(x, y, z)$ is the complex-valued velocity potential function.

Hence the basic equations (1.3b), (1.11) and (1.14) in linearized water wave theory reduce to the following equations:

$$\frac{\partial^2 \phi}{\partial x^2} + \frac{\partial^2 \phi}{\partial y^2} + \frac{\partial^2 \phi}{\partial z^2} = 0 \qquad \text{in the fluid region,} \tag{1.16a}$$

$$\frac{\partial \phi}{\partial z} - \nu \phi = 0 \qquad \text{on} \quad z = 0, \tag{1.16b}$$

$$\frac{\partial \phi}{\partial z} = 0 \qquad \text{on} \quad z = -h. \tag{1.16c}$$

1.2.1 Solution for the potential

Assuming harmonic motion along the y-direction, the potential function in the fluid region can be written as

$$\Phi(x, y, z, t) = \mathbf{Re}[\phi(x, z) \exp\{\mathrm{i}(ly - \omega t)\}]. \tag{1.17}$$

where $l = k_0 \sin\theta$ with k_0 being the incident wave number.

Separation of variables method is utilized to find the analytical solution of the potential function in the fluid region. Depending upon the roots of the dispersion relation which can be obtained from equation (1.16b), after using equation (1.16c) in the separation of variables method for solving equation (1.16a), as

$$\nu = k \tanh kh, \tag{1.18}$$

two types of solutions are obtained. For the pair of real roots (one is positive and the other

negative) and the remaining roots (infinitely many purely imaginary values) of equation (1.18), the potential functions for progressive waves and standing or evanescent waves, respectively, are obtained.

The potential function for such n-th mode can be written as

$$\phi_n(x,z) = \exp\left(\pm \mathrm{i}x\sqrt{k_n^2 - l^2}\right) \quad \frac{\cosh k_n(z+h)}{\cosh k_n h}. \tag{1.19}$$

Note that $(\pm)$ sign is for the direction of the waves.

1.3 General theory for flow inside porous medium

Before going into the theory of flow inside a porous material, it is important to have some idea about what a porous medium signifies. Porous medium mostly consists of pores through which fluid (be it gas or liquid such as water) can pass. The skeleton part of the medium is mainly solid (but foam is considered to be porous though). A porous medium may be an aggregate of large number of particles like sand, gravels or a solid containing many capillaries such as porous rock. Many natural substances like sponge, soil, biological materials (bone, lungs etc.) are some examples of porous material. There are also many man-made porous materials such as cement, ceramics etc.

A *saturated porous medium* is the one in which all void space is filled with fluid. But there are some porous materials like soil near the ground surface, in which the void is partially filled with liquid and the remaining part is occupied by air. Flow through this type of porous material is termed *unsaturated*.

The actual path of a fluid particle inside a porous structure cannot be followed analytically due to the complexity of the microscopic flow in the pores. In order to overcome the complexity, the gross effect of the phenomenon represented by a microscopic law applied to the fluid mass such as the space averaged change with respect to the space and time in the macroscopic quantities is needed to be considered. The characterizing property of a porous material is its *porosity*. It is a non-dimensional quantity which measures the void space in the material; and is the fraction of the volume of void over the total volume of the material. If V_v and V_T are, respectively, the volume of void and the total volume of the porous material, then the porosity γ of the material is defined by

$$\gamma = \frac{V_v}{V_T}.$$

Depending upon the pore size, porous structures can be categorized into three types,

namely, microporous (smaller than 2 nanometers), mesoporous (between 2 and 50 nanometers) and macroporous (larger than 50 nanometers). Metallic foams are good examples of porous materials with higher porosity (ranging from 0.6 to 0.95). The construction of these types of materials can be carried out through a number of means, the main one being the "lost-foam casting". Porous structures, with high porosity but with considerable stability, to be used as breakwater in ocean and coastal engineering can be constructed from low melting metals and alloys such as copper, aluminium, lead, tin, zinc, etc. The porous structure under consideration in this thesis is taken as such type of structure. Figure 1.1 presents a rough visual representation of the present structural model. The main methods of construction of

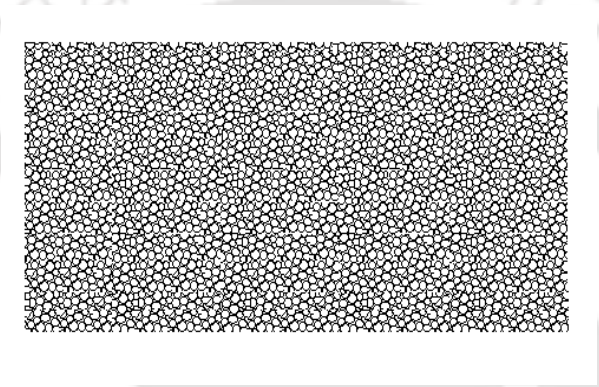

Figure 1.1: Front view of the structural model

these types of materials are briefly discussed below:

1. Casting: In this method, a blowing agent (preferably metal hydride) is added to the molten metal. There are three different types of casting methods:
   (a) Foaming,
   (b) Lost-foam casting,
   (c) Infiltration.
2. Deposition: In this method, physical or chemical reaction is performed between the metal and latex crystal.
3. Gas-eutectic transformation: In this process, molten metal is saturated with gas.
4. Powder metallurgy: Powder or metal fibres are used to create porous materials. Three types of this process are
   (a) Powder sintering,

(b) Compacting with foaming agent,

(c) Fibre metallurgy.

For the problems taken up in this thesis, we consider it important to discuss the flow in the porous region, in particular, in detail since there are non-standard formulations associated in this region in comparison to the other regions which are occupied by fluid only.

Small amplitude wave motion in three dimensions is considered within an undeformable porous medium. It is assumed that the porous structure is homogeneous and isotropic (uniform properties of the material in all directions). The fluid motion follows the continuity equation and the equation of motion in terms of the seepage fluid velocity $\boldsymbol{U}$ and dynamic pressure P, which are given by

$$\boldsymbol{\nabla}\cdot\boldsymbol{U} = 0, \tag{1.20a}$$

$$S\frac{\partial \boldsymbol{U}}{\partial t} + \frac{\boldsymbol{\nabla} P}{\rho} + f\omega\,\boldsymbol{U} = \boldsymbol{0}. \tag{1.20b}$$

The inertial coefficient S (a real quantity) is defined by

$$S = 1 + C_M(1-\gamma)/\gamma. \tag{1.21}$$

The physical significance and derivation of equations (1.20a,b) and (1.21) are described in Appendix A.

A pore velocity potential $\Phi(x, y, z, t)$ is introduced to describe the wave-induced fluid motion in the porous medium:

$$\boldsymbol{U} = \boldsymbol{\nabla}\Phi. \tag{1.22}$$

Integration of equation of motion (1.20b) leads to Bernoulli's equation

$$S\frac{\partial \Phi}{\partial t} + \frac{P}{\rho} + f\omega\Phi = \boldsymbol{0}. \tag{1.23}$$

The solution is assumed to be harmonic in time. So the fluid velocity, dynamic pressure and velocity potential, respectively, can be written as

$$\boldsymbol{U} = \boldsymbol{u}(x, y, z)\exp(-\mathrm{i}\omega t), \qquad P = p(x, y, z)\exp(-\mathrm{i}\omega t), \qquad \Phi = \phi(x, y, z)\exp(-\mathrm{i}\omega t), \tag{1.24}$$

where $\boldsymbol{u}, p$ and ϕ are spatial functions independent of time. Substitution of these values into

equations (1.20a,b) and (1.22) leads to the equations

$$\boldsymbol{\nabla}\cdot\boldsymbol{u} = 0\,, \tag{1.25a}$$

$$\frac{\boldsymbol{\nabla} p}{\rho} + \omega R\boldsymbol{u} = \boldsymbol{0}\,, \tag{1.25b}$$

$$\boldsymbol{u} = \boldsymbol{\nabla}\phi\,. \tag{1.25c}$$

Using equation (1.25c) in equation (1.25a), the spatial potential function ϕ satisfies Laplace's equation

$$\boldsymbol{\nabla}^2\phi = 0. \tag{1.26}$$

If the free surface is defined by $z = \eta(x, y, t)$, then the linearized dynamic free surface boundary condition can be obtained from equation (1.23) with $P = \rho g\eta$ as

$$\eta = -\frac{\omega R}{g}\phi(x, y, z)\exp(-\mathrm{i}\omega t) \qquad \text{at} \qquad z = 0. \tag{1.27}$$

The linearized kinematic free surface boundary condition can be written as

$$\frac{\partial}{\partial z}\{\phi(x, y, z)\exp(-\mathrm{i}\omega t)\} = \frac{\partial \eta}{\partial t} \qquad \text{at} \qquad z = 0. \tag{1.28}$$

Combining equations (1.27) and (1.28), we obtain the following single free surface condition:

$$\frac{\partial \phi}{\partial z} - \mathrm{i}\nu R\phi = 0 \qquad \text{at} \qquad z = 0. \tag{1.29}$$

The condition at the impermeable bottom is

$$\frac{\partial \phi}{\partial n} = 0, \qquad z = -h(x, y), \tag{1.30}$$

where $\partial/\partial n$ represents differentiation along the normal to the bottom boundary $h(x, y)$ which depicts a variable bottom topography.

It is to be noted that by taking $f = 0$ and $S = 1$, i.e., $R = -\mathrm{i}$, the porous medium is reduced to a water region and hence the corresponding free surface condition (1.29) reduces to the free surface condition in the water region as follows:

$$\frac{\partial \phi}{\partial z} - \nu\phi = 0 \qquad \text{at} \qquad z = 0. \tag{1.31}$$

For a flat ocean-bed at $z = -h$, when h is a constant, the general solution of the wave motion within a porous medium can be obtained as follows by solving equations (1.26)–(1.30) (with $h(x, y) = h$ in equation (1.30)) for the potential in x and z with the help of the technique of separation of variables:

$$\phi(x, z) = \sum_{n=0}^{\infty} \left[\tilde{A}_n \exp(\mathrm{i}k_n x) + \tilde{B}_n \exp(-\mathrm{i}k_n x) \right] Z_n(h, z), \tag{1.32a}$$

where $\tilde{A}_n$ and $\tilde{B}_n$ are constants and $Z_n(h, z)$ is the depth-dependent function defined by

$$Z_n(h, z) = \frac{\cosh k_n(h + z)}{\cosh k_n h}, \quad n = 0, 1, 2, \cdots, \tag{1.32b}$$

with the complex wave number k_n satisfying the complex dispersion relation

$$\mathrm{i}R\nu = k_n \tanh k_n h. \tag{1.32c}$$

The characteristics of waves in the porous medium can be described by dimensionless complex wave numbers $k_n h$. It is known that for a non-dissipative medium ($f = 0$), k_0 is purely real, while $k_n (n \geq 1)$ are purely imaginary. For a dissipative medium, it is noted that the influence of the friction factor f is to damp the wave motion. This damping can be achieved by adding an imaginary part to k_0 and real parts to $k_n (n \geq 1)$. By doing so, the amplitude of both propagating modes and evanescent modes will decay.

The dispersion relation for water region is obtained by putting $R = -\mathrm{i}$ in equation (1.32c), i.e.,

$$\nu = k_n \tanh k_n h. \tag{1.33}$$

1.4 Roots of the dispersion relations

Since the roots of the dispersion relations play an important role in each solution, we deem it suitable to discuss these roots in brief. Different dispersion relations will arise for different upper surfaces, bottom surfaces and also for different media. The procedures to solve the dispersion relation in both the water region and porous structure are discussed.

1.4.1 Water region

The dispersion relation can be written as

$$\frac{h\omega^2}{g} = \mathcal{K}\tanh(\mathcal{K}) \quad \text{where} \quad \mathcal{K} = kh.$$

The only positive real root is $\mathcal{K}_0$ and other infinite number of imaginary roots are $i\mathcal{K}_n$ $(n = 1, 2, \cdots)$ with the property $(n - \frac{1}{2})\pi < \mathcal{K}_n < n\pi$ where $\mathcal{K}_n$ are real positive roots of

$$\frac{h\omega^2}{g} = -\mathcal{K}\tan(\mathcal{K}).$$

An approximate value of $\mathcal{K}_0$ is given by Chamberlain and Porter (1999) as

$$\mathcal{K}_0 = \varepsilon\left(1 - \frac{4(1-(1+\varepsilon)e^{-2\varepsilon})}{2\varepsilon + \sinh 2\varepsilon}\right)^{-1/4}, \quad \text{where} \quad \varepsilon = \frac{h\omega^2}{g}. \tag{1.34}$$

To approximate $\mathcal{K}_n$ $(n = 1, 2, \cdots)$, we again use an iterative method suggested by Chamberlain and Porter (1999):

$$\begin{aligned} & \mathcal{K}_{n,m+1} = u_n(\mathcal{K}_{n,m}), \quad m = 0, 1, 2, \cdots, \\ \text{where} \quad & u_n(a_n) = a_n \Bigg/ \sqrt{1 - \frac{2(a_n\tan a_n + \varepsilon)\sin 2a_n}{\varepsilon(sin2a_n + 2a_n)}}, \\ & \mathcal{K}_{n,0} = \beta_n = n\pi - \frac{\pi}{2}\tanh\frac{2\varepsilon}{n\pi^2}. \end{aligned}$$

Once we obtain the values of $\mathcal{K}_n$ $(n = 0, 1, 2, \cdots)$, k_n can be calculated by using the relation $\mathcal{K}_n = k_n h$. The computed values of k_n up to $n = 9$ and the corresponding errors defined by

$$\text{error} = \left|\frac{\omega^2}{g} - k_n \tanh k_n h\right|$$

for five different values of νh, are shown in Table 1.1.

1.4.2 Porous medium

To find the roots of the dispersion relation in porous medium, we adopt the perturbation method described in Mendez and Losada (2004). We write the dispersion relation (1.32c) in

k \ $\omega^2 h/g$	0.8	2.4	4	5.6	7.2
k_0	0.129144	0.304621	0.500334	0.700019	0.900001
error	1.09×10^{-4}	9.78×10^{-8}	1.2×10^{-7}	6.82×10^{-10}	2.35×10^{-12}
k_1	0.358716512	0.293083907	0.255376475	0.237186651	0.227269341
error	3.38×10^{-6}	8.25×10^{-5}	3.16×10^{-6}	6.16×10^{-7}	3.03×10^{-5}
k_2	0.76923896	0.737081275	0.70858633	0.685956885	0.668946851
error	9.42×10^{-9}	3.18×10^{-7}	5.33×10^{-8}	2.95×10^{-8}	5.82×10^{-6}
k_3	1.16741591	1.146095457	1.125854415	1.10764779	1.091929653
error	3.46×10^{-10}	1.22×10^{-8}	2.9×10^{-9}	1.53×10^{-9}	6.08×10^{-7}
k_4	1.562808797	1.546850796	1.531346698	1.516747902	1.503367495
error	3.39×10^{-11}	1.22×10^{-9}	3.26×10^{-10}	1.61×10^{-10}	8.57×10^{-8}
k_5	1.957114003	1.944359751	1.931837491	1.91979012	1.908411965
error	5.64×10^{-12}	2.04×10^{-10}	5.77×10^{-11}	2.74×10^{-11}	1.68×10^{-8}
k_6	2.350880537	2.34025753	2.329768642	2.319558178	2.309750185
error	1.3×10^{-12}	4.73×10^{-11}	1.38×10^{-11}	6.38×10^{-12}	4.23×10^{-9}
k_7	2.744340758	2.735238196	2.726220039	2.717378591	2.70879657
error	3.81×10^{-13}	1.38×10^{-11}	4.09×10^{-12}	1.86×10^{-12}	1.29×10^{-9}
k_8	3.137610078	3.12964697	3.121740384	3.113952778	3.106341623
error	1.29×10^{-13}	4.74×10^{-12}	1.42×10^{-12}	6.38×10^{-13}	4.59×10^{-10}
k_9	3.53075236	3.52367504	3.516637405	3.509683622	3.502855064
error	6.38×10^{-14}	1.84×10^{-12}	5.61×10^{-13}	2.57×10^{-13}	1.83×10^{-10}

Table 1.1: Variation of k_n $(n = 0, 1, \ldots 9)$ in water region against νh

the porous medium as

$$F(\mathcal{K}, \psi) = \psi\mathcal{K}\tanh\mathcal{K} - \nu h = 0, \quad \mathcal{K} = kh, \quad \psi = \frac{1}{S + \mathrm{i}f}. \tag{1.35}$$

According to this approach, a small perturbation $\delta\psi$ in ψ results in a small change $\delta\mathcal{K}$ in the dimensionless wave number $\mathcal{K}$. Explicit form of $\delta\mathcal{K}$ is given by

$$\delta\mathcal{K} = -\delta\psi \left(\frac{\partial F}{\partial \psi}\right) / \left(\frac{\partial F}{\partial \mathcal{K}}\right). \tag{1.36}$$

We use the following iterative method to find $\mathcal{K}$ for a given ψ:

- $\delta\psi = (\psi - \psi_0)/N_1$, N_1= number of steps.
- Calculate $\delta\mathcal{K}_i$ from equation (1.36) as a function of $\mathcal{K}_{i-1}$, ψ_{i-1} and $\delta\psi$.
- $\mathcal{K}_i = \mathcal{K}_{i-1} + \delta\mathcal{K}_i$.

k \ f	0.5	1	1.5
k_0	0.209582043+0.087073752 i	0.190113248+0.177255053 i	0.188784204+0.330981239 i
error	6.088×10^{-4}	2.577×10^{-3}	4.291×10^{-3}
k_1	0.034850072+0.320598836 i	0.078695433+0.30819979 i	0.098513603+0.2243096 i
error	4.036×10^{-4}	2.175×10^{-3}	5.829×10^{-3}
k_2	0.016265784+0.752644764 i	0.033109619+0.751697394 i	0.051249515+0.749936038 i
error	4.895×10^{-4}	1.977×10^{-3}	4.653×10^{-3}
k_3	0.010712259+1.156581663 i	0.021579671+1.15623102 i	0.032770985+1.155614837 i
error	4.956×10^{-4}	1.997×10^{-3}	4.552×10^{-3}
k_4	0.00800041+1.554740104 i	0.016063729+1.55454238 i	0.024255669+1.554201877 i
error	4.975×10^{-4}	1.998×10^{-3}	4.527×10^{-3}
k_5	0.006387924+1.950679756 i	0.012807253+1.950544698 i	0.01929021+1.950314516 i
error	4.984×10^{-4}	1.999×10^{-3}	4.516×10^{-3}
k_6	0.005317679+2.345527954 i	0.010653146+2.345425652 i	0.016024482+2.345252369 i
error	4.989×10^{-4}	1.999×10^{-3}	4.511×10^{-3}
k_7	0.004555127+2.739757607 i	0.009121222+2.739675152 i	0.013709369+2.739536041 i
error	4.992×10^{-4}	1.999×10^{-3}	4.508×10^{-3}
k_8	0.003984101+3.133602524 i	0.007975388+3.133533327 i	0.011981092+3.133416897 i
error	4.994×10^{-4}	1.999×10^{-3}	4.506×10^{-3}
k_9	0.003540428+3.527191734 i	0.00708578+3.527132015 i	0.010641+3.527031725 i
error	4.995×10^{-4}	2×10^{-3}	4.504×10^{-3}

Table 1.2: Variation of k_n $(n = 0, 1, \ldots 9)$ in porous medium against f for $\omega^2 h/g = 1.6$ and $S = 1$

- Repeat the procedure until $\psi = \psi_{N_1} = \psi_{N_1-1} + \delta\psi$ is found.

When we take $\psi_0 = 1$, it corresponds to the dispersion relation for the water region and the corresponding $\mathcal{K}_0$ can be obtained by the method described in subsection 1.4.1.

The computed values of k_n up to $n = 9$ and the corresponding error defined by

$$\text{error} = \left|\frac{\omega^2}{g}(S + \mathrm{i}f) - k_n \tanh k_n h\right|$$

against three different values of f, are shown in Table 1.2. The value of S considered here is $S = 1.0$.

Having stated the preamble and discussed the basic equations for the flow inside both water and porous regions, we now proceed towards a brief review on the works carried out by researchers in the last few decades in the area of damping and scattering of waves by porous structures/ocean-beds.

1.5 Brief history of previous works and motivation

The concept of porous media is used in many areas of applied science and engineering: filtration, mechanics (acoustics, geomechanics, soil mechanics, rock mechanics), engineering (petroleum engineering, bioremediation, construction engineering), geosciences (hydrogeology, petroleum geology, geophysics), biology, biophysics, material science etc. A few examples of application of porous materials is enlisted here. Clement *et al.* (1996) developed analytical solutions to model changes in porosity, specific surface area and permeability caused by biomass accumulation in porous media. The macroscopic models that were developed were found to be simple and useful tools for estimating changes in various porous media properties during bioremediation of contaminated aquifers. Blunt (1998) considered a capillary equilibrium-based network model to compute oil recovery and Amott wettability indices in intermediate-wet porous media. He investigated the models with varying contact angles, and where different fractions of the pore space are oil-wet. Oil recovery showed a complex, non-monotonic dependence with both contact angle and oil-wet fraction. Anglin *et al.* (2008) investigated the utility of porous silicon for applications in microelectronics, optoelectronics, chemical and biological sensors and biomedical devices. Xia *et al.* (2011) employed a rheological model to describe viscoelastic attenuation in saturated porous rocks and they concluded that the model was helpful for the understanding of wave propagation in the temperature domain. These works amply justify that fluid flow through porous media is a subject of immense common interest and has, hence, emerged as a separate significant field of study. In coastal areas, porous structures are widely used as breakwaters to protect harbours, inlets and beaches from wave action, and as dissipating sea-walls to attenuate the wave energy in harbours. Because of this enormous significance of porous structures interacting with ocean waves, we are motivated to investigate some specific cases of reflection and damping by a porous structure.

Many aspects of interaction between waves and porous media have been studied extensively. Theoretical solutions for reflection and transmission coefficients for certain types of porous structures have been analyzed previously by a number of researchers. The most widely used model of wave-induced flow in porous medium is the one developed by Sollitt and Cross (1972). According to this approach, dissipation of wave energy inside a porous medium was taken into account through a linearized friction term f which was evaluated by an iterative procedure. Madsen (1974) developed a simple solution for reflection and transmission from a rectangular porous structure under normal incidence of long waves based on the linearized form of the governing equations and a linearized form of the flow resistance formula. Massel and

Mei (1977) presented a linearized long-wave approximation for random waves impacting on a porous breakwater. The statistical reflection and transmission coefficients were presented in terms of standard deviation and wave spectra. Madsen (1983) obtained a theoretical solution for the reflection of linear shallow-water waves from a vertical porous wave absorber placed on a horizontal bottom. The friction term describing the energy loss inside the absorber was linearized and thereafter, by using Lorentz principle of equivalent work, the reflection coefficient was determined as a function of the parameters describing the incoming waves and the absorber characteristics. Kirby and Dalrymple (1983) investigated the diffraction of obliquely incident surface waves by an asymmetric trench in which a numerical solution was developed by matching the particular solutions for each subregion of constant depth along the vertical boundaries. An approximate solution based on plane-wave modes was derived and compared with the numerical solution. Sulisz (1985) formulated a theory to predict wave reflection and transmission at an infinite rubble-mound breakwater under normal wave incidence. Comparison with the experimental data was made with reasonable agreement and the resultant wave amplitude in front of the breakwater was estimated within an error of few percentage. The approach of Sollitt and Cross (1972) was adopted by Dalrymple *et al.* (1991) to analyze the reflection and transmission of oblique incident waves from infinitely long porous structures. It was found that the oscillation induced by the incident waves reduced with an increase in the thickness of the porous structure. Losada *et al.* (1993) extended this study to the case of an infinitely long, homogeneous, vertical structure capped with an impervious element under oblique incident wave. Wave sheltering provided by the breakwater was determined along with the distribution of wave-induced pressure along the base of the breakwater. It was found that linear pressure gradient assumption usually applied for uplift forces on the breakwater crown was inaccurate. Mallayachari and Sundar (1994) took into account the effects of an uneven ocean-bed. The variation of the reflection coefficient with the porosity of the wall, its friction factor and the relative wall width was studied. Twu and Liu (1994) investigated the elimination of re-reflected waves in a wave channel by installing a porous medium in front of a wavemaker. It was found that the re-reflected waves could be eliminated by simply varying the thickness of the porous medium according to the wave period. Chamberlain and Porter (1995) utilized the variational principle and the Galerkin method to obtain a similar equation, which they termed as the modified mild slope equation, like the one in Mallayachari and Sundar (1994), for linear water wave refraction-diffraction by a bed undulation. Staziker and Porter (1995) further extended the above work by introducing the extended mild slope equation. Zhu (2001) used wave induced refraction-diffraction equations for surface waves in the region occupied by

a porous structure. The orthogonality of the depth-dependent functions was utilized. It was suggested that a porous sea-wall having moderate porosity and friction factor could act as an effective wave absorber whereas width of the porous wall affected only the reflection characteristic of long waves. Zhu and Chwang (2001) extended this work by considering a composite porous wave absorber. It was found that minimum reflection could occur in a certain range of width of the porous structure for various parameters. Moreover, the lowest reflection was not observed for normal incident waves but was observed for oblique waves. Twu *et al.* (2002) investigated the characteristics of wave damping for the vertically stratified porous breakwater under oblique wave action. It was found that irrespective of the angle of incidence, the wave energy loss was proportional to the thickness and porosity of the structure, although using vertically stratified porous structure was not effective as an wave absorber for a structure not having very large thickness.

Many analytical investigations on water wave interaction with submerged porous structure have also been carried out. Rojanakamthorn *et al.* (1989) developed a mathematical model of wave transmission over a submerged breakwater with the help of newly derived equations for waves over a porous layer under the mild slope assumption. The model was verified by considering trapezoidal as well as rectangular-shaped breakwaters. Losada *et al.* (1996a, 1996b) studied the effect of oblique incidence, structure geometry and porous material properties on the hydrodynamic properties over and inside the submerged porous breakwater in details. Two different types of models, namely an eigenfunction expansion 3-D model and a 2-D model based on mild slope equation in order to tackle breakwater slope, were presented. Chen *et al.* (2006) investigated wave reflection by a submerged porous structure placed in front of an impermeable vertical breakwater using a newly derived time-dependent mild slope equation. It was observed that a trapezoidal shaped breakwater reduced the reflection more in comparison to a triangular one. Lee and Cheng (2007) introduced a new approach of solving wave scattering process by a submerged porous structure in multiple regions. The theory was validated by comparing it with other various available results and a scope of extending the theory to achieve the mild slope equation was proposed in the meantime.

Water wave interaction with different types of breakwater consisting of porous or impermeable plates placed horizontally as well as vertically has been investigated by many researchers. Chwang (1983) developed a porous-wavemaker theory in order to investigate small amplitude surface wave in water of finite depth, generated by the horizontal oscillation of a porous vertical plate. Dalrymple and Martin (1990) carried out a study on the reflection and transmission coefficients by a long linear array of rigid vertical walls having periodic gap. Various hydro-

dynamic phenomena, both in front of and behind the breakwater, were discussed. Porter and Evans (1995) presented a complementary solution for water wave scattering by vertical barriers in the case of finite water depth with the help of Galerkin approximation which converted the singular integral equation into a system of algebraic equations. Yu (1995) introduced a newly derived relation for the fluid motion through a thin porous structure and it was observed that for a semi-infinite porous wall, increasing the inertial effect of the wall causes higher amplitude of waves behind the wall. Das *et al.* (1997) studied oblique water wave diffraction by two thin, parallel, fixed vertical impermeable barriers with gaps. Three different types of configurations were considered for the investigation and it was concluded that a submerged double barrier configuration was preferable to a submerged single barrier. The effect of the porous effect parameter of the barrier as well as the distance between the barrier and the vertical wall were investigated. Cox *et al.* (1998) carried out an experimental investigation of hydrodynamic performance of a partially immersed wave absorbing breakwater which consisted of seaward vertical perforated wall and shoreward vertical rigid wall and was connected above the water surface by a rigid horizontal plate. In order to alter the old breakwater for a yacht club near Sydney, Australia, this structure was proposed, and with a suitable design, a significantly reduced reflection and transmission coefficients were obtained. Wu *et al.* (1998) investigated wave reflection by a vertical wall with a horizontal porous plate with the help of linearized water wave theory and eigenfunction expansion method. It was observed that by changing the porous effect parameter of the porous plate, reflection could be controlled. Sahoo *et al.* (2000a) investigated oblique surface wave scattering by permeable barriers by considering four different types of barrier configurations and they observed that a finite angle of incidence and the porous effect of the barrier could reduce the reflection. Sahoo *et al.* (2000b) extended this work by replacing the infinite channel with a semi-infinite one with the help of a rigid vertical wall, where trapping of waves took place. Liu *et al.* (2008) discussed hydrodynamic properties of a modified two-layer breakwater with an upper horizontal porous plate and a lower horizontal impermeable plate. With a suitably chosen porosity of the upper porous plate, the uplift wave force on both the plates could be controlled and a prediction of enhanced hydrodynamic performance was also made if the lower plate was porous too. Liu and Li (2011a) presented an alternative analytical solution of the water wave motion over a horizontal porous-plate breakwater through the introduction of symmetric and anti-symmetric parts of the solution. The convergence of the method was satisfactory and matched well with other previous analytical solutions. Liu and Li (2011b) also investigated the hydrodynamic performance of a double curtain-wall breakwater consisting of a sea-ward porous wall and a shore-ward impermeable

wall. It was observed from the numerical results that with the proper choice of the structure parameters, both the reflection and transmission coefficients could be suppressed below 0.5 at a wide range of the relative water depth. Hsu and Huang (2011) introduced a new partial-slipping boundary condition to investigate a hydrodynamic property of the water wave which was incident parallel to thin porous wall. In order to find proper boundary conditions on a thin porous wall for viscous flow, viscous boundary layer effect was considered in this study. Cho and Kim (2013) investigated the interaction of oblique monochromatic incident waves with a submerged horizontal porous plate. Cho *et al.* (2013) extended this problem by investigating the interaction of oblique incident waves with dual submerged horizontal porous plates including viscous effect through Darcy's law. It was concluded that the upper horizontal porous plate played a major role in blocking the wave but the presence of lower horizontal porous plate played an important role when tidal variation was large.

Various researchers have also investigated wave diffraction problems involving porous cylinders. Wang and Ren (1994) investigated the wave interaction with a concentric surface-piercing two-cylinder system of which the outer one was porous and of thin annular radius, and the inner one impermeable. The free surface elevation and the hydrodynamic forces acting on both the cylinders were determined analytically. Darwiche *et al.* (1994) extended this problem by considering some part of the upper portion of the outer cylinder to be fully porous. Williams *et al.* (2000) and Sankarbabu *et al.* (2007) considered an array of bottom-mounted surface-piercing porous cylinders, whose outer walls were porous and inner region was impermeable. The effects of various wave and structural parameters on the hydrodynamic set-up were presented. Zhao *et al.* (2010) investigated wave interaction with a cylindrical breakwater consisting of a porous sidewall and an impermeable bottom along with a horizontal porous plate either beneath or coincident with the water surface. The effects of porosity and the inner horizontal plate were presented.

A number of notable works have also been accomplished with regard to porous beds. Gu and Wang (1991) investigated water wave interaction with porous ocean-beds of granular material through theory as well as experiment by taking into account inertial and non-linear resistance. Silva *et al.* (2002) utilized Green's second identity and extended the mild slope equations in investigating wave scattering by an arbitrary porous bottom. Lee *et al.* (2002) discussed the interaction of waves and a finite porous bed based on Biot's poro-elasticity theory (1956). It was shown in their result that the effect of parameters significantly altered the wave characteristics. Martha *et al.* (2007) discussed the problem of scattering of obliquely incident surface water waves by a small porous undulation on an ocean-bed. The solution was approached by assuming

a perturbation analysis in conjunction with Fourier transform technique and in terms of the smallness of an undulation parameter. Li and Jeng (2008) evaluated wave induced pore pressure and effective stresses on a porous ocean-bed near a breakwater head in order to investigate the influence of several wave and soil parameters.

Having studied the above works and realizing that not much work has been accomplished for (*i*) reflection and damping by a finite porous structure placed on elevated as well as multi-step bottoms and (*ii*) scattering by a dual porous plate configuration, we are motivated to solve water wave problems due to the presence of an elevated and a multi-step bottom under a finite porous structure and also due to the presence of two thin parallel vertical surface piercing porous plates of different heights and porous effect parameters in an infinite channel of constant depth. As far as our knowledge is concerned, till now no one else has attempted problems of this sort and we are hopeful that our results will throw some new lights on these topics. These problems are considered significant from the point of view of selecting an appropriate porous structure as breakwater/wave absorber to save the harbours, inlets etc.

1.6 Outline of the thesis

This thesis is arranged in eight chapters with the present chapter dealing with the basic ideas and relevant equations, previous important works and our motivation to carry out the present investigation.

In Chapter 2, we study the reflection of oblique ocean water waves by a vertical rectangular porous structure placed on an elevated horizontal bottom and against a rigid vertical wall. An incident wave propagates through the porous structure and gets reflected by a vertical solid wall which supports the structure at one end. Boundary value problems are set up in the two different consecutive media, and by using the matching conditions along the vertical boundary, a system of linear equations is deduced. The roots of the dispersion relation are used in setting up the system of equations. Reflection coefficient is obtained by solving this system of equations. The behaviour of the reflection coefficient due to different relevant parameters is studied. The effect of various parameters, such as depth, number of evanescent modes, porosity, structure width etc., on the reflection coefficient is studied graphically.

A study on wave damping by a vertical porous structure placed near and away from a rigid vertical wall is carried out in Chapter 3. The rectangular porous structure is placed on a small rectangular elevation. An incident wave of small amplitude propagates through the structure - some portion gets reflected back while some portion gets transmitted to a third

region bounded vertically by a rigid wall which is considered to be at a finite distance from the porous structure, and also away from the wall at a large distance as a separate case. Boundary value problems are set up in all three regions and by using the matching conditions along the vertical boundaries, a system of linear equations is deduced. The overall reflection and damping phenomena is studied with respect to different relevant parameters. The dependence of the reflection coefficient on the thickness (width) of the porous structure is investigated for different numbers of modes and porosity. Moreover, energy loss (in %) for different values of evanescent modes and porosity is also investigated.

Chapter 4 deals with the reflection of oblique ocean water waves by a vertical porous structure placed on a horizontal multi-step bottom. The reflection phenomenon is investigated for two forms of the bottom topography: first a 2-step one and then a p-step one. An oblique incident wave propagates through the porous structure and gets reflected by the steps and a vertical solid wall which supports the structure at one end. Boundary value problems are set up in the two different consecutive media, the first medium being water and the second medium being the porous structure consisting of p vertical regions - one above each step. The behaviour of the reflection coefficient due to different relevant parameters is studied. The effect of various parameters, such as depth, porosity, structure width and angle of incidence, on the reflection coefficient is studied graphically for both cases.

Chapter 5 is devoted to the problem related to the damping of oblique ocean waves by a porous structure placed on a multi-step bottom. Here some portion of the oblique wave, incident on the porous structure, gets reflected by the multi-step bottom and the porous structure, and the remaining portion propagates in the water region following the porous structure. Two cases are considered: first a solid vertical wall placed at a finite distance from the porous structure in the water region following the porous structure and then a special case of an unbounded water region following the porous structure. In both cases, boundary value problems are set up in the three different regions, the first region being water, the second being the porous structure consisting of p vertical regions - one above each step and the third being water again. In the first case, the behaviour of the reflection and the dimensionless amplitude of the progressive transmitted wave due to different relevant parameters is studied. The investigation is also carried out for the second case, i.e., when the wall is absent. Now due to this condition, transmission coefficient appears in the solution of this problem. Energy loss due to the propagation of oblique water wave through the porous structure is also carried out. The effects of various parameters, such as number of evanescent modes, porosity, friction factor, structure width, number of steps and angle of incidence, on the reflection coefficient

and the dimensionless amplitude of the progressive transmitted wave is studied graphically. Energy loss due to different porosity, friction factor, structure width and angle of incidence is also studied.

Chapter 6 deals with the wave damping by two thin vertical parallel porous plates of different heights placed at finite distance from each other. An infinite channel of finite depth is divided into three regions in each of which different velocity potentials are considered and the corresponding boundary value problems are formulated. By means of eigenfunction expansion and least square method, a complete analytical solution in each of the regions is obtained. With the help of the matching conditions along the vertical boundaries between any two successive regions, the reflection and transmission coefficients and hence the energy loss, are obtained numerically by applying a matrix method. Numerical study on the reflection coefficient and the amplitude of the transmitted wave as well as the energy loss is carried out for various relevant parameters such as porous effect parameter, heights of both the plates, distance between the plates and the angle of incidence.

Chapter 7 is devoted to the work which is an extension of the work carried out in Chapter 6 by considering the dual porous plates fully submerged in water. Boundary value problems are formulated in each of the water regions and the same solution procedure as described in Chapter 6 is employed. The reflection and transmission coefficients are computed numerically along with the energy loss and the effect of various relevant parameters such as porous effect parameters, height of the plates and distance between them, distance from the free surface. Moreover, a comparative study with the work carried out in Chapter 6, i.e., when the porous plates touch the free surface, is also performed.

Chapter 8 summarizes all the results obtained in this thesis – mainly emphasizing the important observations. This chapter also suggests future directions for similar kind of investigations.

In all the problems considered, justification of our model is presented by matching it with the available ones. In each chapter, the results are presented through a sizeable number of graphs and also through tables wherever deemed necessary.

Chapter 2

Reflection of oblique ocean water waves by a vertical rectangular porous structure placed on an elevated horizontal bottom

In this chapter, the cases of water wave reflection due to the presence of a porous structure, placed on an elevated bottom or on a horizontal ocean-bed, in the presence of a rigid vertical wall is investigated with the help of linear water wave theory. The behaviour of the reflection coefficient and the dimensionless amplitude of the transmitted wave are studied graphically for various relevant parameters and the corresponding observations are made.

2.1 Mathematical formulation

Let us consider a vertical rectangular porous structure, a very small portion of which is above the free surface, on a horizontal elevated bottom at a height d above the horizontal ocean bottom, which is at a uniform depth h_1 from the free surface, and resting against a rigid vertical wall. Using Cartesian coordinates (x, y, z), we define the positive x-direction as the direction of the wave incident on the porous structure at $x = 0$, the z-direction vertically upwards and the mean free surface $z = 0$. The horizontal bottom under the water and porous regions, are considered, respectively, at $z = -h_1$ and $z = -h_2 = -h_1 + d$. The wave gets

reflected by the vertical wall at $x = L$ (figure 2.1). According to Sollitt and Cross (1972), velocity potentials can be assumed to exist within the porous structure as well as in the fluid region. The fluid is assumed to be incompressible, homogeneous and inviscid, and the motion irrotational. We define two velocity potentials, namely $\Phi_1(x, y, z, t) = \phi_1(x, z) \exp(ily - i\omega t)$ and $\Phi_2(x, y, z, t) = \phi_2(x, z) \exp(ily - i\omega t)$, for the water and porous regions, respectively. The variation of the potential functions in the y-direction is considered same in all the regions to satisfy the matching conditions along the vertical boundaries (by Snell's law).

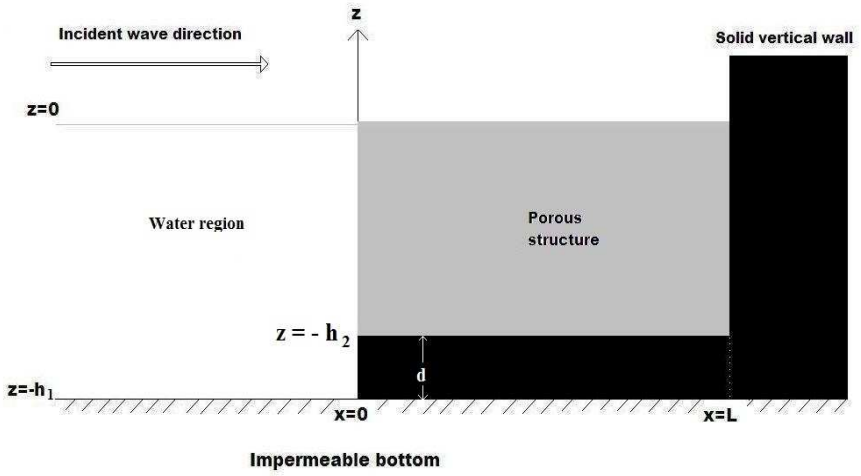

Figure 2.1: Schematic diagram of the problem

Since the ocean-bed is elevated to $z = -h_2, 0 < x < L$, on which the structure is placed, replacing h by h_2 in equations (1.32b,c) will, respectively, give the depth-dependent function and complex dispersion relation in the porous region for our present problem.
The governing equation and the boundary conditions for the water region are

$$\nabla^2\phi_1 - l^2\phi_1 = 0; \qquad -\infty < x < 0, \qquad -h_1 < z < 0, \tag{2.1a}$$

$$\frac{\partial\phi_1}{\partial z} - \nu\phi_1 = 0; \qquad -\infty < x < 0, \qquad z = 0, \tag{2.1b}$$

$$\frac{\partial\phi_1}{\partial z} = 0; \qquad -\infty < x < 0, \qquad z = -h_1, \tag{2.1c}$$

$$\frac{\partial\phi_1}{\partial x} = 0; \qquad x = 0, \qquad -h_1 < z < -h_2. \tag{2.1d}$$

The governing equation and the boundary conditions in the porous medium are

$$\boldsymbol{\nabla}^2\phi_2 - l^2\phi_2 = 0; \qquad 0 < x < L, \qquad -h_2 < z < 0, \tag{2.2a}$$

$$\frac{\partial\phi_2}{\partial z} - \mathrm{i}\nu R\phi_2 = 0; \qquad 0 < x < L, \qquad z = 0, \tag{2.2b}$$

$$\frac{\partial\phi_2}{\partial z} = 0; \qquad 0 < x < L, \qquad z = -h_2, \tag{2.2c}$$

$$\frac{\partial\phi_2}{\partial x} = 0; \qquad x = L, \qquad -h_2 < z < 0. \tag{2.2d}$$

In addition to the governing equation and different boundary conditions for each of the two regions, there exist matching conditions along the common boundary of these regions. These conditions imply the continuity of pressure and mass flux. For our problem, they are given by, along the boundary $x = 0$, $-h_2 \le z \le 0$:

$$\phi_1 = \mathrm{i}R\phi_2, \tag{2.3a}$$

$$\frac{\partial\phi_1}{\partial x} = \gamma\frac{\partial\phi_2}{\partial x}. \tag{2.3b}$$

Derivation of the matching conditions (2.3a,b) is detailed in Appendix B.

2.2 Reflection by the porous structure

The velocity potential $\phi_1(x, z)$ in the water region is given by the following form after using separation of variables method:

$$\phi_1(x,z) = \{\exp(\mathrm{i}K_{1,0}x) + R_0\exp(-\mathrm{i}K_{1,0}x)\}Z_{1,0}(h_1,z) + \sum_{n=1}^{\infty} R_n\exp(-\mathrm{i}K_{1,n}x)Z_{1,n}(h_1,z), \tag{2.4}$$

where the depth-dependent function $Z_{1,n}(h_1, z)$ and $K_{1,n}$ are, respectively, given by

$$Z_{1,n}(h_1,z) = \frac{\cosh k_{1,n}(h_1+z)}{\cosh k_{1,n}h_1}, \quad n = 0, 1, 2, \ldots, \tag{2.5a}$$

$$K_{1,n} = (k_{1,n}^2 - l^2)^{1/2}, \tag{2.5b}$$

with $k_{1,n}$ satisfying the dispersion relation

$$\nu = k_{1,n}\tanh k_{1,n}h_1, \tag{2.5c}$$

which has one positive real root $k_{1,0}$ corresponding to the incident and reflected modes of wave propagation, and infinitely many purely imaginary roots $k_{1,n}$; $n = 1, 2, \cdots$, which correspond to the evanescent modes.

By considering a linear combination up to the N-th term, $\phi_1(x, z)$ can be expressed as

$$\phi_1(x,z) = \{\exp(\mathrm{i}K_{1,0}x) + R_0 \exp(-\mathrm{i}K_{1,0}x)\} Z_{1,0}(h_1, z) + \sum_{n=1}^{N} R_n \exp(-\mathrm{i}K_{1,n}x) Z_{1,n}(h_1, z). \quad (2.6)$$

In the porous region, the horizontal impermeable bottom is considered at $z = -h_2$. Hence, the integrals in this porous region must be from $z = -h_2$ to $z = 0$ in order to meet the matching conditions and we are required to compute relevant integrals from $z = -h_2$ to $z = 0$. By using separation of variables method, the velocity potential $\phi_2(x, z)$ can be written as

$$\phi_2(x,z) = \sum_{n=0}^{\infty} \tilde{A}_n \cos(K_{2,n}x) + \tilde{B}_n \sin(K_{2,n}x) Z_{2,n}(h_2, z), \quad (2.7)$$

where $\tilde{A}_n$ and $\tilde{B}_n$ are arbitrary constants; the depth-dependent function $Z_{2,n}(h_2, z)$ in the porous region and $K_{2,n}$ are given, respectively, by

$$Z_{2,n}(h_2, z) = \frac{\cosh k_{2,n}(h_2 + z)}{\cosh k_{2,n} h_2}, \quad n = 0, 1, 2, \ldots \quad (2.8a)$$

$$\text{and} \quad K_{2,n} = (k_{2,n}^2 - l^2)^{1/2}, \quad (2.8b)$$

where $k_{2,n}$ satisfies the dispersion relation

$$\mathrm{i}R\nu = k_{2,n} \tanh k_{2,n} h_2. \quad (2.8c)$$

Using the boundary condition (2.2d), we obtain $\tilde{B}_n = \tilde{A}_n \tan K_{2,n} L$. By considering a linear combination of solutions up to the N-th term, $\phi_2(x, z)$ can be expressed as

$$\phi_2(x,z) = \sum_{n=0}^{N} \mathcal{A}_n \cos K_{2,n}(L - x) Z_{2,n}(h_2, z), \quad (2.9)$$

where $\mathcal{A}_n = \dfrac{\tilde{A}_n}{\cos K_{2,n} L}$.

It will be convenient to split the depth-dependent integrals into two since the depth-dependent function $Z_{2,n}(h_2, z)$ does not exist in the region $z = -h_1$ to $z = -h_2$, and con-

sequently express the integral in this region in terms of an integral over $-h_2 \leq z \leq 0$. So in the water region, by taking the help of the orthogonality of $Z_{1,n}(h_1, z)$, we have

$$\int_{-h_1}^{-h_2} Z_{1,m} Z_{1,n} dz + \int_{-h_2}^{0} Z_{1,m} Z_{1,n} dz = 0, \tag{2.10a}$$

and

$$\int_{-h_1}^{-h_2} Z_{1,n}^2 dz + \int_{-h_2}^{0} Z_{1,n}^2 dz = a_{1,n}, \tag{2.10b}$$

where

$$a_{1,m} = \int_{-h_1}^{0} Z_{1,m}^2 dz = \frac{h_1 \tanh K_{1,m} h_1}{2K_{1,m} h_1} \left(1 + \frac{2K_{1,m} h_1}{\sinh 2K_{1,m} h_1}\right).$$

Applying the boundary condition (2.1d), along with the matching conditions (2.3a,b), appropriately to the potentials, we get the following equations:

$$\mathrm{i}K_{1,0}(1 - R_0) Z_{1,0} - \sum_{n=1}^{N} R_n \mathrm{i}K_{1,n} Z_{1,n} = 0, \tag{2.11a}$$

$$(1 + R_0) Z_{1,0} + \sum_{n=1}^{N} R_n Z_{1,n} = \mathrm{i}R \sum_{n=0}^{N} \mathcal{A}_n \cos(K_{2,n} L) Z_{2,n}, \tag{2.11b}$$

$$K_{1,0}(1 - R_0) Z_{1,0} - \sum_{n=1}^{N} R_n K_{1,n} Z_{1,n} = -\mathrm{i}\gamma \sum_{n=0}^{N} \mathcal{A}_n K_{2,n} \sin(K_{2,n} L) Z_{2,n}. \tag{2.11c}$$

By using the orthogonality property of $Z_{1,0}(h_1, z)$ and equations (2.10a,b), the above equations reduce to

$$K_{1,0}(1 + R_0)[a_{1,0} - \alpha_{0,0}] + \sum_{n=1}^{N} R_n K_{1,n} \alpha_{0,n} = 0, \tag{2.12a}$$

$$(1 + R_0)\alpha_{0,0} + \sum_{n=1}^{N} R_n \alpha_{0,n} = \mathrm{i}R \sum_{n=0}^{N} \mathcal{A}_n \cos(K_{2,n} L) \mathcal{B}_{1,0,n}, \tag{2.12b}$$

$$K_{1,0}(1 - R_0)\alpha_{0,0} - \sum_{n=1}^{N} R_n K_{1,n} \alpha_{0,n} = -\mathrm{i}\gamma \sum_{n=0}^{N} \mathcal{A}_n K_{2,n} \sin(K_{2,n} L) \mathcal{B}_{1,0,n}, \tag{2.12c}$$

where

$$\mathcal{B}_{1,m,n} = \int_{-h_2}^{0} Z_{1,m} Z_{2,n} dz = \frac{1}{K_{1,m}^2 - K_{2,n}^2} \left[\nu(1 - \mathrm{i}R) - \frac{K_{1,m} \sinh K_{1,m}(h_2 - h_1)}{\cosh K_{1,m} h \cosh K_{2,n} h_2}\right],$$

$$\alpha_{m,m} = \int_{-h_2}^{0} Z_{1,m}^2 dz = \frac{-K_{1,m}h_2 - \sinh K_{1,m}(h_2-h_1)\cosh K_{1,m}(h_2-h_1)}{2K_{1,m}\cosh^2 K_{1,m}h_1} + \frac{\tanh K_{1,m}h_1}{2K_{1,m}},$$

$$\alpha_{m,n} = \int_{-h_2}^{0} Z_{1,m}Z_{1,n}dz = -\frac{1}{2\cosh K_{1,m}h_1 \cosh K_{1,n}h_1} \times \left[\frac{\sinh(h_1-h_2)(K_{1,m}+K_{1,n})}{K_{1,m}+K_{1,n}} + \frac{\sinh(h_1-h_2)(K_{1,m}-K_{1,n})}{K_{1,m}-K_{1,n}}\right].$$

Combining equations (2.12a) and (2.12c), we have

$$K_{1,0}(1-R_0)a_0 = -\mathrm{i}\gamma \sum_{n=0}^{N} \mathcal{A}_n K_{2,n} \sin(K_{2,n}L)\mathcal{B}_{0,n}. \tag{2.13a}$$

Similarly using the orthogonality of $Z_{1,m}(h_1, z)$ (for each m) and proceeding as before will give rise to the following equations:

$$R_m K_{1,m} a_{1,m} - \mathrm{i}\gamma \sum_{n=0}^{N} \mathcal{A}_n K_{2,n} \sin(K_{2,n}L)\mathcal{B}_{m,n} = 0, \tag{2.13b}$$

$$(1+R_0)\alpha_{m,0} + \sum_{n=1}^{N} R_n \alpha_{m,n} = \mathrm{i}R \sum_{n=0}^{N} \mathcal{A}_n \cos(K_{2,n}L)\mathcal{B}_{m,n}. \tag{2.13c}$$

Roots of the dispersion relations in both the water and porous regions are computed by the methods described in Section 1.4. From equations (2.12b), (2.13a–c), we construct a system of linear equations with $(2N+2)$ equations and $(2N+2)$ unknowns as follows:

$$\boldsymbol{MX} = \boldsymbol{b},$$

where $\boldsymbol{M}$ is a square matrix of size $(2N+2)$,

$$\boldsymbol{X} = [R_0, R_1, \ldots R_N, \mathcal{A}_0, \mathcal{A}_1, \ldots \mathcal{A}_N]^T$$

is the unknown vector,

and $$\boldsymbol{b} = [K_{1,0}a_0, \underbrace{0, \ldots 0}_{\text{N times}}, -\alpha_{0,0}, \cdots -\alpha_{N,0}]^T.$$

By solving this system we will be able to evaluate $|R_0|$ and subsequently discuss the reflection phenomenon within the porous structure.

2.3 Determination of friction factor

In order to study the reflection phenomenon, it is very essential to determine the friction factor (f) which is dependent on the incoming wave amplitude (a_i) and the porous structure characteristics. Lorentz principle of equivalent work, which states that the average rate of energy dissipation should be identical whether evaluated using the true non-linear resistance law or its linearized equivalent, is used to determine f. In order to compute the values of the appropriate friction factor corresponding to porosity γ, we follow Madsen (1983) and solve the following equation numerically for f by using secant method with two initial choices of friction factor as $f = 0$ and $f = 1.0$:

$$G \equiv \alpha_0 \frac{(1-\gamma)^3}{\gamma}\left(\frac{vT}{2\pi\delta_0^2}\right) + \beta_0 \frac{(1-\gamma)}{\gamma^2}\frac{a_i}{2\pi\delta_0} T\sqrt{\frac{g}{h_2}}\Lambda - f = 0, \tag{2.14}$$

where $\alpha_0 = 1000$, $\beta_0 = 2.8$, v = kinematic viscosity, T = wave period, δ_0 = grain size of the porous material, a_i = incident wave amplitude, h_2 = height of the porous structure and

$$\begin{aligned} \Lambda &= \frac{\int_0^L \int_0^T |U^*| U^{*2} \mathrm{dtdx}}{\int_0^L \int_0^T U^{*2} \mathrm{dtdx}}, \\ U^* &= \mathrm{Re}\left\{ \frac{2\epsilon[\exp(-\mathrm{i}\kappa x) - \exp\{\mathrm{i}\kappa(x-2L)\}]}{1+\epsilon+(1-\epsilon)\exp(-\mathrm{i}2\kappa L)} \exp(\mathrm{i}\omega t) \right\}, \end{aligned}$$

with $\epsilon = \gamma/\sqrt{1-\mathrm{i}f}$ and $\kappa = \omega\sqrt{1-\mathrm{i}f}/\sqrt{gh_2}$.

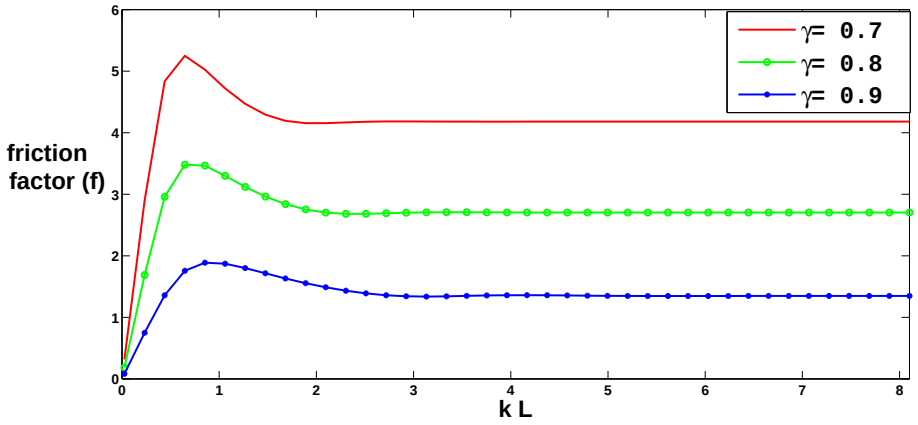

Figure 2.2: Variation of friction factor f against dimensionless width kL of the porous structure for different porosity γ with $h_1 = 21$, $\delta_0 = 0.2$, $T = 17.3$ and $a_i = 0.87$

In figure 2.2, we plot friction factor (f) against dimensionless wave absorber (kL) where

k is defined by $k = \omega/\sqrt{gh_1}$ (h_1 is the depth of the water region) for different values of porosity. Oscillation in values of friction factor is observed for lower values of the width of the wave absorber, but the oscillation vanishes with increasing width and it results in achieving constant values of friction factor afterwards. It is also observed that lower porosity gives rise to higher friction factor while higher values of porosity result in lower friction factors - as per our expectation.

2.4 Numerical results

For computational purpose, we consider some specific values of the parameters such as $d/h_1 = 1/8$; $L/h_1 = 1$; $S = 1$ and $\gamma = 0.3, 0.5, 0.7$.

First we investigate the effect of the number of evanescent modes on the reflection coefficient $|R_0|$ against the dimensionless wave numbers νh_1. It is to be noted that due to the presence of the elevated bottom, evanescent modes will gain higher amplitude at the obstacle and will interact with the incident wave. From figure 2.3, we observe that up to approximately $\nu h_1 < 0.765$, i.e., for long waves, reflection can be described by the propagating mode ($N = 0$) only. On the other hand, for short waves, the effect of number of evanescent modes is evident, that is, higher number of modes gives rise to higher reflection. For intermediate values of νh_1 in the range $0.765 < \nu h_1 < 2.2$ (approx.), the evanescent modes and the incident wave neutralize each other and it is observed that higher the number of modes lower is the reflection. Further, for each number of evanescent modes, $|R_0|$ attains a fixed value as we keep on increasing the value of νh_1.

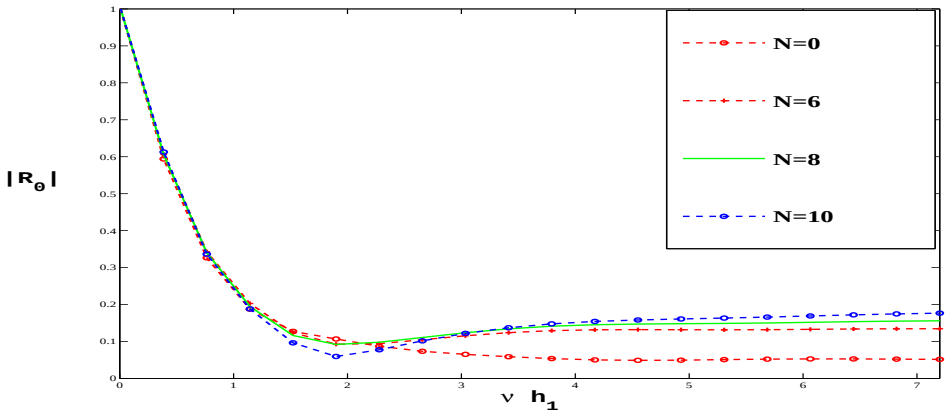

Figure 2.3: Variation of $|R_0|$ against νh_1 for different evanescent modes N with $L/h_1 = 1$, $d/h_1 = 0.125$ and $\gamma = 0.9$

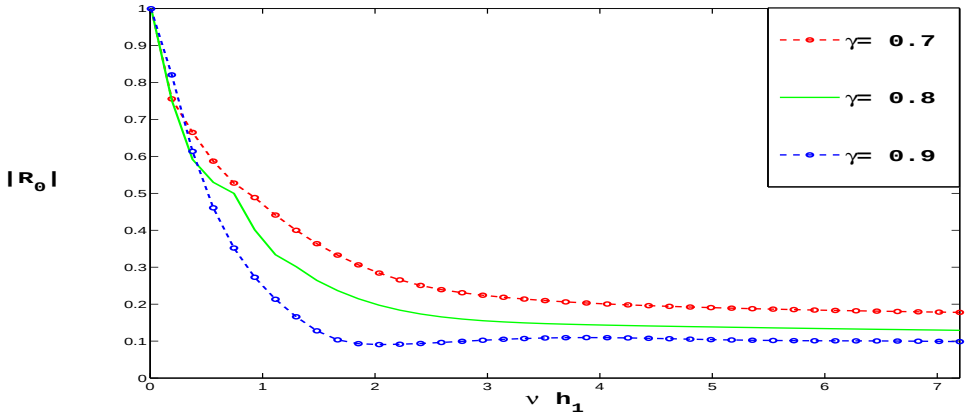

Figure 2.4: Variation of $|R_0|$ against νh_1 for different γ with $L/h_1 = 1$, $d/h_1 = 0.125$ and N=4

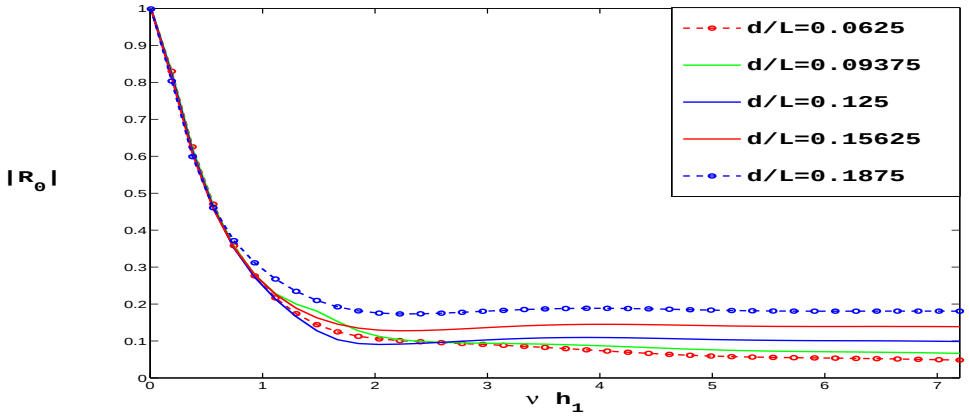

Figure 2.5: Variation of $|R_0|$ against νh_1 for different d/L with $L/h_1 = 1$, $\gamma = 0.9$ and $N = 4$

Porosity of the structure plays an important role in the reflection characteristics. Figure 2.4 shows that for the highest value of porosity considered ($\gamma = 0.9$), $|R_0|$ is considerably low. In other words, as porosity reduces, we encounter higher reflection coefficient. This is physically feasible since higher porosity ensures that a significant amount of waves pass through the porous structure and hence reflection will be less corresponding to higher porosity.

Moreover, an investigation on the effect of the elevation d/L of the impermeable bottom under the porous structure is carried out. $|R_0|$ is plotted against the dimensionless wave numbers νh_1 for five different values of d/L ($0.0625 \leq d/L \leq 0.1875$) in figure 2.5 and it is observed that for long waves, reflection is quite high for all the values of the elevation of the bottom, but it reduces significantly for intermediate and short waves. In the higher range of

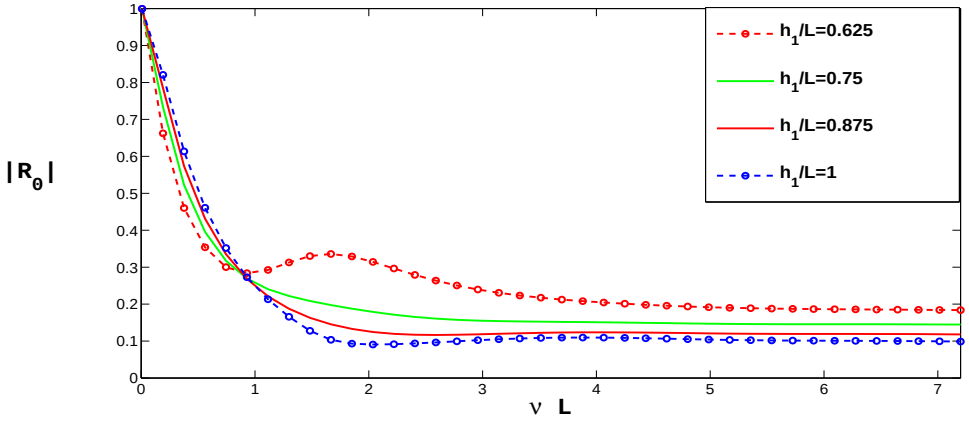

Figure 2.6: Variation of $|R_0|$ against νL for different h_1/L with $d/L = 0.125$, $\gamma = 0.9$ and $N = 4$

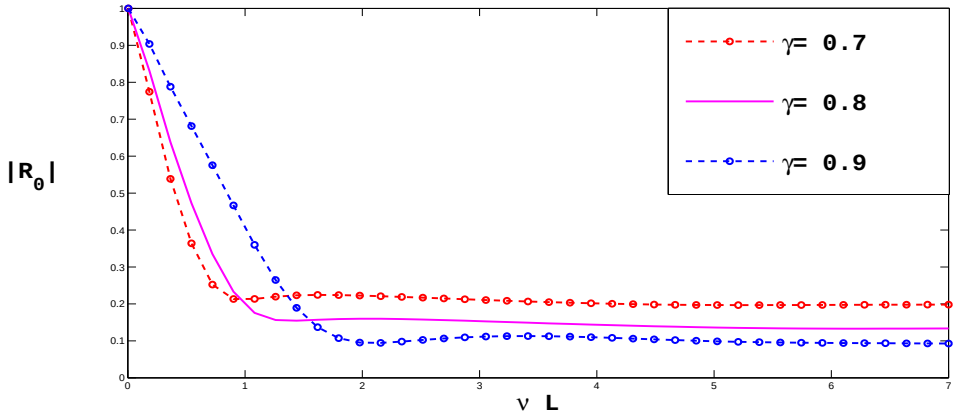

Figure 2.7: Variation of $|R_0|$ against νL for different γ with $d/h_1 = 0.125$, $\nu = 0.5$ and $N = 4$

wave numbers (short waves), reflection is more or less steady. Further, it is observed that higher the elevation higher is the reflection. An increase in d/L results in decrease in the volume of the porous structure and hence relatively less amount of waves will pass through the porous structure. Therefore higher reflection is observed for higher value of d/L - in the line of our expectation.

In order to examine the effect of depth or equivalently the height of the porous structure for a fixed elevated bottom, the reflection coefficient $|R_0|$ is plotted against νL (figure 2.6). It is observed that as the height of the porous structure is increased, i.e., when the elevation is reduced, the reflection coefficient decreases. Volume of the porous structure will increase with an increase in h_1 (keeping d fixed). Hence lower reflection is expected for higher h_1. Now the

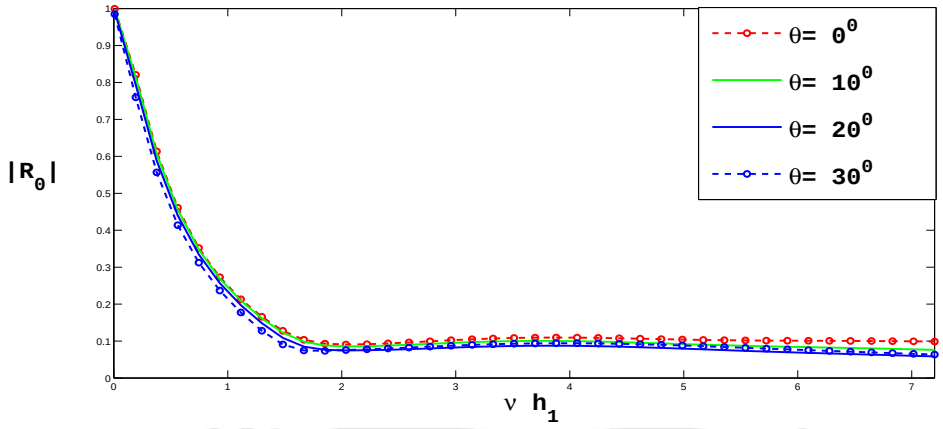

Figure 2.8: Variation of $|R_0|$ against νh_1 for different incident wave angle θ with $d/h_1 = 0.125$, $N = 4$ and γ=0.9

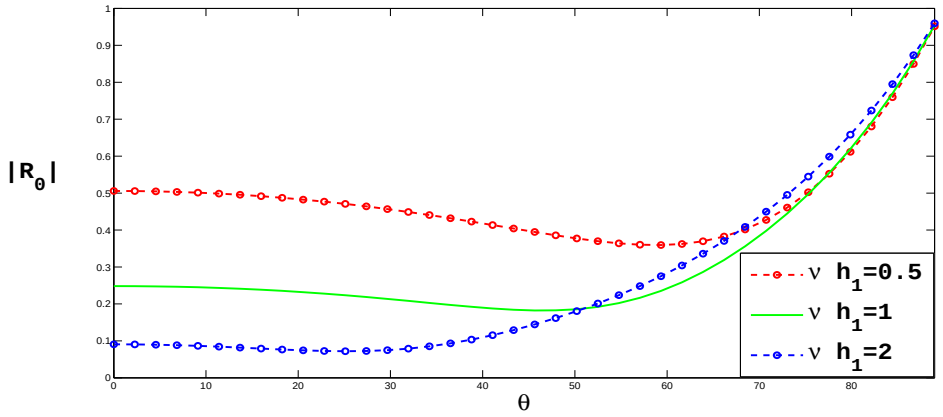

Figure 2.9: Variation of $|R_0|$ against incident wave angle θ for different wave number with $d/h_1 = 1$, $N = 4$ and γ=0.9

effect of the evanescent modes is prominent when there is a depth difference between the two regions. It is observed from the curve corresponding to $h_1/L = 0.625$ where oscillation takes place due to the cancelation of the incident wave and evanescent modes. Higher values of $|R_0|$ in the case of relatively short waves ($\nu L > 1$) (approx.) are observed for lower values of h_1/L because of the dominance of the evanescent waves over the incident wave. All the curves do not converge but higher fixed values of $|R_0|$ are obtained for higher values of h_1/L. Moreover, it is observed that $|R_0|$ is stagnant for $\nu L = 0.9$, irrespective of the values of h_1/L.

Figure 2.7 shows the variation of $|R_0|$ against the dimensionless width νL of the porous structure for different values of porosity. It is observed that $|R_0|$ decreases rapidly with an

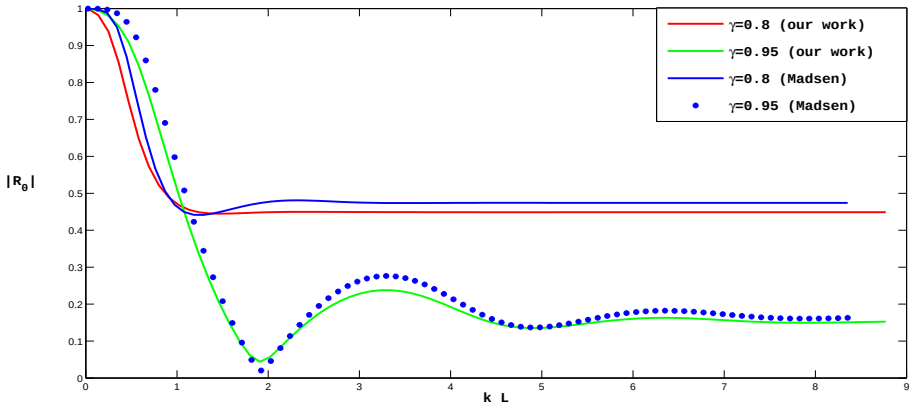

Figure 2.10: Variation of reflection coefficient $|R_0|$ against dimensionless width of porous structure for different porosity γ with $h_1 = 21$, $\delta_0 = 0.2$, $T = 17.3$, $a_i = 0.87$ and $N = 4$ (Comparison with Madsen (1983))

increase in νh_1 for lower porosity as compared to the higher ones and attains a fixed value afterwards which is higher for lower porosity. With higher porosity, relatively significant amount of waves will pass through the porous structure which results in lower reflection coefficient. The steep portion of the curve indicates the minimum width of the porous structure required in order to reduce the reflection. It is also observed that the steep portion tends to shift towards left with a decrease in the value of the porosity taken. This is due to the fact that for lower porosity, fewer waves enter the porous structure and hence, compared to higher porosity, thinner porous structure is required to absorb the wave energy.

Now we study the variation of $|R_0|$ against the dimensionless wave numbers νh_1 for different values of angle of incidence θ. It is observed from figure 2.8 that as we increase θ, the value of $|R_0|$ decreases. The higher values of $|R_0|$ occur for lower range of the wave numbers and they decrease very rapidly to attain different fixed values in the higher range for each case. This is because minimum reflection does not occur at $\theta = 0$ but occurs at higher values of θ only. So with an increase in the value of θ, the reflection coefficient keeps on decreasing until it reaches the specific value of θ of minimum reflection.

We also study the variation of $|R_0|$ against the angle of incidence θ for different values of dimensionless wave numbers νh_1. In figure 2.9, we plot $|R_0|$ against the angle of incidence θ for different wave numbers. Higher reflection coefficients are observed for long waves (lower wave numbers) as compared to short waves (higher wave number) up to some specific value of θ. This occurrence can be explained through linear water wave theory. The fluid layer

affected by the wave motion for relatively short waves is thinner than that of relatively long waves. Hence higher reflection occurs in the case of relatively long waves. Further, the values of $|R_0|$ do not differ much for different wave numbers, i.e., there is no appreciable variation of reflection coefficient beyond this value of angle of incidence. This happens because of higher oblique incidence due to which most of the waves get reflected irrespective of the nature of the wave and hence negligible variation in the reflection coefficient occurs.

In order to ascertain that our model is effective, we compare the reflection coefficients plotted against the dimensionless porous structure width for two values of porosity with those obtained in the work of Madsen (1983). This is accomplished by taking $d = 0$, i.e., by placing the structure on a flat ocean-bed instead of an elevated bottom. The excellent agreement between our result and Madsen's result can be observed from figure 2.10. This confirms that our model is valid and hence can be employed effectively to investigate various issues related to the scattering of waves by a rectangular porous structure.

2.5 Particular Case: Porous structure on a horizontal bottom with a rigid vertical wall

2.5.1 Formulation

Here the geometry of the problem is same as in the previous case except for the fact that there is no elevation of the horizontal bottom under the porous structure, i.e., now $h_1 = h_2$ (refer to figure 2.1).

The boundary value problem in the water region is now given by equations (2.1a–c) because the obstacle at $x = 0$, $-h_1 < z < -h_2$ vanishes which renders condition (2.1d) redundant. The governing equation and the boundary conditions in the porous region are given by the same set of equations (2.2a–d) with h_2 replaced by h_1. The same applies to the matching conditions (2.3a,b) with the only change being the range of z replaced by $-h_1 < z < 0$.

2.5.2 Solution

Following the same procedure adopted earlier, we construct a system of linear equations with $(2N + 2)$ unknowns as

$$(1 + R_0)a_{1,0} = \mathrm{i}R\sum_{n=0}^{N} C_n \cos(K_{2,n}L)E_{0,n}, \tag{2.15a}$$

$$\mathrm{i}K_{1,0}(1-R_0)a_{1,0} = -\gamma\sum_{n=0}^{N} C_n K_{2,n}\sin(K_{2,n}L)E_{0,n}, \tag{2.15b}$$

$$R_m a_{1,m} = \mathrm{i}R\sum_{n=0}^{N} C_n\cos(K_{2,n}L)E_{m,n}, \quad m=1,\ldots,N, \tag{2.15c}$$

$$\mathrm{i}K_{1,m}R_m a_{1,m} = -\gamma\sum_{n=0}^{N} C_n K_{2,n}\sin(K_{2,n}L)E_{m,n}, \quad m=1,\ldots,N, \tag{2.15d}$$

where $E_{m,n}$ are given by

$$E_{m,n} = \int_{-h_1}^{0} Z_{1,m}Z_{2,n}dz = \frac{\nu(\mathrm{i}R-1)}{K_{2,n}^2-K_{1,m}^2}.$$

Equations (2.15a–d) can be written as the system

$$\boldsymbol{A}\boldsymbol{X} = \boldsymbol{c},$$

where $\boldsymbol{A}$ is a square matrix of size $(2N+2)$,

$\boldsymbol{X} = [R_0, R_1, \ldots R_N, C_0, C_1, \ldots C_N]^T$ is the unknown vector,

and $\boldsymbol{c} = [-a_0, \underbrace{0,\ldots 0}_{\text{N-times}}, \tilde{a_0}, \underbrace{0,\ldots 0}_{\text{N-times}}]^T$,

with $\tilde{a}_m = K_{1,m}a_m$.

By solving the above system of linear equations, we evaluate and discuss the reflection coefficient for this particular case.

2.5.3 Numerical results

Comparing figures 2.3 and 2.8–2.9 with figures 2.11 and 2.15–2.16, respectively, we observe that the overall reflection is higher when the bottom elevation is more. But by comparing figures 2.4 and 2.7 with figures 2.12 and 2.14, respectively, we observe that $d/L = 1/8$ results in lower reflection compared to the case with no elevation under the porous structure for $\gamma = 0.7$, 0.8 whereas $\gamma = 0.9$ results in higher reflection. This is due to the fact that porosity dominates over the bottom elevation which is small in comparison to the height of the porous structure. It is observed from figure 2.13 that all curves converge to each other at $\nu L = 6$. The stagnation

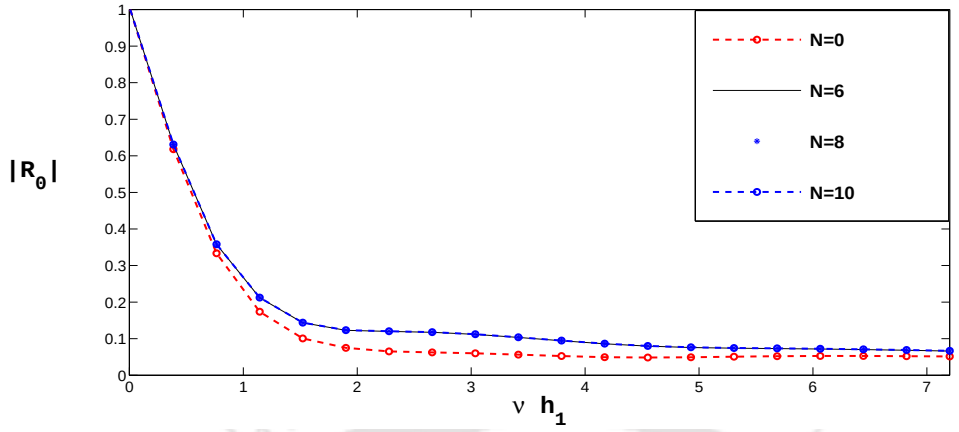

Figure 2.11: Variation of $|R_0|$ against νh_1 for different numbers of evanescent modes N with $L/h_1 = 1$ and $\gamma = 0.9$

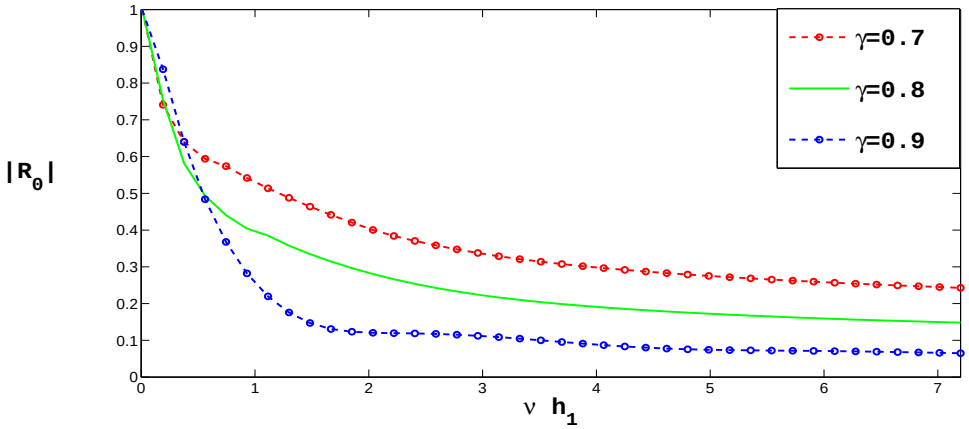

Figure 2.12: Variation of $|R_0|$ against νh_1 for different γ with $L/h_1 = 1$ and $N = 4$

point of $|R_0|$ is at $\nu L = 1.2$ (approx.). Comparison of figure 2.13 with figure 2.6 shows that the oscillation in $|R_0|$ for $h_1/L = 0.625$ in figure 2.13 vanishes since there does not exist any bottom elevation under the porous structure and the evanescent modes do not assume a significant role in interacting with the incident wave. Now, without elevation, stagnation point occurs at higher wave numbers as against at lower wave numbers in the elevated bottom case.

2.6 Conclusion

Based on linear water wave theory, the reflection coefficient for oblique water waves scattering by a vertical rectangular porous structure placed on an elevated horizontal bottom and bounded

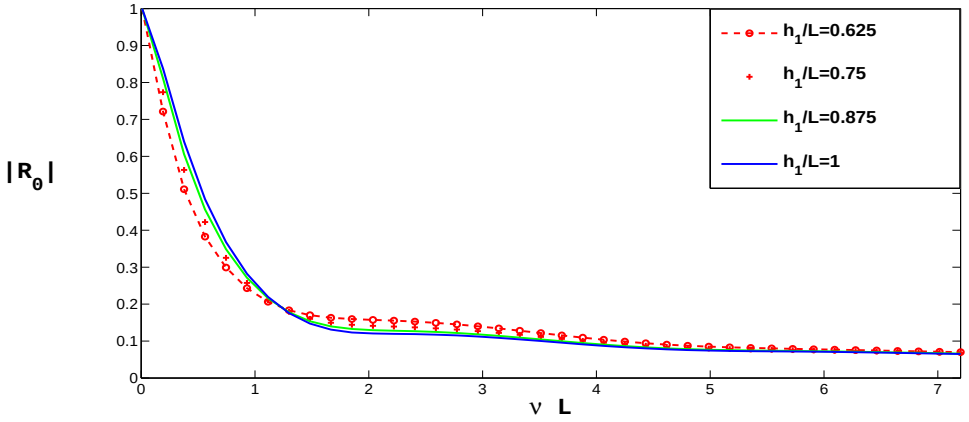

Figure 2.13: Variation of $|R_0|$ against νL for different h_1/L with $\gamma = 0.9$ and $N = 4$

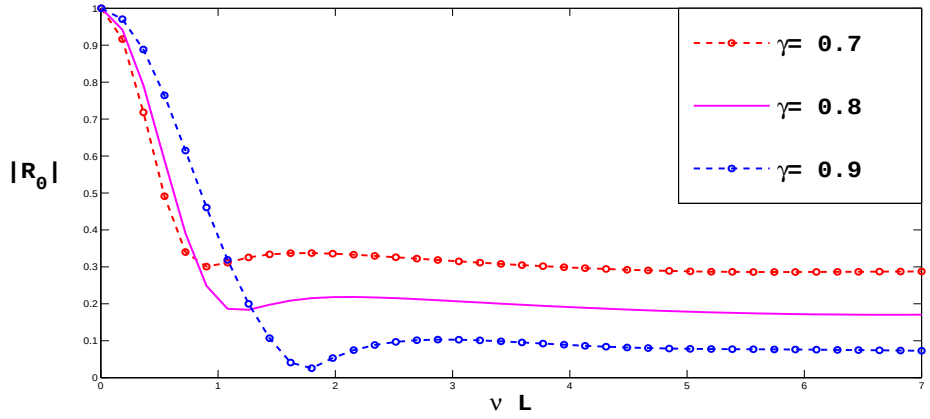

Figure 2.14: Variation of $|R_0|$ against νL for different γ with $L/h_1 = 1$, $\nu = 0.5$ and $N = 4$

vertically by a solid vertical wall is considered. By setting up the boundary value problems and appropriate matching conditions, and using the orthogonality of the depth functions, a system of linear equations is derived. In order to do so, roots of the dispersion relations in both porous and water regions are found numerically. It is observed that the propagating mode controls the reflection phenomenon up to a certain wave number. For short waves, the effect of number of evanescent modes is clearly visible, that is, higher number of modes gives rise to higher reflection. But for intermediate values of the wave number, the evanescent modes and the incident wave neutralize each other and it is observed that higher number of modes produces lower reflection. An increment in the height of the elevated bottom results in higher reflection coefficient, whereas increments in the depth and the values of porosity of the porous structure

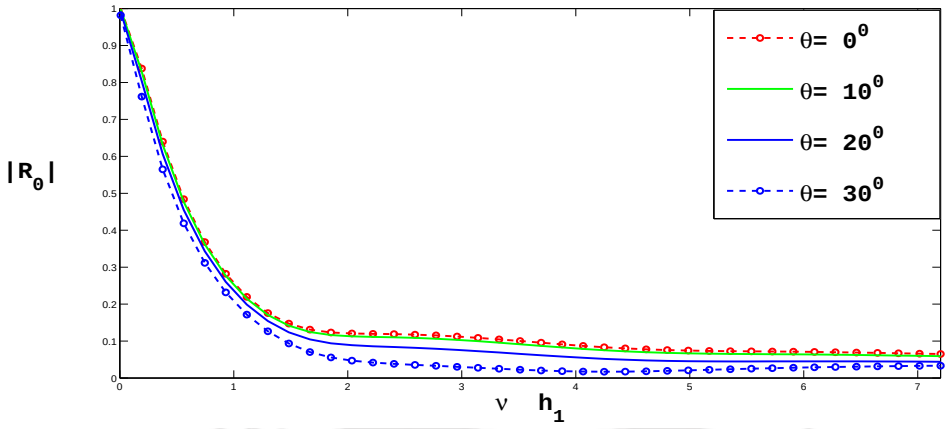

Figure 2.15: Variation of $|R_0|$ against νh_1 for different incident wave angle θ with $L/h_1 = 1$, $N = 4$ and γ=0.9

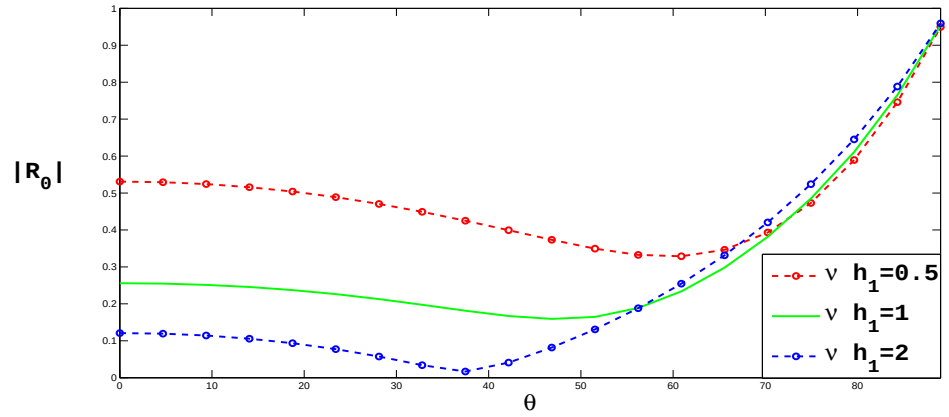

Figure 2.16: Variation of $|R_0|$ against incident wave angle θ for different wave number with $L/h_1 = 1$, $N = 4$ and γ=0.9

lead to a fall in the values of reflection coefficient. There exists a specific wavelength of the incident wave for which the reflection coefficient is invariant with respect to the height of the porous structure. An increment in incident wave angle results in lower reflection coefficient. The value of reflection coefficient is higher for long waves compared to short ones, but the difference in the values of the reflection coefficients decreases as we increase the incident wave angle; and for the higher values of incident wave angle, the values of the reflection coefficient converge. Observations on reflection are made for a certain range of bottom elevation, and the corresponding results are compared with the particular case, i.e., for no elevation of the ocean bottom under the porous structure. Graphically we observe more reflection in the above-

mentioned particular case compared to the elevated bottom case except for the case of different values of porosity where the reverse effect is observed due to the dominance of porosity over the bottom elevation. For the validity of our mathematical model, we compare our work with Madsen (1983) by plotting reflection coefficient against dimensionless width of the porous structure for different values of porosity and we arrive at excellent agreement in this regard. This shows that our model will be effective for solving the class of problems of wave scattering by vertical porous structures.

Chapter 3

Water wave damping by a vertical porous structure placed near and away from a rigid vertical wall

In this chapter, the water wave scattering problem due to the presence of a porous structure placed on an elevated impermeable bed at constant depth and at some distance from a rigid vertical wall is attempted. The scattering phenomenon as well as the associated energy loss are studied for different relevant parameters for two cases, namely, the one in which the porous structure is placed near a rigid vertical wall and also the one when the porous structure is placed far away from the wall.

3.1 Mathematical formulation

For simplicity in analysis let us consider the breakwater as a rectangular porous structure of width L and height h_2 placed on a horizontal bottom at a small height d above the horizontal ocean bottom, which is at a depth h_1 from the mean free surface. Using Cartesian coordinates (x, y, z), we define the positive x-direction as the direction of the wave incident on the porous structure at $x = 0$, the z-direction vertically upwards and the mean free surface as $z = 0$. The horizontal bottoms under the water region and the porous structure are considered, respectively, at $z = -h_1$ and $z = -h_2 = -h_1 + d$. We further consider a water region again between the porous structure and the rigid vertical wall placed at a distance

$x = D$ (figure 3.1). The wave gets partially reflected by the porous structure and the rest gets

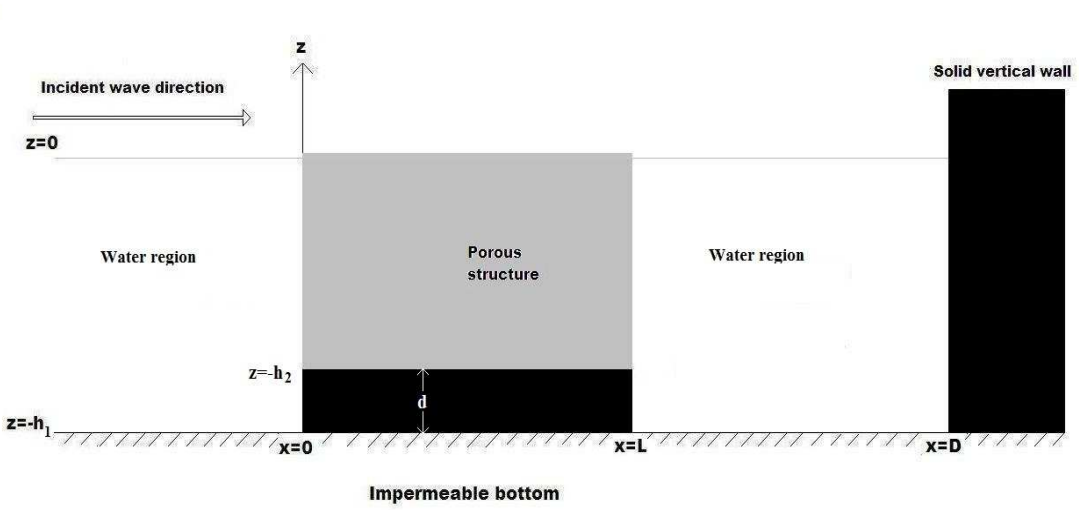

Figure 3.1: Schematic diagram of the problem

transmitted through the structure to the third region where it again gets reflected by the solid vertical wall. We define three velocity potentials, namely $\Phi_1(x, y, z, t) = \phi_1(x, z) \exp(ily - i\omega t)$, $\Phi_2(x, y, z, t) = \phi_2(x, z) \exp(ily - i\omega t)$ and $\Phi_3(x, y, z, t) = \phi_3(x, z) \exp(ily - i\omega t)$, in the water region, the porous structure and the water region between the porous structure and the solid vertical wall, respectively. For convenience we refer to the left water region, porous region and the right water region as region I, region II and region III, respectively.

The governing equation and the boundary conditions in region I, $-\infty < x < 0$, $-h_1 < z < 0$, are

$$\nabla^2\phi_1 - l^2\phi_1 = 0; \qquad -\infty < x < 0, \qquad -h_1 < z < 0, \tag{3.1a}$$

$$\frac{\partial\phi_1}{\partial z} - \nu\phi_1 = 0; \qquad -\infty < x < 0, \qquad z = 0, \tag{3.1b}$$

$$\frac{\partial\phi_1}{\partial z} = 0; \qquad -\infty < x < 0, \qquad z = -h_1, \tag{3.1c}$$

$$\frac{\partial\phi_1}{\partial x} = 0; \qquad x = 0, \qquad -h_1 < z < -h_2. \tag{3.1d}$$

Here it is to be noted that since we consider only a small elevation d under the porous structure, we use the same velocity potential throughout this region, i.e., we approximate ϕ_1 for the depth $z = 0$ to $z = -h_1$ though in reality we should have considered ϕ_1 separately for $z = 0$

to $z = -h_2$ and for $z = -h_2$ to $z = -h_1$.

The governing equation and the boundary conditions in region II, $0 < x < L$, $-h_2 < z < 0$, are

$$\boldsymbol{\nabla}^2\phi_2 - l^2\phi_2 = 0; \qquad 0 < x < L, \qquad -h_2 < z < 0, \tag{3.2a}$$

$$\frac{\partial\phi_2}{\partial z} - \mathrm{i}\nu R\phi_2 = 0; \qquad 0 < x < L, \qquad z = 0, \tag{3.2b}$$

$$\frac{\partial\phi_2}{\partial z} = 0; \qquad 0 < x < L, \qquad z = -h_2. \tag{3.2c}$$

The governing equation and the boundary conditions in region III, $L < x < D$, $-h_1 < z < 0$, are given by

$$\boldsymbol{\nabla}^2\phi_3 - l^2\phi_3 = 0; \qquad L < x < D, \qquad -h_1 < z < 0, \tag{3.3a}$$

$$\frac{\partial\phi_3}{\partial z} - \nu\phi_3 = 0; \qquad L < x < D, \qquad z = 0, \tag{3.3b}$$

$$\frac{\partial\phi_3}{\partial z} = 0; \qquad L < x < D, \qquad z = -h_1, \tag{3.3c}$$

$$\frac{\partial\phi_3}{\partial x} = 0; \qquad x = D, \qquad -h_1 < z < 0, \tag{3.3d}$$

$$\frac{\partial\phi_3}{\partial x} = 0; \qquad x = L, \qquad -h_1 < z < -h_2. \tag{3.3e}$$

The matching conditions along the boundaries $x = 0$ and $x = L$ are

$$\phi_1 = \mathrm{i}R\phi_2; \qquad x = 0, \qquad -h_2 \le z \le 0, \tag{3.4a}$$

$$\frac{\partial\phi_1}{\partial x} = \gamma\frac{\partial\phi_2}{\partial x}; \qquad x = 0, \qquad -h_2 < z < 0, \tag{3.4b}$$

$$\mathrm{i}R\phi_2 = \phi_3; \qquad x = L, \qquad -h_2 \le z \le 0, \tag{3.4c}$$

$$\gamma\frac{\partial\phi_2}{\partial x} = \frac{\partial\phi_3}{\partial x}; \qquad x = L, \qquad -h_2 < z < 0. \tag{3.4d}$$

3.2 Reflection and damping by the porous structure

In region I, the velocity potential $\phi_1(x, z)$ is same as the one defined in Chapter 2. Hence $\phi_1(x, z)$, depth dependent function $Z_{1,n}$ and wave number $K_{1,n}$ satisfy equations (2.6), (2.5a) and (2.5b), respectively, along with the dispersion relation (2.5c).

In region II, the horizontal impermeable bottom is considered at $z = -h_2$. Hence, the integrals in the porous region must be from $z = -h_2$ to $z = 0$ in order to meet the matching

conditions and it is required that we compute relevant integrals from $z = -h_2$ to $z = 0$. By using separation of variables method, the velocity potential ϕ_2 in $0 < x < L$, $-h_2 < z < 0$ can be written after truncating n at $n = N$ as

$$\phi_2(x,z) = \sum_{n=0}^{N} \{A_n \exp(\mathrm{i}K_{2,n}x) + B_n \exp[-\mathrm{i}K_{2,n}(x-L)]\} Z_{2,n}(h_2,z), \tag{3.5}$$

where A_n and B_n are arbitrary constants and $K_{2,n} = \sqrt{k_{2,n}^2 - l^2}$; $Z_{2,n}(h_2,z)$ and $k_{2,n}$ satisfy equations (2.8a) and (2.8b), respectively.

In region III, $L < x < D$, $-h_1 < z < 0$, the velocity potential can be written as, after truncating n at $n = N$,

$$\phi_3(x,z) = \sum_{n=0}^{N} \{C_n \exp\big[\mathrm{i}K_{3,n}(x-L)\big] + D_n \exp\big[-\mathrm{i}K_{3,n}(x-D)\big]\} Z_{3,n}(h_1,z), \tag{3.6a}$$

where C_n and D_n are arbitrary constants and the depth-dependent function $Z_{3,n}(h_1,z)$ is given by

$$Z_{3,n}(h_1,z) = \frac{\cosh k_{3,n}(h_1+z)}{\cosh k_{3,n}h_1}, \quad n = 0,1,2,\ldots \tag{3.6b}$$

The dimensionless amplitude of the progressive transmitted wave is defined as $|C_0|$. The quantities $K_{3,n}$ and $k_{3,n}$ satisfy the same relations that hold for $K_{1,n}$ and $k_{1,n}$, respectively, i.e., equations (2.5b) and (2.5c).

Since the waves transmitted from the porous structure gets completely reflected by the solid wall placed at $x = D$, the following relation holds true for D_n:

$$D_n = C_n \exp(\mathrm{i}K_{3,n}r), \tag{3.7}$$

where $r = D - L$. Hence $\phi_3(x,z)$ can be written as

$$\phi_3(x,z) = \sum_{n=0}^{N} C_n \{\exp\big[\mathrm{i}K_{3,n}(x-L)\big] + \exp\big[-\mathrm{i}K_{3,n}(x-2D+L)\big]\} Z_{3,n}(h_1,z). \tag{3.8}$$

When energy loss is discussed during the whole process of scattering, the following definition will be used:

$$E_{\text{loss}} = (1 - |R_0|^2 - |C_0|^2) \times 100\%. \tag{3.9}$$

In region I, taking the help of the orthogonality of $Z_{1,n}(h,z)$, we have

$$\int_{-h_1}^{-h_2} Z_{1,m}Z_{1,n}\mathrm{d}z + \int_{-h_2}^{0} Z_{1,m}Z_{1,n}\mathrm{d}z = 0, \tag{3.10a}$$

$$\int_{-h_1}^{-h_2} Z_{1,n}^2\mathrm{d}z + \int_{-h_2}^{0} Z_{1,n}^2\mathrm{d}z = a_{1,n}. \tag{3.10b}$$

Now using equations (3.1d) and (3.3e), we arrive at

$$K_{1,0}(1-R_0)Z_{1,0} - \sum_{n=1}^{N} R_n K_{1,n} Z_{1,n} = 0, \tag{3.11a}$$

$$\sum_{n=0}^{N} K_{3,n}\big\{\exp\big(-\mathrm{i}K_{3,n}L\big) - \exp\big[-\mathrm{i}K_{3,n}(L-2D)\big]\big\}C_n = 0. \tag{3.11b}$$

Furthermore, using the orthogonality property of $Z_{1,0}$ and $Z_{1,m}$ $(m = 1,\dots N)$ in equations (3.11a,b) and integrating over $-h_1$ to $-h_2$ and then using equations (3.10a,b), we have

$$K_{1,0}(1-R_0)(a_{1,0}-\alpha_{0,0}) - \sum_{n=1}^{N} R_n K_{1,n}\alpha_{0,n} = 0, \tag{3.12a}$$

$$-K_{1,0}(1-R_0)\alpha_{m,0} - R_m K_{1,m}(a_{1,m}-\alpha_{m,m}) + \sum_{n=1(\neq m)}^{N} R_n K_{1,n}\alpha_{m,n} = 0, \tag{3.12b}$$

$$\begin{aligned} &K_{3,0}C_0\big\{\exp\big(-\mathrm{i}K_{3,0}L\big) + \exp\big[-\mathrm{i}K_{3,0}(L-2D)\big]\big\}(a_{1,0}-\alpha_{0,0}) \\ &\quad - \sum_{n=1}^{N} C_n K_{3,n}\big\{\exp\big(-\mathrm{i}K_{3,n}L\big) - \exp\big[-\mathrm{i}K_{3,n}(L-2D)\big]\big\}\alpha_{0,n} = 0, \end{aligned} \tag{3.12c}$$

$$\begin{aligned} &-\sum_{n=1(\neq m)}^{N} C_n K_{3,n}\big\{\exp\big(-\mathrm{i}K_{3,n}L\big) - \exp\big[-\mathrm{i}K_{3,n}(L-2D)\big]\big\}\alpha_{m,n} \\ &\quad + K_{3,m}T_m\big\{\exp\big(-\mathrm{i}K_{3,0}L\big) + \exp\big[-\mathrm{i}K_{3,0}(L-2D)\big]\big\}(a_{1,m}-\alpha_{m,m}) = 0. \end{aligned} \tag{3.12d}$$

Thereafter using the matching conditions (3.4a–d) on ϕ_1, ϕ_2 and ϕ_3, we have

$$(1+R_0)Z_{1,0} + \sum_{n=1}^{N} R_n Z_{1,n} = \mathrm{i}R\sum_{n=0}^{N}[A_n + B_n\exp(\mathrm{i}K_{2,n}L)]Z_{2,n}, \tag{3.13a}$$

$$\mathrm{i}K_{1,0}(1-R_0)Z_{1,0} - \sum_{n=1}^{N} R_n \mathrm{i}K_{1,n}Z_{1,n} = \gamma\sum_{n=0}^{N} K_{2,n}\left[A_n - B_n\exp(\mathrm{i}K_{2,n}L)\right]Z_{2,n}, \tag{3.13b}$$

$$\sum_{n=0}^{N} C_n[1+\exp(-2\mathrm{i}K_{3,n}L)]Z_{3,n} = \mathrm{i}R\sum_{n=0}^{N}[A_n\exp(\mathrm{i}K_{2,n}L)+B_n]Z_{2,n}, \tag{3.13c}$$

$$\sum_{n=0}^{N} C_n[1-\exp(-2\mathrm{i}K_{3,n}L)]K_{3,n}Z_{3,n} = \gamma\sum_{n=0}^{N} K_{2,n}\,[A_n\exp(\mathrm{i}K_{2,n}L)-B_n]Z_{2,n}. \tag{3.13d}$$

Similarly, using the orthogonality property of $Z_{1,0}$ and $Z_{1,m}$ $(m = 1,\dots N)$ and equations (3.12a–d) in the above equations, we obtain the following system of equations:

$$K_{1,0}a_{1,0}R_0 + \gamma\sum_{n=0}^{N} K_{2,n}\,[A_n - B_n\exp(\mathrm{i}K_{2,n}L)]\,\mathcal{B}_{1,0,n} = K_{1,0}a_{1,0}, \tag{3.14a}$$

$$K_{1,m}a_{1,m}R_m + \gamma\sum_{n=0}^{N} K_{2,n}\,[A_n - B_n\exp(\mathrm{i}K_{2,n}L)]\,\mathcal{B}_{1,m,n} = 0, \tag{3.14b}$$

$$\alpha_{0,0}R_0 + \sum_{n=1}^{N} R_n\alpha_{0,n} - \mathrm{i}R\sum_{n=0}^{N}[A_n + B_n\exp(\mathrm{i}K_{2,n}L)]\mathcal{B}_{1,0,n} = -\,\alpha_{0,0}, \tag{3.14c}$$

$$\alpha_{m,0}R_m + \sum_{n=1}^{N} R_n\alpha_{m,n} - \mathrm{i}R\sum_{n=0}^{N}[A_n + B_n\exp(\mathrm{i}K_{2,n}L)]\mathcal{B}_{1,m,n} = -\,\alpha_{m,0}, \tag{3.14d}$$

and

$$-\mathrm{i}R\sum_{n=0}^{N}[A_n\exp(\mathrm{i}K_{2,n}L)+B_n]\mathcal{B}_{1,0,n} + \sum_{n=0}^{N} C_n[1+\exp(2\mathrm{i}K_{3,n}r)]\alpha_{0,n} = 0, \tag{3.15a}$$

$$-\mathrm{i}R\sum_{n=0}^{N}[A_n\exp(\mathrm{i}K_{2,n}L)+B_n]\mathcal{B}_{1,m,n} + \sum_{n=0}^{N} C_n[1+\exp(2\mathrm{i}K_{3,n}r)]\alpha_{m,n} = 0, \tag{3.15b}$$

$$K_{3,0}a_{1,0}[1-\exp(2\mathrm{i}K_{3,0}r)]C_0 - \gamma\sum_{n=0}^{N} K_{2,n}\,[A_n\exp(\mathrm{i}K_{2,n}L) - B_n]\,\mathcal{B}_{1,0,n} = 0, \tag{3.15c}$$

$$K_{3,m}a_{1,m}[1-\exp(2\mathrm{i}K_{3,m}r)]T_m - \gamma\sum_{n=0}^{N} K_{2,n}\,[A_n\exp(\mathrm{i}K_{2,n}L) - B_n]\,\mathcal{B}_{1,m,n} = 0, \tag{3.15d}$$

where the coefficients $\mathcal{B}_{1,m,n}$ are defined as

$$\begin{aligned}\mathcal{B}_{1,m,n} &= \int_{-h_2}^{0} Z_{1,m}Z_{2,n}\mathrm{d}z = \int_{-h_2}^{0} Z_{3,m}Z_{2,n}\mathrm{d}z \\ &= \frac{1}{K_{1,m}^2 - K_{2,n}^2}\left[\nu(1-\mathrm{i}R) - \frac{K_{1,m}\sinh K_{1,m}(h_2-h_1)}{\cosh K_{1,m}h_1\cosh K_{2,n}h_2}\right].\end{aligned} \tag{3.16}$$

Using equations (3.14a–d) and (3.15a–d), we construct a matrix system as follows:

$$\boldsymbol{MX} = \boldsymbol{b},$$

where $\boldsymbol{M}$ is a square matrix of size $(4N+4)$,

$$\boldsymbol{X} = [R_0, R_1, \ldots R_N, A_0, A_1, \ldots A_N, B_0, B_1, \ldots B_N, C_0, C_1, \ldots C_n]^T$$

is the unknown vector,

and $$\boldsymbol{b} = [K_{1,0}P_0, \underbrace{0, \ldots 0}_{\text{N times}}, -a_{0,0}, \cdots - a_{N,0}, \underbrace{0 \ldots 0}_{\text{(2N+2) times}}]^T.$$

By solving this system we will be able to evaluate $|R_0|$ and $|C_0|$, and subsequently study the overall reflection phenomenon by the porous structure.

3.3 Numerical results

It is to be noted that the computed values of f, as described in Chapter 2, are used here also.

We now proceed to evaluate the reflection coefficient and the dimensionless amplitude of the progressive transmitted wave against the width of the porous structure and investigate their dependence on the number of evanescent modes and porosity. As the location of the rigid wall also plays an important role in studying these phenomena, we consider two cases - first with the wall at a distance nearer to the structure and then the wall at a very large distance away from it. For all the results we obtain, small horizontal bottom elevation $d/h_1 = 1/8$ under the porous structure and dimensionless wave number $\nu h = 5.102$ are considered. When the wall is near the structure, we consider the width $r = D - L$ of region III as $10h_1$ while r is taken as $100h_1$ when the wall is considered at a very large distance.

We define the dimensionless quantity L/h_1 to be the width of the porous structure for computational purpose. Figures 3.2 and 3.3 give the plots of reflection coefficient and the dimensionless amplitude of the progressive transmitted wave, respectively, against the width of the porous structure for different numbers of evanescent modes. Here we consider $r = 10h_1$, $\gamma = 0.9$ and $C_M = 0$. For discussing reflection, we consider different numbers of evanescent modes: $N = 1, 4, 9, 11, 14$. Figure 3.2 shows that as the width of the porous structure is increased, the reflection coefficient $|R_0|$ decreases initially for all numbers of modes. As N, the number of evanescent modes, increases, the corresponding reflection coefficients converge as can be seen for the plots for $N = 9, 11, 14$.

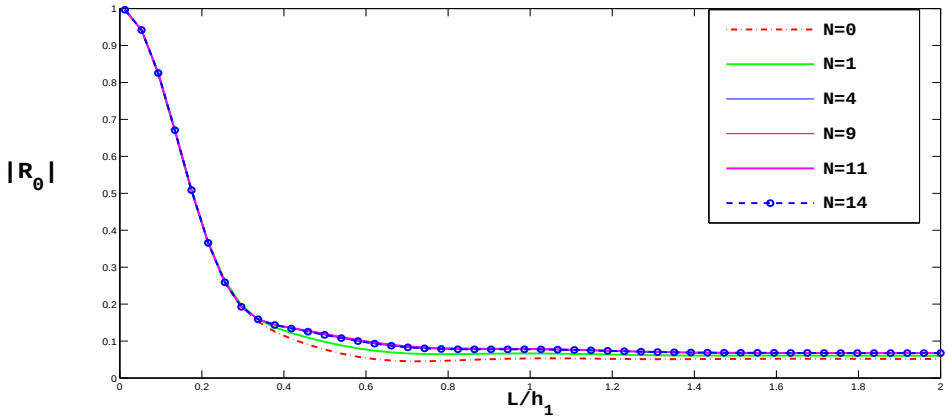

Figure 3.2: Variation of reflection coefficient $|R_0|$ against dimensionless width of porous structure for different numbers of evanescent modes N with $d/h_1 = 1/8$, $r/h_1 = 10$ and $\gamma = 0.9$; vertical wall placed nearer to the structure

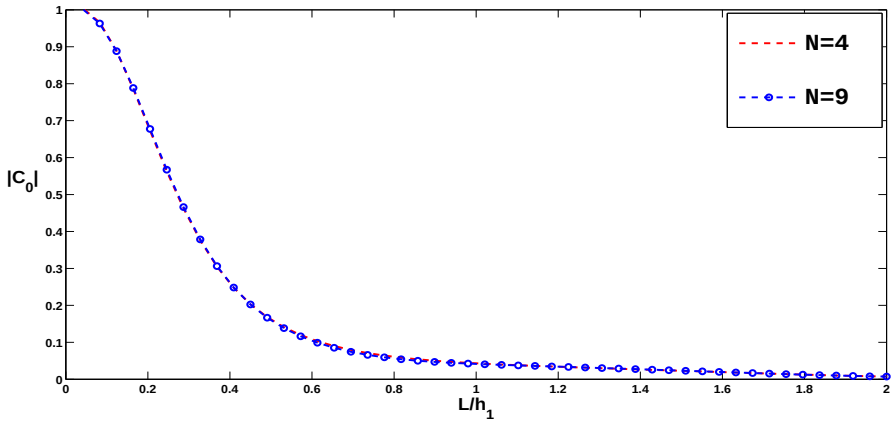

Figure 3.3: Variation of $|C_0|$ against dimensionless width of porous structure for different numbers of evanescent modes N with $d/h_1 = 1/8$, $r/h_1 = 10$ and $\gamma = 0.9$; vertical wall placed nearer to the structure

Similarly, figure 3.3 shows the dimensionless amplitude $|C_0|$ of the progressive transmitted wave for the same set of parameters corresponding to $N = 4$ and $N = 9$. $|C_0|$ also decreases as the width of the porous structure is increased and all the curves, irrespective of the number of modes included, converge together. It is observed that $|C_0|$ vanishes when the porous structure is very wide. Consideration of the values of N up to $N = 9$ is sufficient since the results obtained with $N = 9$ are more or less the same as those obtained for $N = 1, 2, \ldots, 8$. Therefore, for clear viewing without much overlapping, we here show the plots only for $N = 4, 9$.

Figures 3.4 and 3.5 give the plots of the reflection coefficient and the dimensionless am-

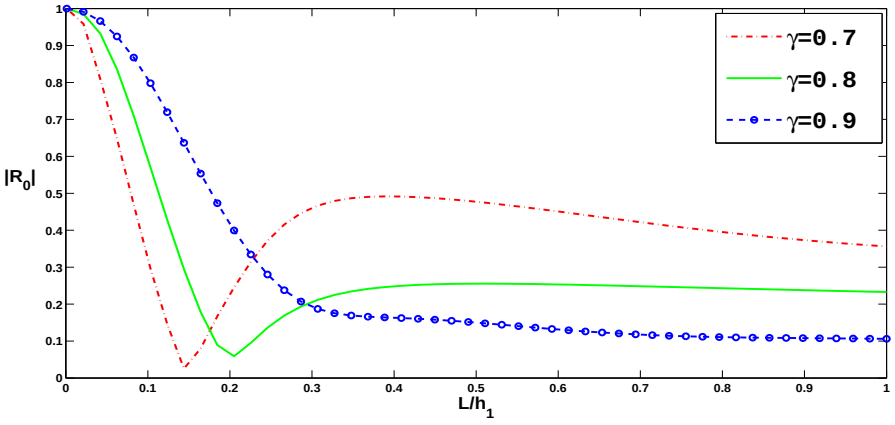

Figure 3.4: Variation of reflection coefficient $|R_0|$ against dimensionless width of porous structure for different porosity γ with $d/h_1 = 1/8$, $r/h_1 = 10$ and $N = 4$; vertical wall placed nearer to the structure

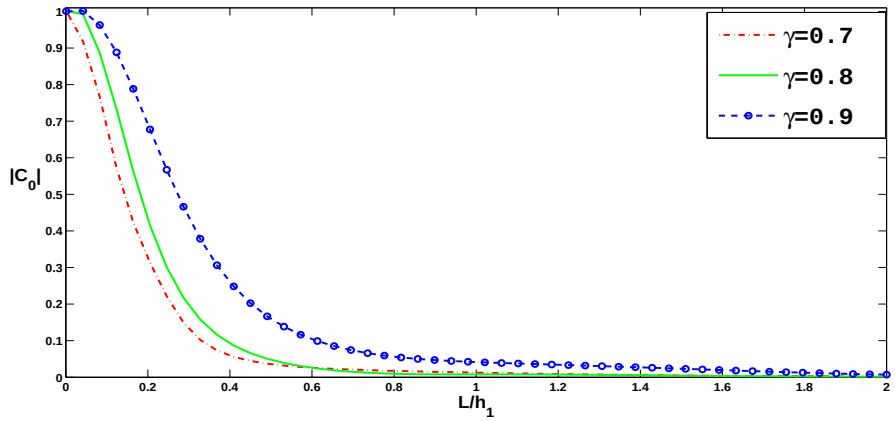

Figure 3.5: Variation of $|C_0|$ against dimensionless width of porous structure for different porosity γ with $d/h_1 = 1/8$, $r/h_1 = 10$ and $N = 4$; vertical wall placed nearer to the structure

plitude of the progressive transmitted wave, respectively, against the width of the porous structure for different values of porosity where we consider $N = 9$. Figure 3.4 shows that some oscillations in the reflection coefficient exist for lower values of porosity when the structure width is less while they do not exist at all for higher values of porosity, e.g., $\gamma = 0.9$. The reflection coefficient attains a fixed value once the oscillations disappear, irrespective of the values of porosity. It is also observed that after the oscillations vanish, higher porosity gives rise to lower reflection coefficients.

Figure 3.5 shows $|C_0|$ for the same set of parameters. We observe that $|C_0|$ decreases as

the width of the porous structure is increased and all the curves, irrespective of the porosity, ultimately converge to zero.

In order to ascertain that our model is effective, we compare our reflection coefficients plotted against the dimensionless porous structure width with the work of Madsen (1983). This is accomplished by taking $x = D = L$ and $d = 0$, i.e., by eliminating region III and placing the structure on the ocean-bed instead of an elevated bottom. The excellent agreement between our result and Madsen's result can be observed from figure 2.7 of Chapter 2. This confirms that our model is valid and hence can be employed effectively to investigate various issues related to scattering of waves by a porous structure.

3.4 Special Case: Porous structure placed far away from the solid wall

3.4.1 Formulation

Here the governing equations and boundary conditions in region I, region II and region III remain the same.

3.4.2 Solution

The velocity potentials in region I ($-\infty < x < 0$, $-h_1 < z < 0$) and region II ($0 < x < L$, $-h_2 < z < 0$) remain the same as in the previous case. But in region III ($L < x < D$, $-h_1 < z < 0$), the velocity potential now takes the following form:

$$\phi_3(x,z) = \sum_{n=0}^{N} C_n \exp\big[\mathrm{i}K_{3,n}(x-L)\big] Z_{3,n}(h_1,z) + D_0 \exp\big[-\mathrm{i}K_{3,0}(x-D)\big] Z_{3,0}(h_1,z). \quad (3.17)$$

Since the right decaying modes (corresponding to $n = 1, 2, \ldots, N$) decay to zero by the time they reach the solid wall at $x = D$, we use equation (3.3d) for the plane waves (corresponding to $n = 0$). Therefore the following relation holds true for D_0:

$$D_0 = C_0 \exp(\mathrm{i}K_{3,0}r). \quad (3.18)$$

Hence $\phi_3(x,z)$ can be simplified to the following form:

$$\begin{aligned}\phi_3(x,z) &= C_0\left\{\exp\left[\mathrm{i}K_{3,0}(x-L)\right]+\exp\left[-\mathrm{i}K_{3,0}(x-D-r)\right]\right\}Z_{3,0}(h_1,z)\\ &\quad+\sum_{n=1}^{N}C_n\exp\left[\mathrm{i}K_{3,n}(x-L)\right]Z_{3,n}(h_1,z).\end{aligned}\tag{3.19}$$

By applying the same technique adopted earlier, we obtain a system of linear equations as follows:

$$K_{1,0}a_{1,0}R_0+\gamma\sum_{n=0}^{N}K_{2,n}\left[A_n-B_n\exp(\mathrm{i}K_{2,n}L)\right]\mathcal{B}_{1,0,n}=K_{1,0}a_{1,0},\tag{3.20a}$$

$$K_{1,m}a_{1,m}R_m+\gamma\sum_{n=0}^{N}K_{2,n}\left[A_n-B_n\exp(\mathrm{i}K_{2,n}L)\right]\mathcal{B}_{1,m,n}=0,\tag{3.20b}$$

$$\alpha_{0,0}R_0+\sum_{n=1}^{N}R_n\alpha_{0,n}-\mathrm{i}R\sum_{n=0}^{N}[A_n+B_n\exp(\mathrm{i}K_{2,n}L)]\mathcal{B}_{1,0,n}=-\alpha_{0,0},\tag{3.20c}$$

$$\alpha_{m,0}R_m+\sum_{n=1}^{N}R_n\alpha_{m,n}-\mathrm{i}R\sum_{n=0}^{N}[A_n+B_n\exp(\mathrm{i}K_{2,n}L)]\mathcal{B}_{1,m,n}=-\alpha_{m,0},\tag{3.20d}$$

and

$$-\mathrm{i}R\sum_{n=0}^{N}[A_n\exp(\mathrm{i}K_{2,n}L)+B_n]\mathcal{B}_{1,0,n}+C_0[1+\exp(2\mathrm{i}K_{3,0}r)]\alpha_{0,0}+\sum_{n=1}^{N}C_n\alpha_{0,n}=0,\tag{3.21a}$$

$$-\mathrm{i}R\sum_{n=0}^{N}[A_n\exp(\mathrm{i}K_{2,n}L)+B_n]\mathcal{B}_{1,m,n}+C_0[1+\exp(2\mathrm{i}K_{3,0}r)]\alpha_{m,0}+\sum_{n=1}^{N}C_n\alpha_{m,n}=0,\tag{3.21b}$$

$$K_{3,0}[1-\exp(2\mathrm{i}K_{3,0}r)]a_{1,0}C_0-\gamma\sum_{n=0}^{N}K_{2,n}\left[A_n\exp(\mathrm{i}K_{2,n}L)-B_n\right]\mathcal{B}_{1,0,n}=0,\tag{3.21c}$$

$$K_{3,m}a_{1,m}T_m-\gamma\sum_{n=0}^{N}K_{2,n}\left[A_n\exp(\mathrm{i}K_{2,n}L)-B_n\right]\mathcal{B}_{1,m,n}=0.\tag{3.21d}$$

A matrix system can be constructed as per our earlier discussion and the related reflection and transmission can be analyzed.

3.4.3 Numerical results

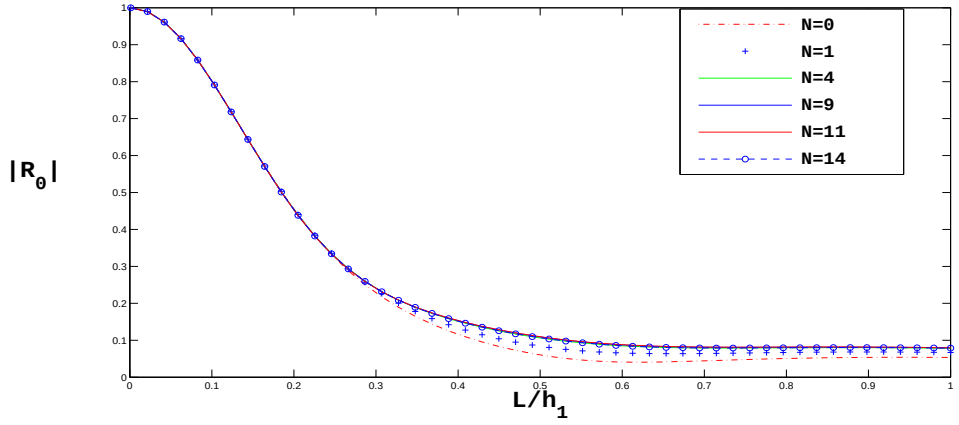

Figure 3.6: Variation of reflection coefficient $|R_0|$ against dimensionless width of porous structure for different numbers of evanescent modes N with $d/h_1 = 1/8$, $r/h_1 = 100$ and $\gamma = 0.9$; vertical wall at a large distance from the structure

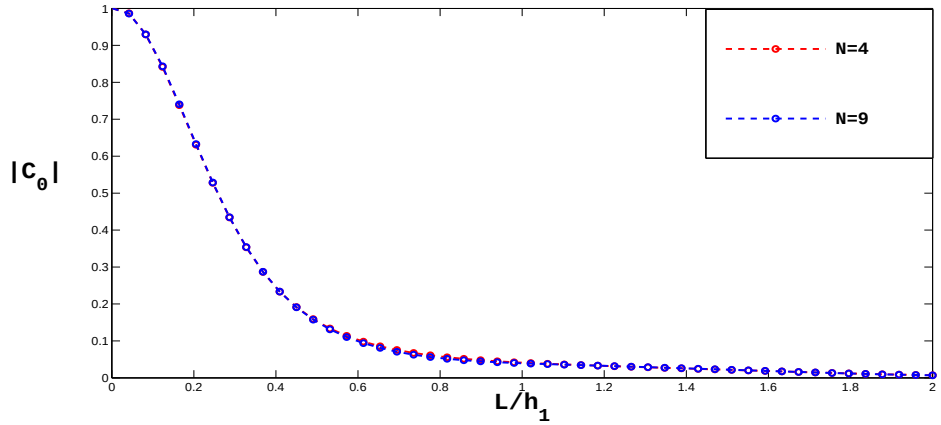

Figure 3.7: Variation of transmission coefficient $|C_0|$ against dimensionless width of porous structure for different numbers of evanescent modes N with $d/h_1 = 1/8$, $r/h_1 = 100$ and $\gamma = 0.9$; vertical wall at a large distance from the structure

Here we consider the wall to be located at a very large distance away from the structure. Reflection coefficient and dimensionless amplitude of the progressive transmitted wave are plotted against the width of the porous structure for different numbers of evanescent modes in figures 3.6 and 3.7 respectively. Here we consider $r = 100h_1$ and $\gamma = 0.9$.

For discussing reflection, we consider different numbers of evanescent modes: $N = 1, 4, 9, 11$ and 14. Figure 3.6 shows that the values of the reflection coefficient $|R_0|$ begin from 1 and

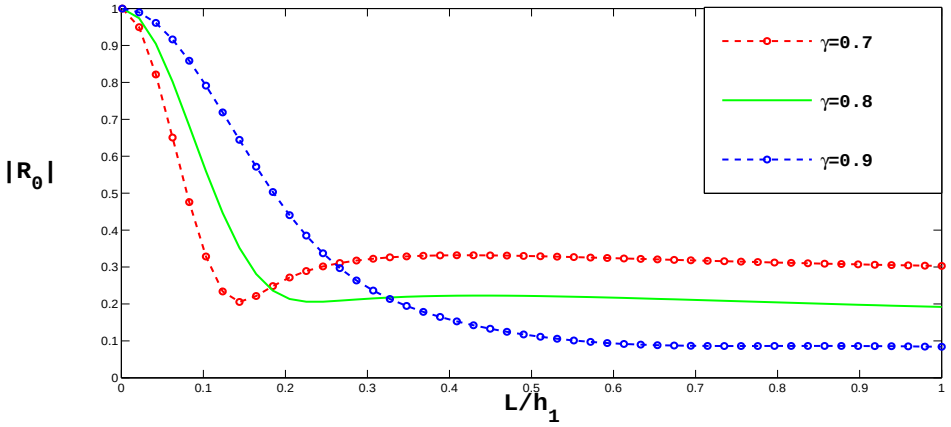

Figure 3.8: Variation of reflection coefficient $|R_0|$ against dimensionless width of porous structure for different porosity γ with $d/h_1 = 1/8$, $r/h_1 = 100$ and $N = 4$; vertical wall at a large distance from the structure

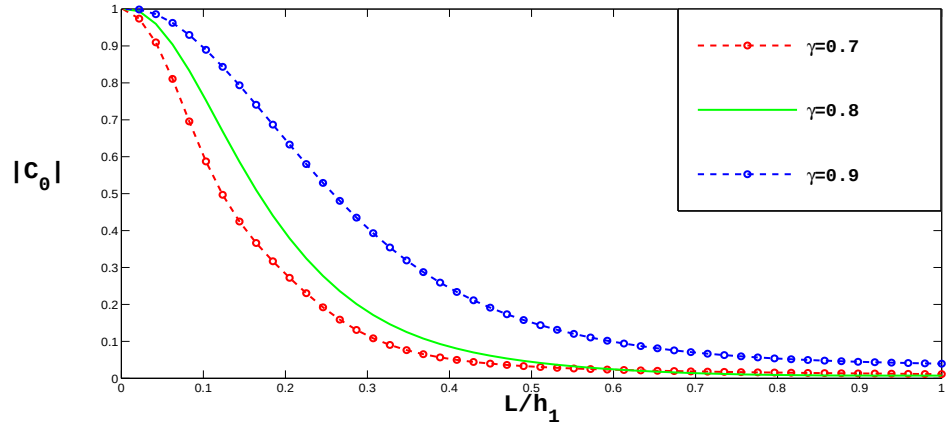

Figure 3.9: Variation of transmission coefficient $|C_0|$ against dimensionless width of porous structure for different porosity γ with $d/h_1 = 1/8$, $r/h_1 = 100$ and $N = 4$; vertical wall at a large distance from the structure

decrease steadily for all numbers of modes as the width of the porous structure is increased. As N, the number of evanescent modes, increases, the corresponding reflection coefficients converge as can be observed from the plots for $N = 9, 11, 14$. Figure 3.7 shows $|C_0|$ for the same set of values. $|C_0|$ decreases steadily as the width of the porous structure is increased and eventually after approximately $L/h_1 = 2.0$, $|C_0|$ vanishes for all numbers of evanescent modes. Also, the values of the coefficient are the same for all the numbers of modes and all L/h_1, and hence we show the plots only for $N = 4, 9$ for clear viewing.

Now we study the effect of porosity γ on reflection coefficient and dimensionless amplitude

of the progressive transmitted wave against the width of the porous structure. Here we consider $N = 10$. Figure 3.8 illustrates more or less the same effects as was observed in figure 3.3 except that the magnitude of oscillation is less in this case. Similarly from figure 3.9 we study $|C_0|$ for the same set of values, which shows that $|C_0|$ decreases as the width of the porous structure increases and finally vanishes after an approximate dimensionless width 1.0 of the porous structure. It is also observed that higher porosity gives rise to higher values of $|C_0|$.

3.5 Energy loss

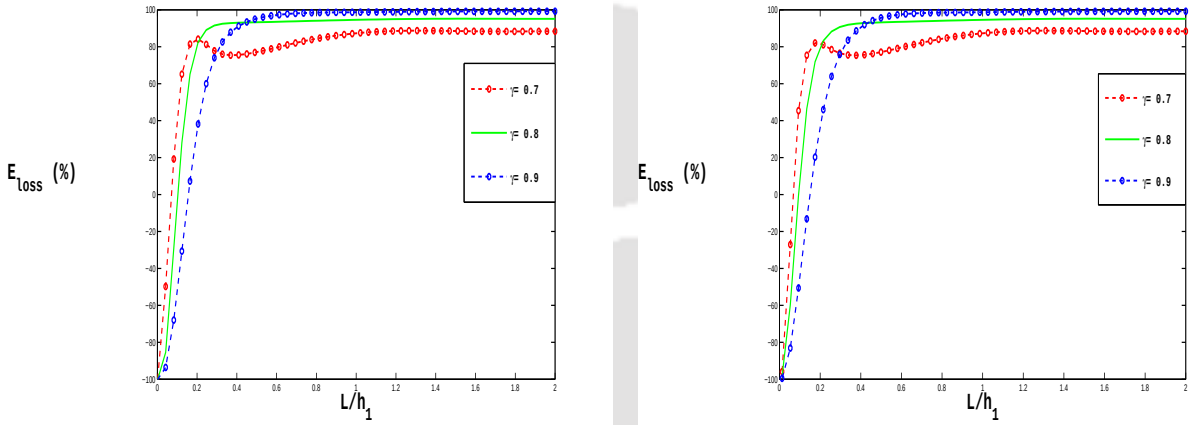

(a) vertical wall placed nearer to the structure ($r/h_1 = 10$) (b) vertical wall at a large distance from the structure ($r/h_1 = 100$)

Figure 3.10: Energy loss (%) against dimensionless width of porous structure for different porosity γ with $d/h_1 = 1/8$

In this section we discuss the effect of the width of the porous structure on energy loss in percent. Figures 3.10 and 3.11 depict the scenario for all the relevant parameters.

Figures 3.10(a) and 3.10(b), respectively, show the energy loss for different values of porosity when the rigid wall is near the structure and at a large distance. Here we consider $N = 9$. Figures 3.11(a) and 3.11(b) show the energy loss for different values of evanescent modes when the wall is near the structure and at a large distance, respectively. Here we consider $\gamma = 0.9$. From figures 3.10 and 3.11, we observe that when the width of the porous structure is zero, i.e., no porous structure is present, the amplitude of the incident wave is same as the amplitude of the transmitted wave in region III and hence $|C_0| = 1$. Therefore, we observe that the left propagating mode arising from the solid wall placed at $x = L$ has the same magnitude, i.e., $|D_0| = 1$. This left propagating mode is responsible for reflection taking place (virtually) at

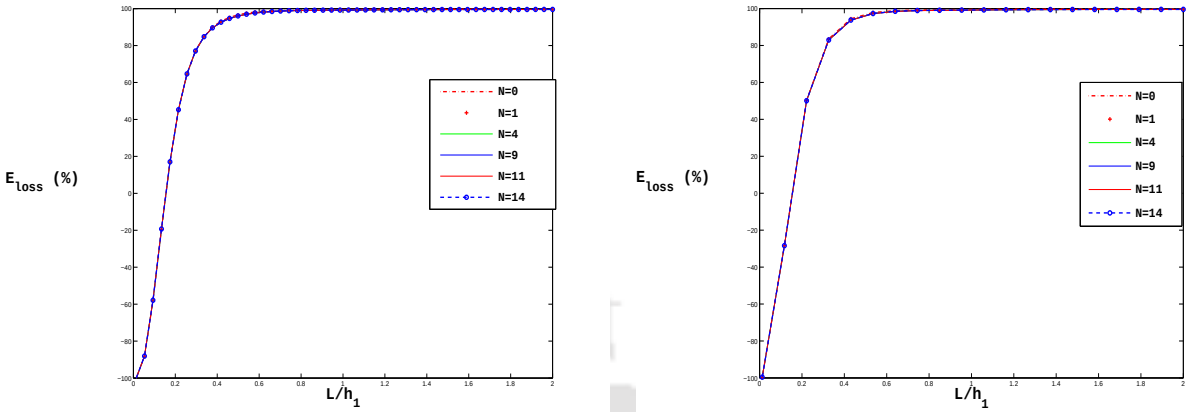

(a) vertical wall placed nearer to the structure ($r/h_1 = 10$) (b) vertical wall at a large distance from the structure ($r/h_1 = 100$)

Figure 3.11: Energy loss (%) against dimensionless width of porous structure for different numbers of evanescent modes N with $d/h_1 = 1/8$, and $\gamma = 0.9$

$x = 0$. Therefore $|R_0| = 1$ in this case resulting (from equation (3.9)) in the following:

$$E_{\text{loss}} = (1 - 1 - 1) \times 100\% = -100\%.$$

But as the width of the porous structure increases, damping starts taking place and energy loss increases very rapidly before it attains a fixed value. We observe from figure 3.10 that except for the case when the porous structure is thin, higher porosity value results in more energy loss irrespective of whether the wall is near the structure or at a large distance. Figure 3.11 shows an interesting observation that the energy loss is same for all numbers of modes considered and is independent of the positioning of the wall.

3.6 Conclusion

Based on linear water wave theory, we examine the reflection coefficient and the dimensionless amplitude of the transmitted wave for water waves reflected and transmitted by a porous structure placed on a raised horizontal bottom and at some distance from a rigid vertical wall. Consequently three regions – (i) an infinite fluid domain, (ii) a finite porous structure and (iii) a finite fluid region (a small horizontal extent and also a very large horizontal extent as two separate cases) are considered. Boundary value problems are set up in each of these regions. Using the matching conditions and the resultant system of equations, we derive the reflection

coefficient $|R_0|$ and and the dimensionless amplitude $|C_0|$ of the transmitted wave. Noting that the friction factor f depends on the porosity γ, we use Lorentz principle of virtual work in finding f the values of which are used throughout in our calculation. Two different cases are considered separately to study the reflection and transmission phenomena, namely, the rigid vertical wall placed near the porous structure and again placed at a very large from it.

It is observed that when the rigid wall is placed nearer to the structure, reflection coefficient $|R_0|$, for different numbers of evanescent modes, decreases rapidly for a thin width of the porous structure and converges for higher numbers of evanescent modes. The dimensionless amplitude $|C_0|$ of the transmitted wave also decreases with an increase in the width of the porous structure and vanishes after $L/h_1 = 2.0$ approximately. For a thin width of the porous structure and lower porosity values, $|R_0|$ shows some oscillations which do not exist for higher porosity values and also when the width of the structure increases. We also find that higher values of porosity results in lower $|R_0|$ after the disappearance of the oscillations. Higher porosity values give rise to higher values of $|C_0|$ which decrease rapidly as the structure width is increased and they ultimately vanish.

For the case when the wall is placed at a very large distance away from the structure, the overall observation is more or less the same with the case when the wall is nearer to the structure.

Moreover, we study energy loss due to the presence of the porous structure for different values of number of modes and porosity. For both the cases of wall placed near the structure and far away from the structure, energy loss curves for different numbers of modes and porosity exhibit similar features. Higher porosity results in higher energy loss, except for a thin porous structure, and energy loss is same for all numbers of modes considered.

Chapter 4

Reflection of oblique water waves by a vertical porous structure placed on a multi-step impermeable bottom

In this chapter, the water wave scattering problem due to the presence of a vertical porous structure, placed on a 2-step or a p-step horizontal bottom and supported by a rigid vertical wall at one end, is solved by using linear water wave theory. The reflection characteristics are investigated for different relevant parameters. First we discuss the problem related to a 2-step bottom.

4.1 Mathematical formulation

Let us consider a vertical porous structure of width $L+D$ placed on a 2-step bottom topography above the horizontal ocean bottom, which is at a constant depth h_1 from the free surface, and resting against a rigid vertical wall. Using Cartesian coordinate system (x, y, z), the positive x-direction is defined as the direction of the normal wave incident on the porous structure at $x = 0$, the positive z-direction is considered vertically upwards and the mean free surface as $z = 0$. Due to the 2-step bottom topography under the porous structure, two different heights of the porous structure exist, namely, h_2 when $0 < x < L$ and h_3 when $L < x < L + D$. The water region $(-\infty < x < 0, -h_1 < z < 0)$ is labeled as region I, the porous structure above the first step $(0 < x < L, -h_2 < z < 0)$ and above the second step

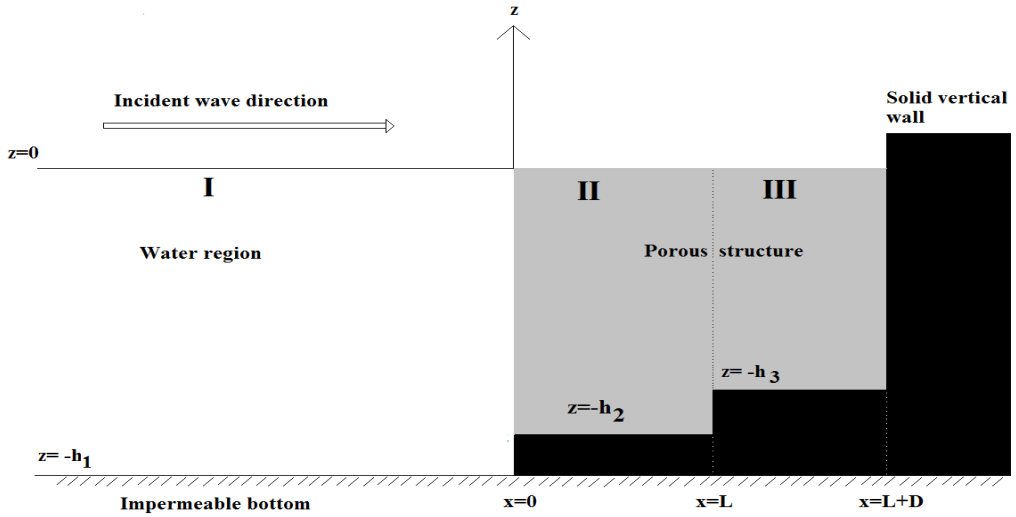

Figure 4.1: Schematic diagram of the problem with a 2-step bottom

($L < x < L + D$, $-h_3 < z < 0$) as region II and region III, respectively (figure 4.1). The horizontal bottom for region I is at $z = -h_1$. After propagating through the porous structure, the incident wave gets reflected by the vertical wall at $x = L + D$. The fluid is assumed to be incompressible, homogeneous and inviscid, and the motion irrotational. We define three velocity potentials $\Phi_1(x, y, z, t) = \phi_1(x, z) \exp(\mathrm{i}ly - \mathrm{i}\omega t)$, $\Phi_2(x, y, z, t) = \phi_2(x, z) \exp(\mathrm{i}ly - \mathrm{i}\omega t)$ and $\Phi_3(x, y, z, t) = \phi_3(x, z) \exp(\mathrm{i}ly - \mathrm{i}\omega t)$ in region I, region II and region III, respectively.

The governing equation and the boundary conditions in region I are

$$\nabla^2\phi_1 - l^2\phi_1 = 0; \quad -\infty < x < 0, \quad -h_1 < z < 0, \tag{4.1a}$$

$$\frac{\partial\phi_1}{\partial z} - \nu\phi_1 = 0; \quad -\infty < x < 0, \quad z = 0, \tag{4.1b}$$

$$\frac{\partial\phi_1}{\partial z} = 0; \quad -\infty < x < 0, \quad z = -h_1, \tag{4.1c}$$

$$\frac{\partial\phi_1}{\partial x} = 0; \quad x = 0, \quad -h_1 < z < -h_2. \tag{4.1d}$$

The governing equation and the boundary conditions in region II are

$$\nabla^2\phi_2 - l^2\phi_2 = 0; \quad 0 < x < L, \quad -h_2 < z < 0, \tag{4.2a}$$

$$\frac{\partial\phi_2}{\partial z} - \mathrm{i}\nu R\phi_2 = 0; \quad 0 < x < L, \quad z = 0, \tag{4.2b}$$

$$\frac{\partial \phi_2}{\partial z} = 0; \qquad 0 < x < L, \qquad z = -h_2, \tag{4.2c}$$

$$\frac{\partial \phi_2}{\partial x} = 0; \qquad x = L, \qquad -h_2 < z < -h_3. \tag{4.2d}$$

The governing equation and the boundary conditions in region III are

$$\boldsymbol{\nabla}^2 \phi_3 - l^2 \phi_3 = 0; \qquad L < x < L + D, \qquad -h_3 < z < 0, \tag{4.3a}$$

$$\frac{\partial \phi_3}{\partial z} - \mathrm{i}\nu R \phi_3 = 0; \qquad L < x < L + D, \qquad z = 0, \tag{4.3b}$$

$$\frac{\partial \phi_3}{\partial z} = 0; \qquad L < x < L + D, \qquad z = -h_3, \tag{4.3c}$$

$$\frac{\partial \phi_3}{\partial x} = 0; \qquad x = L + D, \qquad -h_3 < z < 0. \tag{4.3d}$$

The matching conditions along the vertical boundaries $x = 0$ and $x = L$ are given by

$$\phi_1 = \mathrm{i}R\phi_2; \qquad x = 0, \qquad -h_2 \le z \le 0, \tag{4.4a}$$

$$\frac{\partial \phi_1}{\partial x} = \gamma \frac{\partial \phi_2}{\partial x}; \qquad x = 0, \qquad -h_2 \le z \le 0, \tag{4.4b}$$

$$\phi_2 = \phi_3; \qquad x = L, \qquad -h_3 \le z \le 0, \tag{4.4c}$$

$$\frac{\partial \phi_2}{\partial x} = \frac{\partial \phi_3}{\partial x}; \qquad x = L, \qquad -h_3 \le z \le 0. \tag{4.4d}$$

4.2 Reflection by the porous structure

The velocity potential $\phi_1(x, z)$ in region I is given by the following form after truncating n at $n = N$:

$$\phi_1(x, z) = [\exp(\mathrm{i}K_{1,0}x) + R_0 \exp(-\mathrm{i}K_{1,0}x)]Z_{1,0}(h_1, z) + \sum_{n=1}^{N} R_n \exp(-\mathrm{i}K_{1,n}x)Z_{1,n}(h_1, z), \tag{4.5}$$

where the depth-dependent function $Z_{1,n}(h_1, z)$ and $K_{1,n}$ are same as defined in Chapter 3.

In region II, the horizontal impermeable bottom is considered at $z = -h_2$. Hence, the integrals in this porous region must be from $z = -h_2$ to $z = 0$ in order to meet the matching conditions and it is required that we compute the relevant integrals from $z = -h_2$ to $z = 0$. By using separation of variables method, the velocity potential $\phi_2(x, z)$, after truncating the

infinite sum at $n = N$, can be written as

$$\phi_2(x,z) = \sum_{n=0}^{N} \{A_{2,n} \exp(\mathrm{i}K_{2,n}x) + B_{2,n} \exp[-\mathrm{i}K_{2,n}(x-L)]\} Z_{2,n}(h_2,z), \tag{4.6}$$

where $A_{2,n}$ and $B_{2,n}$ are arbitrary constants; $K_{2,n} = (k_{2,n}^2 - l^2)^{1/2}$ with $k_{2,n}$ satisfying the dispersion relation

$$\mathrm{i}R\nu = k_{2,n} \tanh k_{2,n} h_2, \tag{4.7a}$$

and $Z_{2,n}(h_2,z)$ is the depth-dependent function given by

$$Z_{2,n}(h_2,z) = \frac{\cosh k_{2,n}(h_2+z)}{\cosh k_{2,n} h_2}, \quad n = 0,1,2,\cdots,N. \tag{4.7b}$$

In region III, the horizontal impermeable bottom is considered at $z = -h_3$. Hence, the integrals in the porous region must be from $z = -h_3$ to $z = 0$ in order to meet the matching conditions and it is required that we compute the relevant integrals from $z = -h_3$ to $z = 0$. The velocity potential $\phi_3(x,z)$, after truncating the infinite sum at $n = N$, can be written as

$$\phi_3(x,z) = \sum_{n=0}^{N} \{C_{3,n} \cos[K_{3,n}(x-L-D)]\} Z_{3,n}(h_3,z), \tag{4.8}$$

where $C_{3,n}$ are arbitrary constants; $K_{3,n} = (k_{3,n}^2 - l^2)^{1/2}$ with $k_{3,n}$ satisfying the dispersion relation

$$\mathrm{i}R\nu = k_{3,n} \tanh k_{3,n} h_3, \tag{4.9a}$$

and $Z_{3,n}(h_3,z)$ is the depth-dependent function given by

$$Z_{3,n}(h_3,z) = \frac{\cosh k_{3,n}(h_3+z)}{\cosh k_{3,n} h_3}, \quad n = 0,1,2,\cdots,N. \tag{4.9b}$$

Using the matching conditions (4.4a–d), the following equations in $(4N+4)$ unknowns $R_n, A_{2,n}, B_{2,n}, C_{2,n}$ $(n = 0,1,\ldots,N)$ are obtained:

$$(1+R_0)Z_{1,0} + \sum_{n=1}^{N} R_n Z_{1,n} = \mathrm{i}R \sum_{n=0}^{N} [A_{2,n} + B_{2,n} \exp(\mathrm{i}K_{2,n}L)] Z_{2,n}, \tag{4.10a}$$

$$K_{1,0}(1-R_0)Z_{1,0} - \sum_{n=1}^{N} K_{1,n} R_n Z_{1,n} = \gamma \sum_{n=0}^{N} [A_{2,n} - B_{2,n} \exp(\mathrm{i}K_{2,n}L)] K_{2,n} Z_{2,n}, \tag{4.10b}$$

$$\sum_{n=0}^{N}[A_{2,n}\exp(\mathrm{i}K_{2,n}L)+B_{2,n}]Z_{2,n} = \sum_{n=0}^{N}C_{3,n}\cos(K_{3,n}D)Z_{3,n}, \tag{4.10c}$$

$$\sum_{n=0}^{N}\mathrm{i}K_{2,n}[A_{2,n}\exp(\mathrm{i}K_{2,n}L)-B_{2,n}]Z_{2,n} = \sum_{n=0}^{N}K_{3,n}C_{3,n}\sin(K_{3,n}D)Z_{3,n}. \tag{4.10d}$$

By using the orthogonality property of $Z_{2,m}(h_2,z)$ and $Z_{3,m}(h_3,z)$ (for all $m=0,1,\ldots,N$) in equations (4.10a,b) and (4.10c,d), respectively, the above equations reduce to

$$\sum_{n=0}^{N}\mathcal{B}_{1,n,m}R_n-\mathrm{i}Ra_{2,m}A_{2,m}-\mathrm{i}R\exp(\mathrm{i}K_{2,m}L)a_{2,m}B_{2,m}=-\mathcal{B}_{1,0,m}, \tag{4.11a}$$

$$\sum_{n=0}^{N}\mathcal{B}_{1,n,m}K_{1,n}R_n+\gamma K_{2,m}a_{2,m}A_{2,m}-\gamma K_{2,m}\exp(\mathrm{i}K_{2,m}L)a_{2,m}B_{2,m}=K_{1,0}\mathcal{B}_{1,0,m}, \tag{4.11b}$$

$$\sum_{n=0}^{N}\exp(\mathrm{i}K_{2,n}L)\mathcal{B}_{1,n,m}A_{2,n}+\sum_{n=0}^{N}\mathcal{B}_{1,n,m}B_{2,n}-\cos K_{3,m}(D)a_{3,m}C_{3,m}=0, \tag{4.11c}$$

$$\sum_{n=0}^{N}\mathrm{i}K_{2,n}\exp(\mathrm{i}K_{2,n}L)\mathcal{B}_{1,n,m}A_{2,n}+\sum_{n=0}^{N}\mathrm{i}K_{2,n}\mathcal{B}_{1,n,m}B_{2,n}-K_{3,m}\sin K_{3,m}(D)a_{3,m}C_{3,m}=0, \tag{4.11d}$$

where

$$a_{q,m} = \int_{-h_q}^{0}Z_{q,m}^2dz=\frac{h_q\tanh K_{q,m}h_q}{2K_{q,m}h_q}\left(1+\frac{2K_{q,m}h_q}{\sinh 2K_{q,m}h_q}\right),\quad q=1,2,\ldots,p+2,$$

$$\mathcal{B}_{q,n,m} = \int_{-h_{q+1}}^{0}Z_{q,n}Z_{q+1,m}dz=\begin{cases}\dfrac{1}{K_{1,n}^2-K_{2,m}^2}\left[\nu(1-\mathrm{i}R)-\dfrac{K_{1,n}\sinh K_{1,n}(h_2-h_1)}{\cosh K_{1,n}h_1\cosh K_{2,m}h_2}\right] & \text{when } q=1,\\ \dfrac{1}{K_{2,n}^2-K_{3,m}^2}\left[-\dfrac{K_{2,n}\sinh K_{2,n}(h_3-h_2)}{\cosh K_{2,n}h_2\cosh K_{3,m}h_3}\right] & \text{when } q=2.\end{cases}$$

From equations (4.11a–d) a system of linear equations with $(4N+4)$ equations in $(4N+4)$ unknowns can be constructed as follows:

$$\boldsymbol{MX}=\boldsymbol{b},$$

where $\boldsymbol{M}$ is a square matrix of size $(4N+4)$,

$$\boldsymbol{X} = [R_0, R_1, \ldots R_N, A_{2,0}, A_{2,1}, \ldots A_{2,N}, B_{2,0}, B_{2,1}, \ldots B_{2,N}, C_{3,0}, C_{3,1}, \ldots C_{3,N}]^T$$

is the unknown vector,

and $$\boldsymbol{b} = [-\mathcal{B}_{1,0,0}, -\mathcal{B}_{1,0,1}, \ldots -\mathcal{B}_{1,0,N}, K_{1,0}\mathcal{B}_{1,0,0}, K_{1,0}\mathcal{B}_{1,0,1}, \ldots K_{1,0}\mathcal{B}_{1,0,N}, \underbrace{0, \ldots\ldots\ldots 0}_{(2N+2)\text{ times}}]^T.$$

By solving this system, $|R_0|$ can be evaluated and subsequently the reflection phenomenon within the porous structure can be discussed.

4.3 Numerical results for reflection

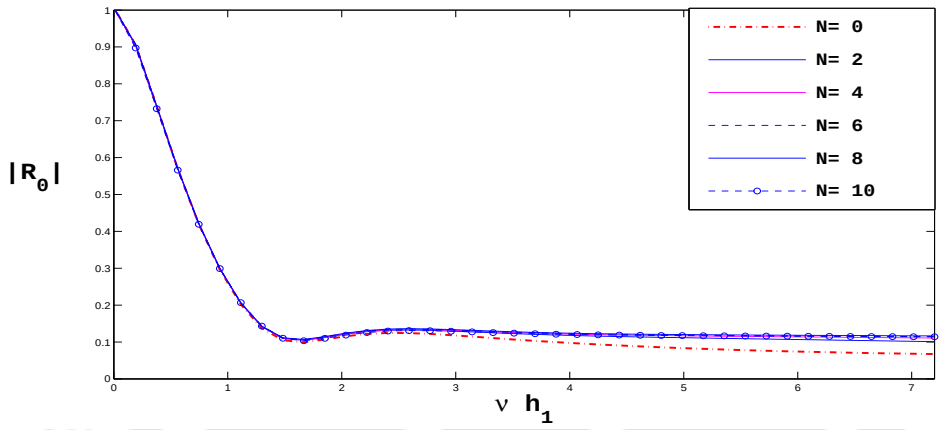

Figure 4.2: Variation of $|R_0|$ against νh_1 for different numbers of evanescent modes N with $f = 1$, $(L + D)/h_1 = 1$, $\theta = 0^0$ and $\gamma = 0.9$

It is to be noted that unlike in Chapters 2 and 3, from now onwards, we consider only fixed values of friction factor f. This is due to the fact that from an application point of view, consideration of a fixed value of f is more appropriate, as supported by a large number of previous works (e.g., Zhu (2001), Twu and Liu (1994)). For computational purpose, some specific values of the parameters are considered: $L/h_1 = 0.5$; $D/h_1 = 0.5$; $D/L = 1$; $f = 1$; $S = 1$; $\gamma = 0.7, 0.8$ and 0.9; $h_1 - h_2 = h_2 - h_3 = h_1/16$; $\theta = 0^0$ and $\nu h_1 = 2$.

First we investigate the effect of the number of evanescent modes on the reflection coefficient $|R_0|$ against wave numbers νh_1. The ratio $(L + D)/h_1 = 1$ is maintained throughout and the values $N = 0, 2, 4, \ldots, 10$ are considered. From figure 4.2, it is observed that up to approximately $\nu h_1 < 2.4$, reflection can be described by the propagating mode $(N = 0)$ only. As the wave number increases, i.e., for short waves, it is evident that the number of evanescent

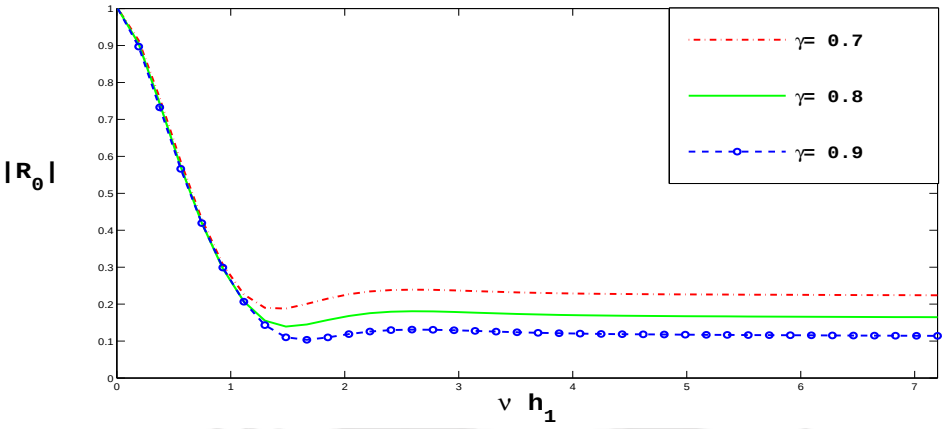

Figure 4.3: Variation of $|R_0|$ against νh_1 for different γ with $(L+D)/h_1 = 1$, $f = 1$, $\theta = 0^0$ and $N = 9$

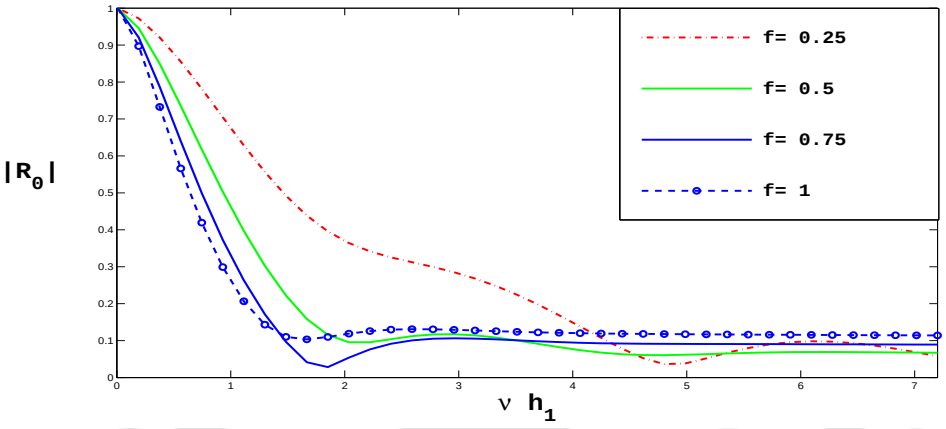

Figure 4.4: Variation of $|R_0|$ against νh_1 for different f with $(L+D)/h_1 = 1$, $\gamma = 0.9$, $\theta = 0^0$ and $N = 9$

modes starts affecting $|R_0|$ but it converges to a fixed value for higher numbers of evanescent modes.

Porosity of the structure plays an important role in the reflection characteristics. Figure 4.3 shows that for relatively long waves ($\nu h_1 < 1$), porosity does not affect reflection, but as the value of the wave number increases, the values of $|R_0|$, corresponding to the highest value of porosity considered ($\gamma = 0.9$), are considerably low. In other words, as the porosity reduces, higher reflection coefficient is encountered.

The effect of the friction factor f on the reflection coefficient is studied for various wave numbers. Figure 4.4 shows oscillation of $|R_0|$ for lower values of the friction factors considered.

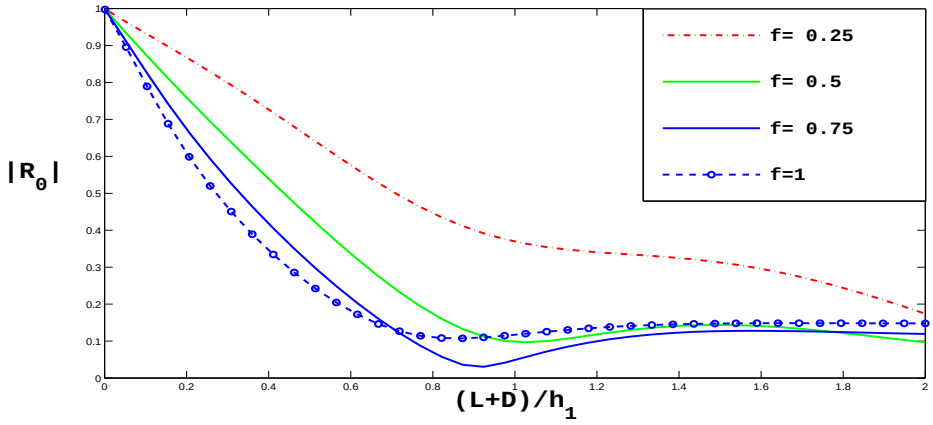

Figure 4.5: Variation of $|R_0|$ against dimensionless width of the porous structure $(L+D)/h_1$ for different f with $\gamma = 0.9$, $\theta = 0^0$ and $N = 9$

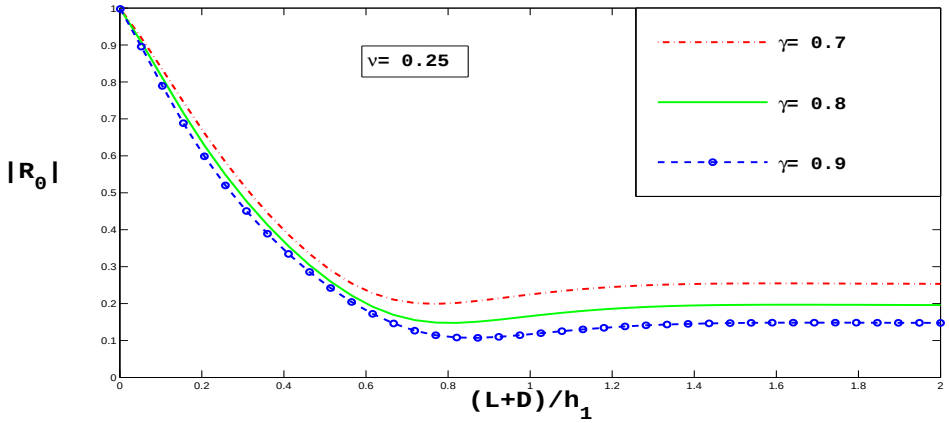

Figure 4.6: Variation of $|R_0|$ against dimensionless width of the porous structure $(L+D)/h_1$ for different γ with $f = 1$, $\theta = 0^0$ and $N = 9$

As the value of f increases, the oscillation vanishes.

Further, figure 4.5 illustrates the effect of friction factor on the reflection coefficient for various dimensionless width $(L+D)/h_1$ of the porous structure. Lower values of f result in oscillation in $|R_0|$ which vanishes with an increase in the value of the friction factor (here, for $f = 1$).

We also study the effect of the dimensionless width of the porous structure on reflection. In figure 4.6, $|R_0|$ is plotted against the dimensionless width of the porous structure for different values of porosity. Reflection coefficient decreases with an increase in $(L+D)/h_1$ before attaining a fixed value for each of the porosity values considered. It is also observed that

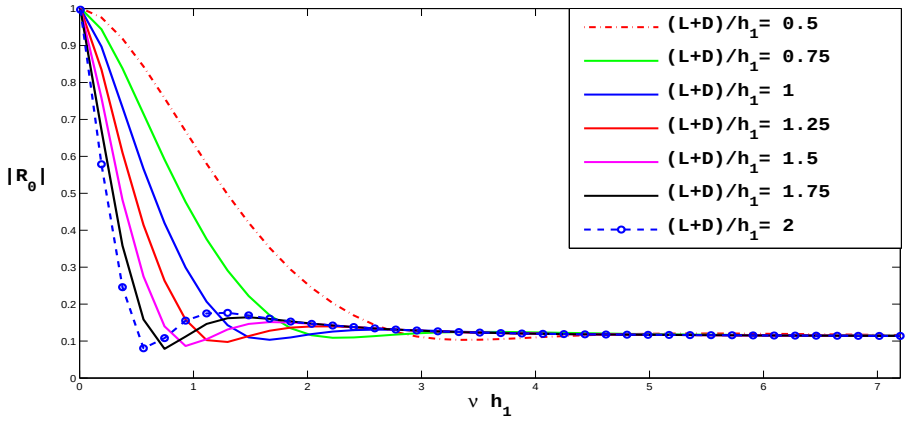

Figure 4.7: Variation of $|R_0|$ against νh_1 for different width of the porous structure $(L+D)/h_1$ with $f = 1$, $\gamma = 0.9$, $\theta = 0^0$ and $N = 9$

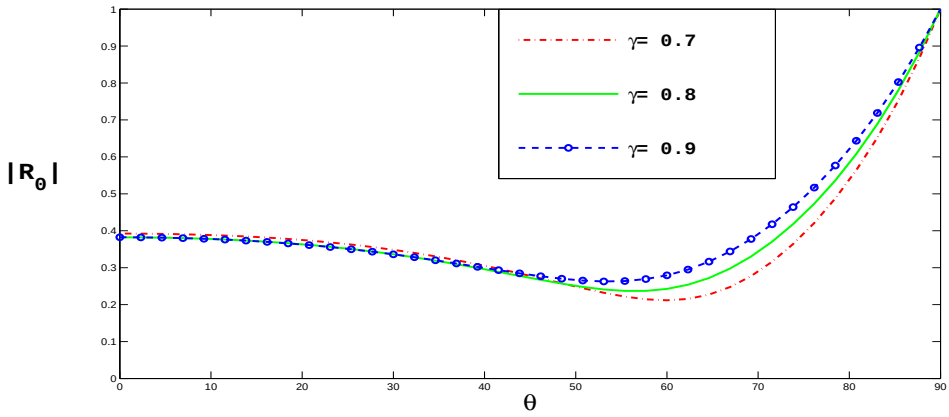

Figure 4.8: Variation of $|R_0|$ against incident wave angle θ for different γ with $(L+D)/h_1 = 1$, $f = 1$ and $N = 9$

higher porosity results in lower reflection coefficient.

Figure 4.7 illustrates the effect of wave number on the reflection coefficient for different values of width $(L + D)/h_1$. It is observed that oscillation in $|R_0|$ exists for lower values of width and it disappears with an increase in width before converging to each other.

Figure 4.8 shows the variation of $|R_0|$ against angle of incidence θ for different values of porosity. It is observed that, for $\theta < 45^0$, $|R_0|$ is more or less the same for different porosity values. But for higher values of θ $(> 45^0)$, $|R_0|$ attains its minimum value for lower value of porosity (here for $\gamma = 0.7$) and then starts increasing before converging to each other.

We further study the effect of wave number on reflection for different angles of incidence θ.

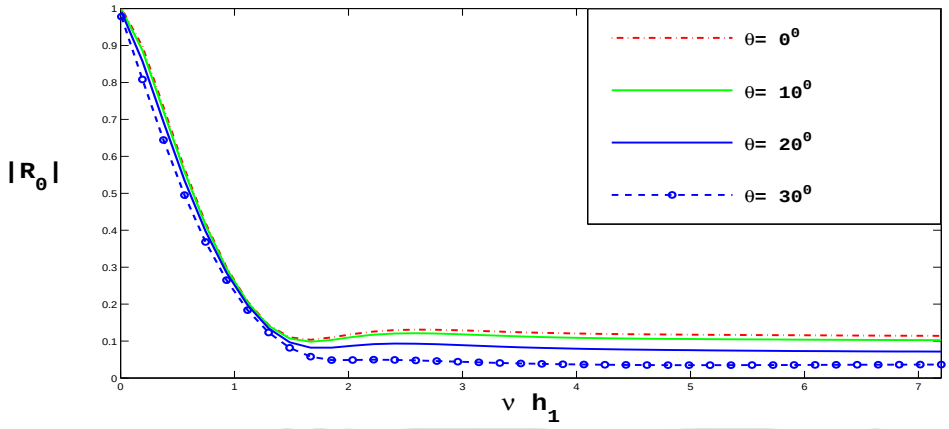

Figure 4.9: Variation of $|R_0|$ against νh_1 for different incident wave angle θ with $(L+D)/h_1 = 1$, $f = 1$, $\gamma = 0.9$ and $N = 9$

Four different values of θ, namely $\theta = 0^0, 10^0, 20^0$ and 30^0, are considered. It is observed from figure 4.9 that for relatively long waves ($\nu h_1 < 1.5$), $|R_0|$ is same for all angles of incidence considered and as the wave number increases further, higher θ gives rise to lower reflection coefficient.

4.4 Scattering by a p-step bottom

4.4.1 Formulation

Here we consider p number of horizontal steps, in place of 2 steps, to represent the uneven bottom topography under the porous structure (figure 4.10). h_{j+1} $(j = 2, 3, \ldots, p+1)$ is considered to be the height of the porous structure above the j-th horizontal step and a velocity potential $\Phi_j(x, y, z, t) = \phi_j(x, z) \exp(\mathrm{i}ly - \mathrm{i}\omega t)$ is defined in the region $x_{j-1} < x < x_j$, $-h_j < z < 0$ for each j where

$$x_1 = 0 < x_2 < \ldots < x_{p+1} = L \qquad \text{with} \qquad x_j - x_{j-1} = l_0.$$

The boundary value problem in the water region is given by equations (4.1a–d) – exactly the same as the 2-step case. The governing equation and the boundary conditions in the j-th $(j = 2, 3, \ldots, p)$ region, which is porous, are

$$\boldsymbol{\nabla}^2\phi_j - l^2\phi_j = 0\,; \qquad x_{j-1} < x < x_j, \qquad -h_j < z < 0, \tag{4.12a}$$

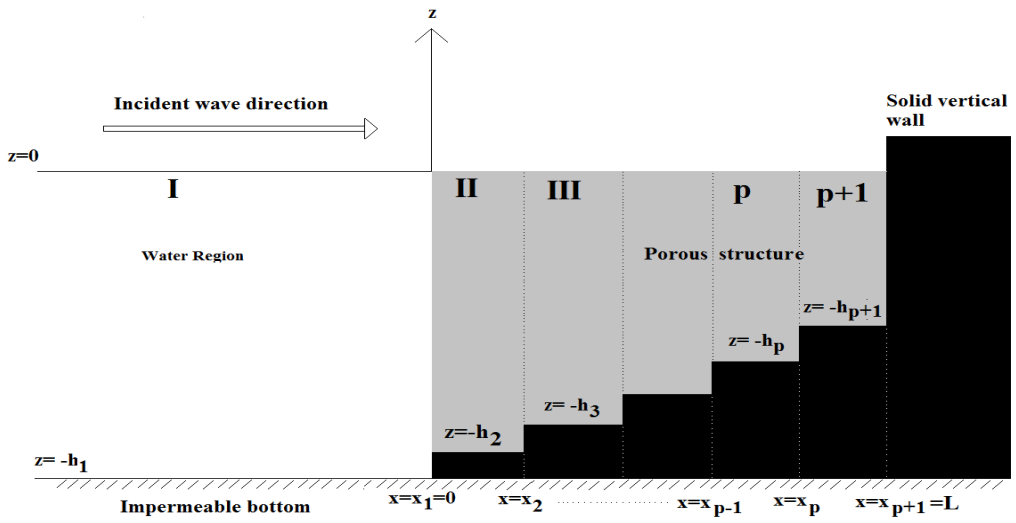

Figure 4.10: Schematic diagram of the problem with a p-step bottom

$$\frac{\partial \phi_j}{\partial z} - \mathrm{i}\nu R\phi_j = 0\,; \qquad x_{j-1} < x < x_j, \qquad z = 0, \tag{4.12b}$$

$$\frac{\partial \phi_j}{\partial z} = 0\,; \qquad x_{j-1} < x < x_j, \qquad z = -h_j, \tag{4.12c}$$

$$\frac{\partial \phi_j}{\partial x} = 0\,; \qquad x = x_j, \qquad -h_j < z < -h_{j+1}. \tag{4.12d}$$

The velocity potential ϕ_{p+1} satisfies equations (4.12a–c) along with one extra condition

$$\frac{\partial \phi_{p+1}}{\partial x} = 0; \qquad x = x_{p+1} = L, \qquad -h_{p+1} < z < 0. \tag{4.13}$$

The matching conditions along the boundary $x = x_1 = 0$, $-h_2 \le z \le 0$, are given by

$$\phi_1 = \mathrm{i}R\phi_2, \tag{4.14a}$$

$$\frac{\partial \phi_1}{\partial x} = \gamma \frac{\partial \phi_2}{\partial x}. \tag{4.14b}$$

The matching conditions along the boundary $x = x_j$, $-h_{j+1} \le z \le 0$ $(j = 2, 3, \ldots p)$, are given by

$$\phi_j = \phi_{j+1}, \tag{4.15a}$$

$$\frac{\partial \phi_j}{\partial x} = \frac{\partial \phi_{j+1}}{\partial x}. \tag{4.15b}$$

4.4.2 Solution

Potential function ϕ_1, depth dependent function $Z_{1,n}(h_1, z)$ and $K_{1,n}$ in region I satisfy equations (2.6) and (2.5a,b), respectively.

Potential function $\phi_j(x, z)$ in the j-th region is given by

$$\phi_j(x,z) = \begin{cases} \sum_{n=0}^{N} \{A_{j,n} \exp\left[\mathrm{i}K_{j,n}(x - x_{j-1})\right] \\ \qquad + B_{j,n} \exp\left[-\mathrm{i}K_{j,n}(x - x_j)\right]\} Z_{j,n}(h_j, z), & j = 2, 3, \ldots, p, \\ \sum_{n=0}^{N} C_{p+1,n} \cos\left[K_{p+1,n}(x - L)\right] Z_{p+1,n}(h_{p+1}, z), & j = p+1, \end{cases} \tag{4.16}$$

where $A_{j,n}$, $B_{j,n}$ and $C_{p+1,n}$ are arbitrary constants; $K_{j,n} = (k_{j,n}^2 - l^2)^{1/2}$ with $k_{j,n}$ satisfying the dispersion relation

$$\mathrm{i}R\nu = k_{j,n} \tanh k_{j,n} h_j, \tag{4.17a}$$

and $Z_{j,n}(h_j, z)$ is the depth-dependent function in region j given by

$$Z_{j,n}(h_j, z) = \frac{\cosh k_{j,n}(h_j + z)}{\cosh k_{j,n} h_j}, \quad j = 2, 3, \cdots, p+1. \tag{4.17b}$$

Now using the matching conditions (4.14a–d) along the boundary $x = x_j$, $-h_j \le z \le 0$ $(j = 1, 2, \ldots, p-1)$, the following equations are obtained:

$$(1 + R_0) Z_{1,0} + \sum_{n=1}^{N} R_n Z_{1,n} = \mathrm{i}R \sum_{n=0}^{N} [A_{2,n} + B_{2,n} \exp(\mathrm{i}K_{2,n} l)] Z_{2,n}, \tag{4.18a}$$

$$K_{1,0}(1 - R_0) Z_{1,0} - \sum_{n=1}^{N} K_{1,n} R_n Z_{1,n} = \gamma \sum_{n=0}^{N} [A_{2,n} - B_{2,n} \exp(\mathrm{i}K_{2,n} l)] K_{2,n} Z_{2,n}, \tag{4.18b}$$

$$\sum_{n=0}^{N} [A_{j,n} \exp(\mathrm{i}K_{j,n} l) + B_{j,n}] Z_{j,n} = \sum_{n=0}^{N} [A_{j+1,n} + B_{j+1,n} \exp(\mathrm{i}K_{j+1,n} l)] Z_{j+1,n}, \tag{4.18c}$$

$$\sum_{n=0}^{N} [A_{j,n} \exp(\mathrm{i}K_{j,n} l) - B_{j,n}] K_{j,n} Z_{j,n} = \sum_{n=0}^{N} [A_{j+1,n} - B_{j+1,n} \exp(\mathrm{i}K_{j+1,n} l)] K_{j+1,n} Z_{j+1,n}. \tag{4.18d}$$

Since the analytical expression for the potential function $\phi_{p+1}(x, z)$ is different from other

potential functions $\phi_j(x,z)$ $(j=1,2,\dots p)$, applying the matching conditions (4.15a–d) along the boundary $x=x_p$ separately, the following equations are obtained :

$$\sum_{n=0}^{N}[A_{p,n}\exp(\mathrm{i}K_{p,n}l)+B_{p,n}]Z_{p,n} = \sum_{n=0}^{N}C_{p+1,n}\cos(K_{p+1,n}l)Z_{p+1,n}(h_{p+1},z), \quad (4.18e)$$

$$\mathrm{i}\sum_{n=0}^{N}[A_{p,n}\exp(\mathrm{i}K_{p,n}l)-B_{p,n}]K_{p,n}Z_{p,n} = \sum_{n=0}^{N}C_{p+1,n}\sin(K_{p+1,n}l)K_{p+1,n}Z_{p+1,n}(h_{p+1},z). \quad (4.18f)$$

Further, using the orthogonality property of $Z_{2,m}$, $Z_{j+1,m}$ $(j=2,3,\dots,p-1)$ and $Z_{p+1,m}$, for each $m=0,1,\dots,N$, in equations (4.18a,b), (4.18c,d) and (4.18e,f), respectively, it follows

$$\sum_{n=0}^{N}\mathcal{B}_{1,n,m}R_n-\mathrm{i}Ra_{2,m}A_{2,m}-\mathrm{i}R\exp(\mathrm{i}K_{2,m}l)a_{2,m}B_{2,m} = -\mathcal{B}_{1,0,m}, \quad (4.19a)$$

$$\sum_{n=0}^{N}\mathcal{B}_{1,n,m}K_{1,n}R_n+\gamma K_{2,m}a_{2,m}A_{2,m}-\gamma K_{2,m}\exp(\mathrm{i}K_{2,m}l)a_{2,m}B_{2,m} = K_{1,0}\mathcal{B}_{1,0,m}, \quad (4.19b)$$

$$\sum_{n=0}^{N}\exp(\mathrm{i}K_{j,n}l)\mathcal{B}_{j,n,m}A_{j,n}+\sum_{n=0}^{N}\mathcal{B}_{j,n,m}B_{j,n}-a_{j+1,m}A_{j+1,m} -\exp(\mathrm{i}K_{j+1,n}l)a_{j+1,m}B_{j+1,m} = 0, \quad (4.19c)$$

$$\sum_{n=0}^{N}K_{j,n}\exp(\mathrm{i}K_{j,n}l)\mathcal{B}_{j,n,m}A_{j,n}-\sum_{n=0}^{N}K_{j,n}\mathcal{B}_{j,n,m}B_{j,n}-K_{j+1,m}a_{j+1,m}A_{j+1,m} -K_{j+1,m}\exp(\mathrm{i}K_{j+1,n}l)a_{j+1,m}B_{j+1,m} = 0, \quad (4.19d)$$

$$\sum_{n=0}^{N}\exp(\mathrm{i}K_{p,n}l)\mathcal{B}_{p,n,m}A_{p,n}+\sum_{n=0}^{N}\mathcal{B}_{p,n,m}B_{p,n}-\cos(K_{p+1,m}l)a_{p+1,m}C_{p+1,m} = 0, \quad (4.19e)$$

$$\mathrm{i}\sum_{n=0}^{N}K_{p,n}\exp(\mathrm{i}K_{p,n}l)\mathcal{B}_{p,n,m}A_{p,n}-\mathrm{i}\sum_{n=0}^{N}K_{p,n}\mathcal{B}_{p,n,m}B_{p,n} -K_{p+1,m}\sin(K_{p+1,m}l)a_{p+1,m}C_{p+1,m} = 0. \quad (4.19f)$$

Equations (4.19a–f) can now be written as the following system:

$$\boldsymbol{AX} = \boldsymbol{c},$$

where $\boldsymbol{A}$ is a square matrix of size $[2p(N+1)]$,

$$\boldsymbol{X} = [R_0, \ldots R_N, A_{2,0}, B_{2,0} \ldots, A_{2,N}, B_{2,N}, \cdots\cdots, A_{p,0}, B_{p,0}, \ldots, A_{p,N}, B_{p,N}, C_{p+1,0} \ldots, C_{p+1,N}]^T \text{ is the unknown vector,}$$

and $$\boldsymbol{c} = [-\mathcal{B}_{1,0,0}, \ldots, \mathcal{B}_{1,0,N}, K_{1,0}\mathcal{B}_{1,0,0}, \ldots, K_{1,0}\mathcal{B}_{1,0,N}, \underbrace{0, \ldots\ldots\ldots\ldots 0}_{2(p-1)(N+1)\text{-times}}]^T.$$

By solving the above system of linear equations, reflection coefficient is to be evaluated.

4.4.3 Numerical results

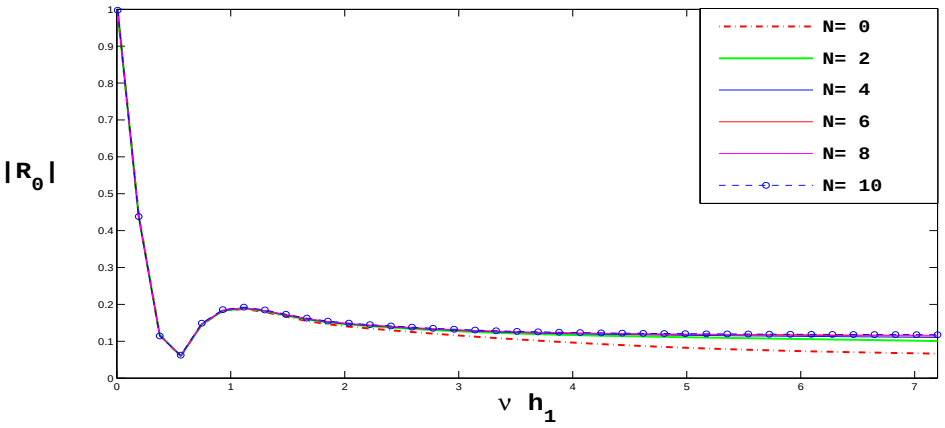

Figure 4.11: Variation of $|R_0|$ against νh_1 for different numbers of evanescent modes N steps $= 8$, $h_{p+1}/h_1 = 0.5$, $f = 1$, $L/h_1 = 2$, $\theta = 0^0$ and $\gamma = 0.9$

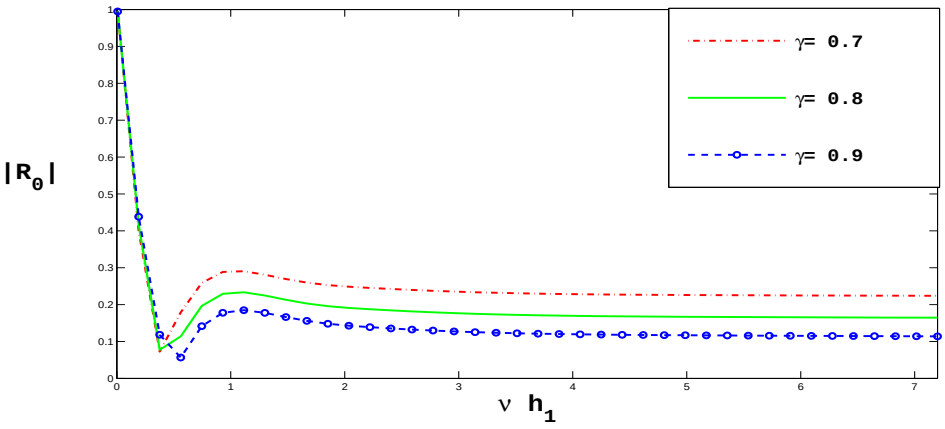

Figure 4.12: Variation of $|R_0|$ against νh_1 for different γ with steps $= 8$, $h_{p+1}/h_1 = 0.5$, $L/h_1 = 2$, $f = 1$, $\theta = 0^0$ and $N = 9$

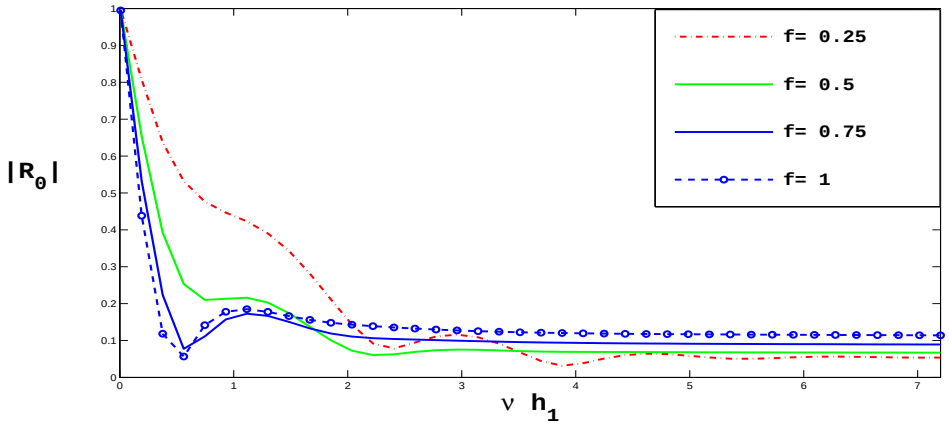

Figure 4.13: Variation of $|R_0|$ against νh_1 for different f with steps $= 8$, $h_{p+1}/h_1 = 0.5$, $L/h_1 = 2$, $\gamma = 0.9$, $\theta = 0^0$ and $N = 9$

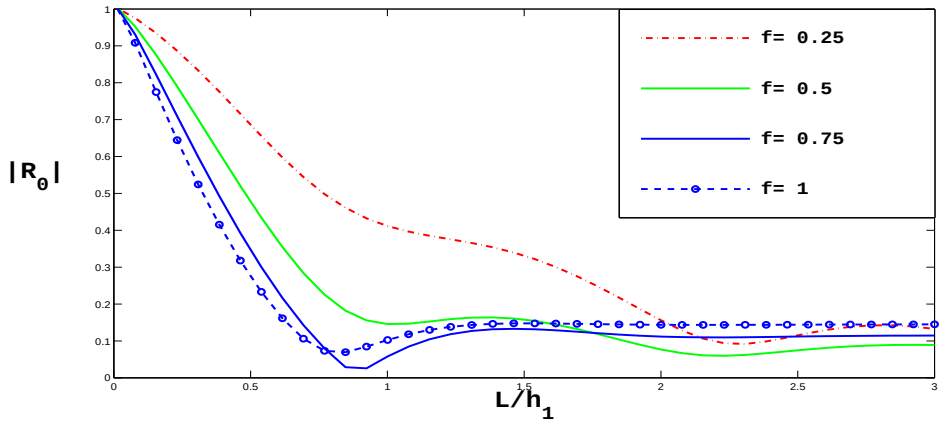

Figure 4.14: Variation of $|R_0|$ against dimensionless width of the porous structure L/h_1 for different f with steps $= 8$, $h_{p+1}/h_1 = 0.5$, $\gamma = 0.9$, $\theta = 0^0$ and $N = 9$

Here the corresponding investigation of different parameters on reflection coefficient is taken up along with two additional studies on number of steps p and height h_{p+1} of the $(p+1)$-th region as compared to the 2-step case, with $L/h_1 = 2$; $f = 1$; $S = 1$; $h_{p+1}/h_1 = 0.5$ and $\gamma = 0.7, 0.8$ and 0.9.

While presenting the reflection coefficient $|R_0|$ by figure 4.11 (against wave number for various number of evanescent modes), figure 4.12 (against wave number for various porosity), figure 4.16 (against width of the porous structure for various porosity), figure 4.17 (against wave number for various width of the porous structure) and figure 4.20 (against wave number for various angles of incidence), it is observed that reflection follows the same pattern as that

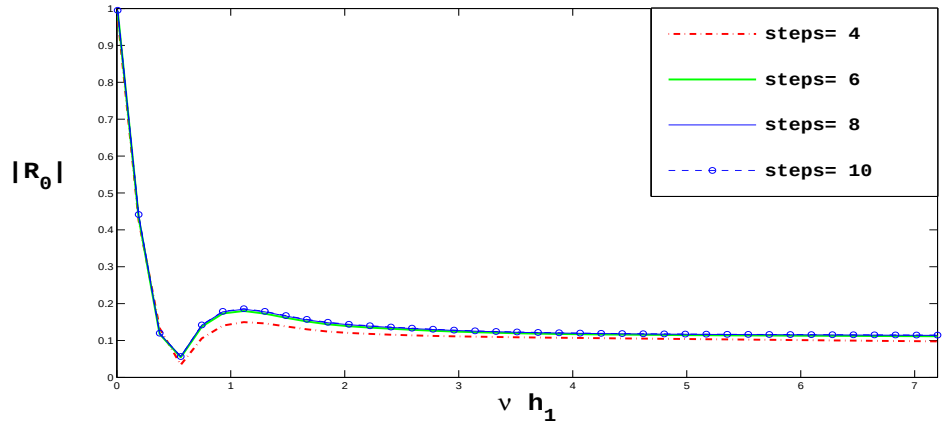

Figure 4.15: Variation of $|R_0|$ against νh_1 for different number of steps with $h_{p+1}/h_1 = 0.5$, $L/h_1 = 2$, $f = 1$, $\gamma = 0.9$, $\theta = 0^0$ and $N = 9$

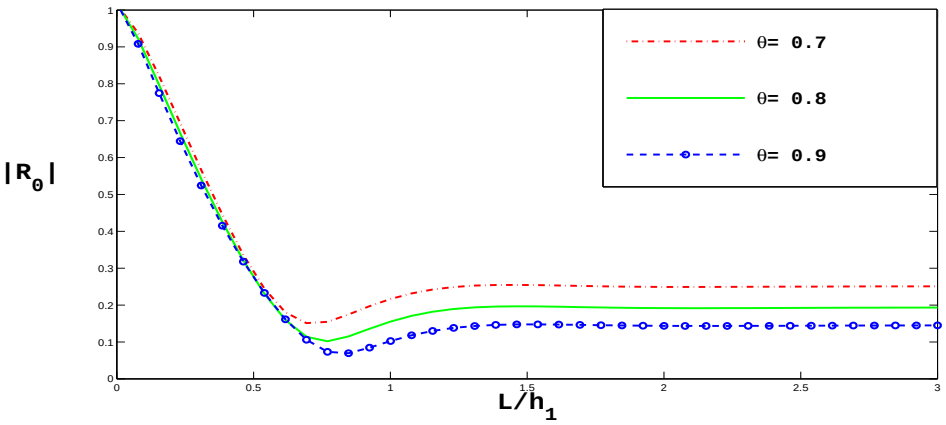

Figure 4.16: Variation of $|R_0|$ against dimensionless width of the porous structure L/h_1 for different γ with steps $= 8$, $h_{p+1}/h_1 = 0.5$, $f = 1$, $\theta = 0^0$ and $N = 9$

of the 2-step case except for the fact that for relatively long waves, oscillation is encountered in the reflection coefficient $|R_0|$ before attaining a constant value for relatively short waves.

Figures 4.13 and 4.14 also suggest the same pattern of the reflection coefficient plotted against νh_1 and L/h_1, respectively, for different friction factors as like that in the 2-step case, except for the fact that oscillation vanishes for relatively lower values of the wave number.

Figure 4.15 shows the effect of wave number on the reflection coefficient for different numbers of steps. Here the number of steps $= 4, 6, 8$ and 10 are considered. In this case also, oscillation in the reflection coefficient is observed for relatively long waves and it disappears with an increase in the value of the wave number. Higher number of steps gives rise to higher

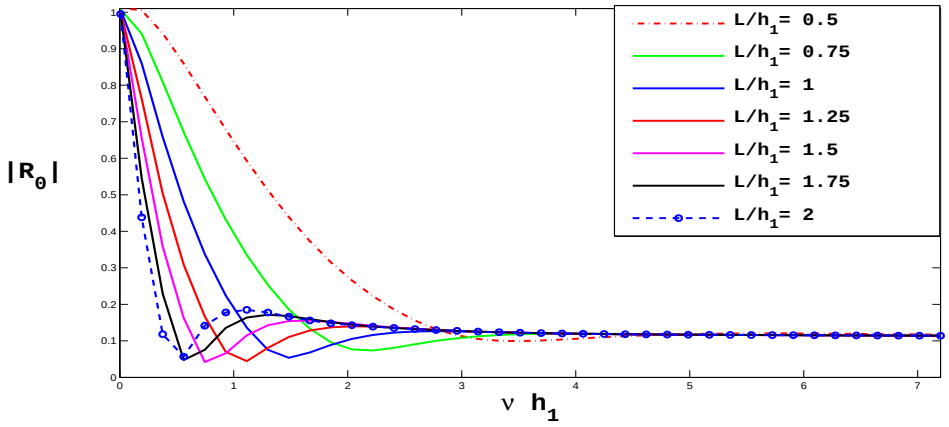

Figure 4.17: Variation of $|R_0|$ against νh_1 for different dimensionless width of the porous structure L/h_1 with steps $= 8$, $h_{p+1}/h_1 = 0.5$, $f = 1$, $\gamma = 0.9$, $\theta = 0^0$ and $N = 9$

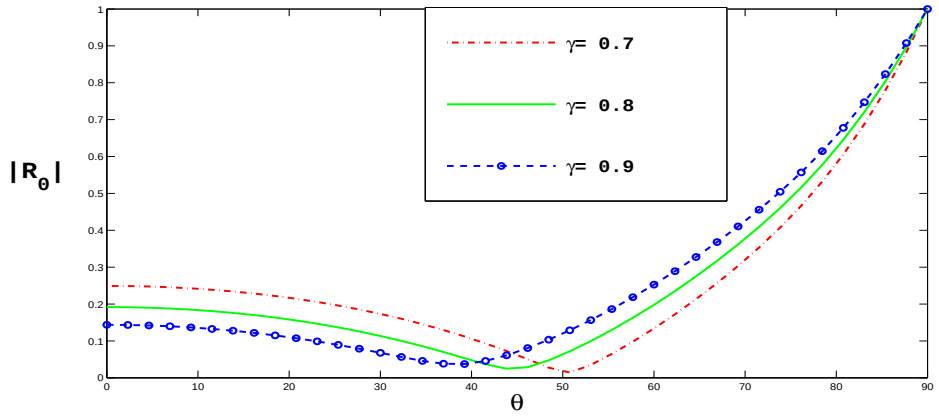

Figure 4.18: Variation of $|R_0|$ against incident wave angle θ for different γ with steps $= 8$, $h_{p+1}/h_1 = 0.5$, $L/h_1 = 2$ $f = 1$ and $N = 9$

reflection coefficient but it converges for sufficiently higher number of steps (here we consider steps $= 8$ and 10).

Further the effect of the angle of incidence θ on the reflection coefficient is studied for different values of porosity (figure 4.18). It is observed that for values of θ up to 40^0 (approx.), higher porosity results in lower reflection coefficient, but as the value of θ increases, the afore-said effect starts reversing and after $\theta = 50^0$ (approx.), higher porosity gives rise to higher reflection before converging to each other for very large values of θ.

We also investigate the effect of the angle of incidence θ on the reflection coefficient for different values of h_{p+1}/h_1, namely $h_{p+1}/h_1 = 0.5, 0.625$ and 0.75 and 6 (figure 4.19). Up to

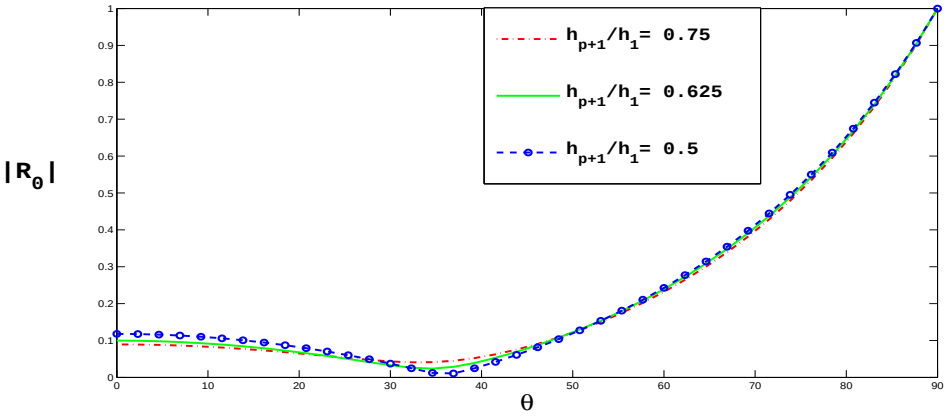

Figure 4.19: Variation of $|R_0|$ against incident wave angle θ for different values of h_{p+1}/h_1 with steps $= 8$, $L/h_1 = 2$, $f = 1$ $\gamma = 0.9$, and $N = 9$

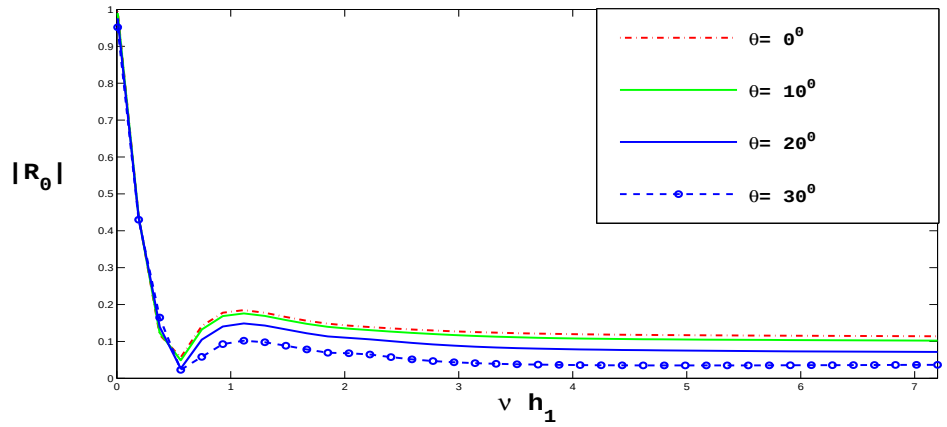

Figure 4.20: Variation of $|R_0|$ against νh_1 for different incident wave angle θ with steps $= 8$, $h_{p+1}/h_1 = 0.5$, $L/h_1 = 2$, $f = 1$, $\gamma = 0.9$ and $N = 9$

$\theta = 28^0$ (approx.), higher h_{p+1}/h_1 results in lower reflection coefficient but as the value of θ is increased further (in $30^0 < \theta < 50^0$), higher h_{p+1}/h_1 gives rise to lower reflection coefficient before converging to each other.

4.5 Comparison between 2-step and p-step bottom

To observe the difference or similarity between the results for both cases, we move forward to compare graphically the two different solutions for 2-step and p-step cases for the same set of parameter values by comparing $|R_0|$ against the wave number and the dimensionless width of

the porous structure for number of steps = 2 and 8. We consider $L/h_1 = 1$; $f = 1$; $S = 1$; $h_{p+1}/h_1 = 0.75$ and $\gamma = 0.9$.

Figures 4.21 and 4.22 show that the values of the reflection coefficients for $\gamma = 0.9$ are more or less the same in both cases. But if lower value of porosity ($\gamma = 0.5$ in this case) is considered, significant difference occurs (figures 4.23 and 4.24). Now it is observed that the 2-step approximation results in lower reflection coefficient as compared to the p-step approximation.

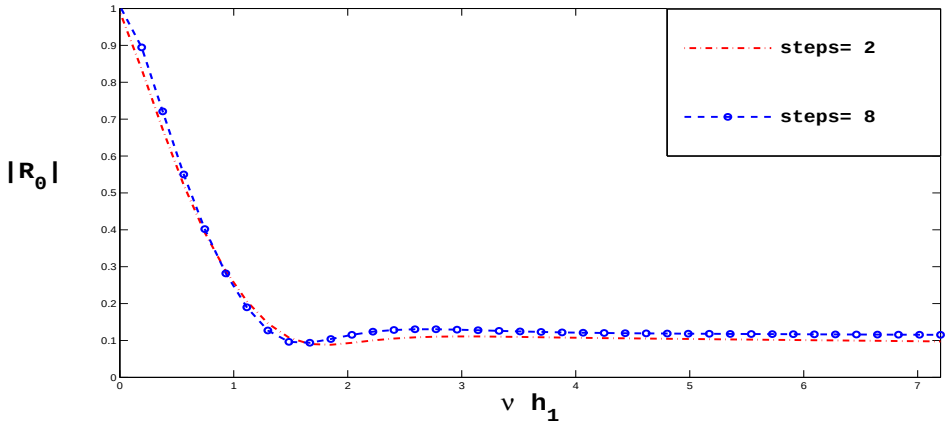

Figure 4.21: Variation of $|R_0|$ against νh_1 for 2 different different number of steps (2-step and 8-step) with $h_{p+1}/h_1 = 0.75$, $L/h_1 = 1$, $f = 1$, $\gamma = 0.9$, $\theta = 0^0$ and $N = 9$

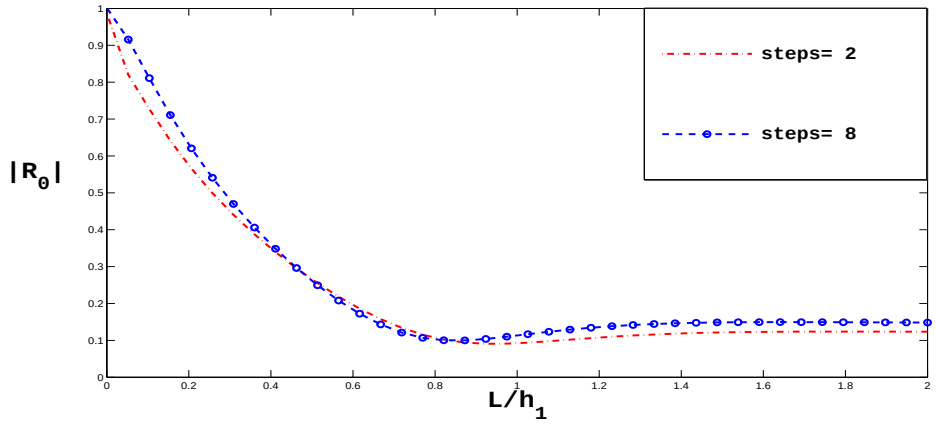

Figure 4.22: Variation of $|R_0|$ against dimensionless width of the porous structure L/h_1 for 2 different different number of steps (2-step and 8-step) with $h_{p+1}/h_1 = 0.75$, $f = 1$, $\gamma = 0.9$, $\theta = 0^0$ and $N = 9$

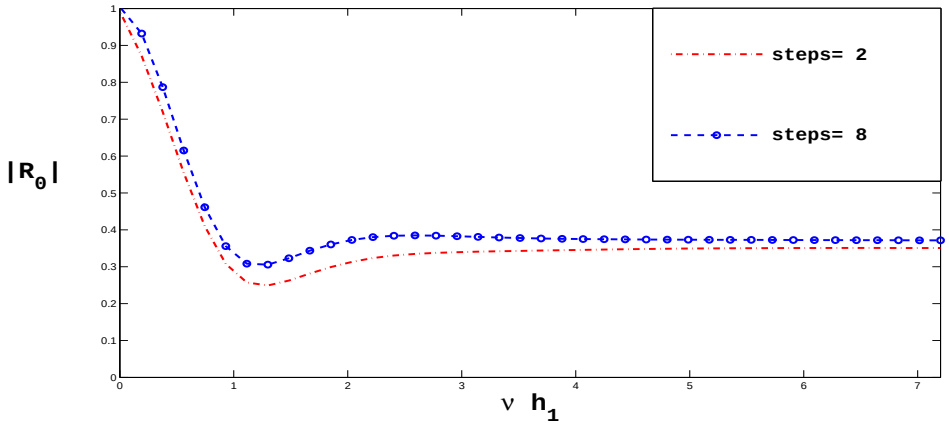

Figure 4.23: Variation of $|R_0|$ against νh_1 for 2 different different number of steps (2-step and 8-step) with $h_{p+1}/h_1 = 0.75$, $L/h_1 = 1$, $f = 1$, $\gamma = 0.5$, $\theta = 0^0$ and $N = 9$

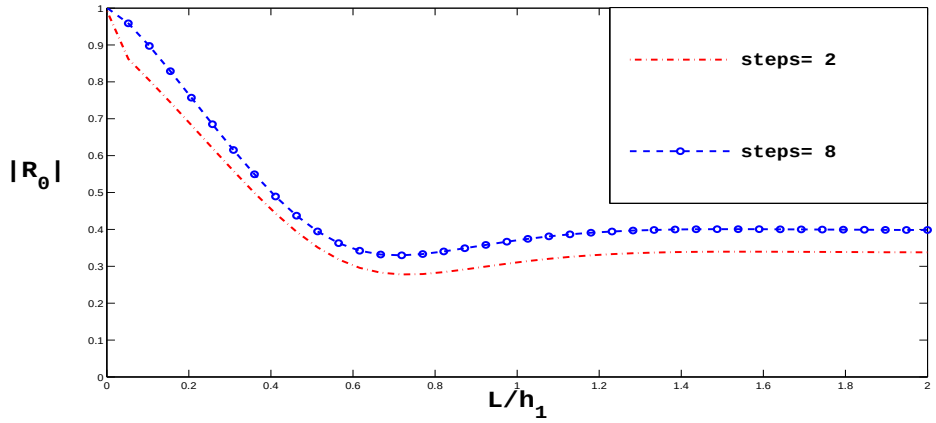

Figure 4.24: Variation of $|R_0|$ against dimensionless width of the porous structure L/h_1 for 2 different different number of steps (2-step and 8-step) with $h_{p+1}/h_1 = 0.75$, $f = 1$, $\gamma = 0.5$, $\theta = 0^0$ and $N = 9$

4.6 Comparison with existing result

In order to ascertain that our model is effective, we compare our reflection coefficients plotted against the dimensionless porous structure width with those in the work of Madsen (1983). This is accomplished by taking $h_1 = h_{p+1}$, i.e., by placing the porous structure on the horizontal ocean-bed instead of a p-step bottom. The excellent agreement between our result and Madsen's result can be observed from figure 4.25. This confirms that our model is valid and hence can be employed effectively to investigate various issues related to scattering of waves by a porous structure placed on a p-step bottom.

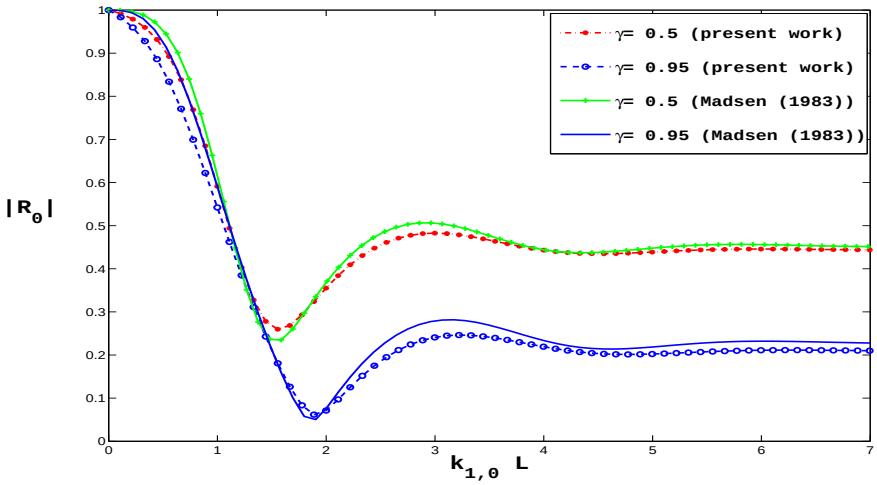

Figure 4.25: Variation of reflection coefficient $|R_0|$ against dimensionless width of porous structure $k_{1,0}L$ for different porosity γ with steps=40, $h_1 = 21$, $h_{p+1} = h_1$, $f = 1$, $\delta = 0.2$, $T = 17.3$, $a_i = 0.87$ and $N = 10$ (Comparison with Madsen (1983))

4.7 Conclusion

Based on linear water wave theory, we investigate the reflection coefficient for oblique water wave scattering by a vertical porous structure placed on an elevated bottom consisting of two steps as well as of p steps. It is observed that the propagating mode controls the reflection phenomenon up to a certain wave number. An increment in the height of the porous structure does not affect the reflection phenomenon after certain width of the structure. Higher value of the reflection coefficient is observed corresponding to lower values of porosity. It is also observed that lower values of friction factor lead to oscillation in the reflection coefficient which vanishes for higher values of friction factor. For relatively long waves, the values of the angle of incidence do not affect $|R_0|$ but for short waves, higher value of angle of incidence results in lower reflection coefficient. Porosity of the structure does not contribute up to a certain range of angle of incidence. The corresponding study of the effect of the number of evanescent modes and porosity for p-step impermeable bottom shows the same pattern, but oscillation for relatively long waves appears for the p-step bottom as against the 2-step bottom. Oscillation in $|R_0|$ for higher values of friction factor vanishes for the p-step ocean-bed at a relatively lower value of the wave number as compared to the 2-step ocean-bed. Increasing number of steps results in higher reflection coefficient but the values converge for sufficiently higher number of steps. For relatively lower value of the angle of incidence, $|R_0|$ takes higher value for lower

porosity but the effect reverses for relatively higher value of the angle of incidence. The same effect mentioned above is observed for different values of depth h_{p+1}. Further, comparison between the reflection coefficients of 2-step and p-step bottoms is carried out for two different values of porosity against wave number and dimensionless width of the porous structure. It is observed that for relatively lower value of porosity, p-step bottom results in lower reflection coefficient. For the validity of our mathematical model, we compare our work with Madsen (1983) by plotting reflection coefficient against dimensionless width of the porous structure for different values of porosity and we arrive at excellent agreement in this regard.

Chapter 5

Damping of oblique ocean waves by a porous structure placed on a multi-step bottom

In this chapter, the problem related to the damping of oblique ocean water waves by a porous structure placed on a multi-step bottom is solved with the help of linear water wave theory. Two different cases, namely a finite water region at the rear of the porous structure bounded by a rigid vertical wall as well as an unbounded water region at the rear of the porous structure, are considered separately for the investigation. The reflection and the transmission coefficients, along with the energy loss, are investigated for various relevant parameters.

5.1 Mathematical Formulation

Let us consider a vertical porous structure of width L along the mean free surface, placed on a p-step bottom topography above the horizontal ocean bottom, which is at a constant depth h_1 from the mean free surface. Using Cartesian coordinate system (x, y, z), the positive x-direction is defined as the direction of the wave incident on the porous structure at $x = 0$, the positive z-direction is considered vertically upwards and the mean free surface as $z = 0$. Due to the p-step bottom topography under the porous structure, p number of different heights of

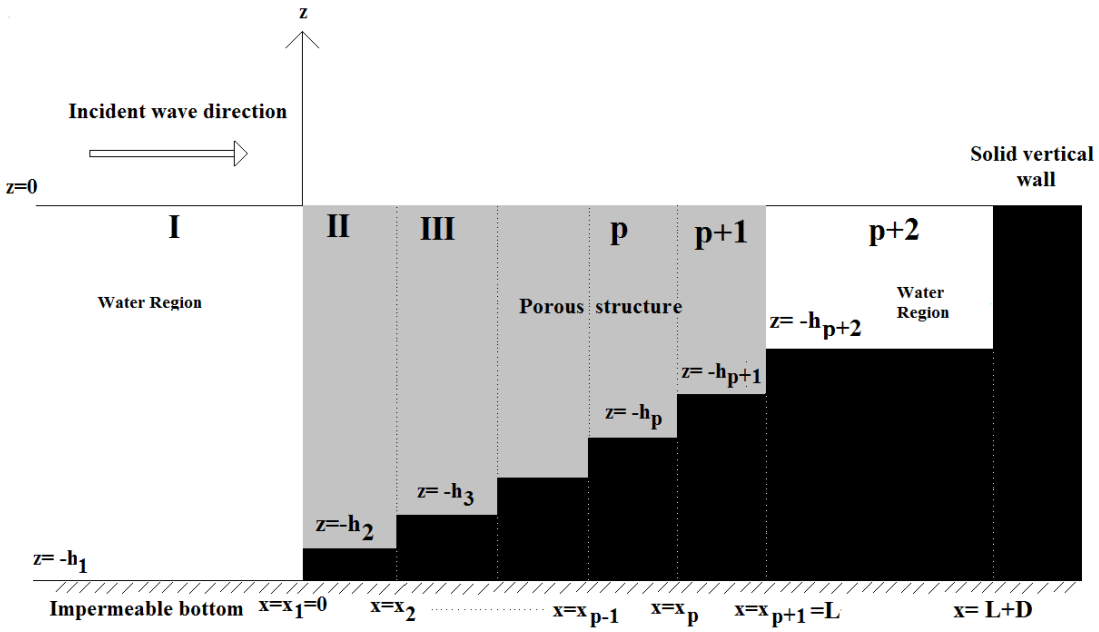

Figure 5.1: Schematic diagram of the problem

the porous structure exist, namely, h_j when $x_{j-1} < x < x_j$ for each $j = 2, 3, \ldots, p+1$, where

$$x_1 = 0 < x_2 < \ldots < x_{p+1} = L \qquad \text{with} \qquad x_j - x_{j-1} = l_0.$$

The water region ($-\infty < x < 0$, $-h_1 < z < 0$) is labeled as region I, the porous structure above the j-th step ($x_{j-1} < x < x_j$, $-h_j < z < 0$) as region $j+1$ with the structure split into a total of p regions (Figure 5.1). Further a water region ($L < x < L + D$, $-h_{p+2} < z < 0$) between the porous structure and the rigid vertical wall placed at a distance $x = L + D$ is considered and labeled as region $p + 2$. The horizontal bottom for region I is considered at $z = -h_1$. After propagating through the porous structure, the wave passes through region $p + 2$ and gets reflected by the vertical wall placed at $x = L + D$. The fluid is assumed to be incompressible, homogeneous and inviscid, and the motion irrotational. We define $p + 2$ velocity potentials $\Phi_j(x, y, z, t) = \phi_j(x, z) \exp(ily - i\omega t)$ in region j for each $j = 1, 2, \ldots, p+2$. The governing equation and the boundary conditions in region I are

$$\nabla^2\phi_1 - l^2\phi_1 = 0; \qquad -\infty < x < 0, \qquad -h_1 < z < 0, \tag{5.1a}$$

$$\frac{\partial \phi_1}{\partial z} - \nu \phi_1 = 0; \qquad -\infty < x < 0, \qquad z = 0, \tag{5.1b}$$

$$\frac{\partial \phi_1}{\partial z} = 0; \qquad -\infty < x < 0, \qquad z = -h_1, \tag{5.1c}$$

$$\frac{\partial \phi_1}{\partial x} = 0; \qquad x = 0, \qquad -h_1 < z < -h_2. \tag{5.1d}$$

The governing equation and the boundary conditions in region j $(j = 2, 3, \ldots, p+1)$ are

$$\boldsymbol{\nabla}^2 \phi_j - l^2 \phi_j = 0; \qquad x_{j-1} < x < x_j, \qquad -h_j < z < 0, \tag{5.2a}$$

$$\frac{\partial \phi_j}{\partial z} - \mathrm{i}\nu R \phi_j = 0; \qquad x_{j-1} < x < x_j, \qquad z = 0, \tag{5.2b}$$

$$\frac{\partial \phi_j}{\partial z} = 0; \qquad x_{j-1} < x < x_j, \qquad z = -h_j, \tag{5.2c}$$

$$\frac{\partial \phi_j}{\partial x} = 0; \qquad x = x_j, \qquad -h_j < z < -h_{j+1}. \tag{5.2d}$$

The governing equation and the boundary conditions in region $p+2$ are

$$\boldsymbol{\nabla}^2 \phi_{p+2} - l^2 \phi_{p+2} = 0; \qquad L < x < L + D, \qquad -h_{p+2} < z < 0, \tag{5.3a}$$

$$\frac{\partial \phi_{p+2}}{\partial z} - \nu \phi_{p+2} = 0; \qquad L < x < L + D, \qquad z = 0, \tag{5.3b}$$

$$\frac{\partial \phi_{p+2}}{\partial z} = 0; \qquad L < x < L + D, \qquad z = -h_{p+2}, \tag{5.3c}$$

$$\frac{\partial \phi_{p+2}}{\partial x} = 0; \qquad x = L + D, \qquad -h_{p+2} < z < 0. \tag{5.3d}$$

The matching conditions along the boundaries $x = 0$, $x = x_j$ $(j = 2, \ldots, p)$ and $x = x_{p+1}$ are given by

$$\phi_1 = \mathrm{i}R\phi_2; \qquad x = 0, \qquad -h_2 \le z \le 0, \tag{5.4a}$$

$$\frac{\partial \phi_1}{\partial x} = \gamma \frac{\partial \phi_2}{\partial x}; \qquad x = 0, \qquad -h_2 \le z \le 0, \tag{5.4b}$$

$$\phi_j = \phi_{j+1}; \qquad x = x_j, \qquad -h_{j+1} \le z \le 0, \tag{5.4c}$$

$$\frac{\partial \phi_j}{\partial x} = \frac{\partial \phi_{j+1}}{\partial x}; \qquad x = x_j, \qquad -h_{j+1} \le z \le 0, \tag{5.4d}$$

$$\mathrm{i}R\phi_{p+1} = \phi_{p+2}; \qquad x = x_{p+1}, \qquad -h_{p+2} \le z \le 0, \tag{5.4e}$$

$$\gamma \frac{\partial \phi_{p+1}}{\partial x} = \frac{\partial \phi_{p+2}}{\partial x}; \qquad x = x_{p+1}, \qquad -h_{p+2} \le z \le 0. \tag{5.4f}$$

5.2 Reflection and damping by the porous structure

The velocity potential $\phi_1(x,z)$ in region I is given by the following form:

$$\phi_1(x,z) = [\exp(\mathrm{i}K_{1,0}x) + R_0\exp(-\mathrm{i}K_{1,0}x)]Z_{1,0}(h_1,z) + \sum_{n=1}^{\infty} R_n \exp(-\mathrm{i}K_{1,n}x)Z_{1,n}(h_1,z), \quad (5.5)$$

where the depth-dependent function $Z_{1,n}(h_1,z)$ and $K_{1,n}$ are same as defined in Chapter 3. We truncate the infinite sum at $n=N$ so as to consider a finite number of evanescent modes N only:

$$\phi_1(x,z) = \{\exp(\mathrm{i}K_{1,0}x) + R_0\exp(-\mathrm{i}K_{1,0}x)\}Z_{1,0}(h_1,z) + \sum_{n=1}^{N} R_n \exp(-\mathrm{i}K_{1,n}x)Z_{1,n}(h_1,z). \quad (5.6)$$

In region j ($j=2,3,\ldots,p+1$, $x_{j-1}<x<x_j$, $-h_j<z<0$), the horizontal impermeable bottom is considered at $z=-h_j$. Hence, the integrals in this porous region must be from $z=-h_j$ to $z=0$ in order to meet the matching conditions and we are required to compute the relevant integrals from $z=-h_j$ to $z=0$. By using separation of variables method, the velocity potential $\phi_j(x,z)$, after truncating the infinite sum at $n=N$, can be written as

$$\phi_j(x,z) = \sum_{n=0}^{N} \left\{A_{j,n}\exp\left[\mathrm{i}K_{j,n}(x-x_{j-1})\right] + B_{j,n}\exp\left[-\mathrm{i}K_{j,n}(x-x_j)\right]\right\} Z_{j,n}(h_j,z), \quad (5.7a)$$

where $A_{j,n}$ and $B_{j,n}$ are arbitrary constants; $K_{j,n} = (k_{j,n}^2 - l^2)^{1/2}$ with $k_{j,n}$ satisfying the dispersion relation

$$\mathrm{i}R\nu = k_{j,n}\tanh k_{j,n}h_j, \quad (5.7b)$$

and $Z_{j,n}(h_j,z)$ is the depth-dependent function in region j given by

$$Z_{j,n}(h_j,z) = \frac{\cosh k_{j,n}(h_j+z)}{\cosh k_{j,n}h_j}, \quad n=0,1,2,\cdots,N. \quad (5.7c)$$

In region $p+2$ ($L<x<L+D$, $-h_{p+2}<z<0$), the horizontal impermeable bottom is considered at $z=-h_{p+2}$. Hence, the integrals in the water region must be from $z=-h_{p+2}$ to $z=0$ in order to meet the matching conditions and we are required to compute the relevant integrals from $z=-h_{p+2}$ to $z=0$. The velocity potential $\phi_{p+2}(x,z)$, after truncating the

infinite sum at $n = N$, can be written as

$$\phi_{p+2}(x,z) = \sum_{n=0}^{N} \{C_n \exp[\mathrm{i}K_{p+2,n}(x-L)] + D_n \exp[-\mathrm{i}K_{p+2,n}(x-L-D)]\} Z_{p+2,n}(h_{p+2},z), \tag{5.8a}$$

where C_0 is the dimensionless amplitude of the progressive transmitted wave; C_n $(n = 1, 2, \ldots, N)$ and D_n $(n = 0, 1, \ldots, N)$ are arbitrary constants; $K_{p+2,n} = (k_{p+2,n}^2 - l^2)^{1/2}$ with $k_{p+2,n}$ satisfying the dispersion relation

$$\nu = k_{p+2,n} \tanh k_{p+2,n} h_{p+2}, \tag{5.8b}$$

and $Z_{p+2,n}(h_{p+2}, z)$ is the depth-dependent function in region $p+2$ given by

$$Z_{p+2,n}(h_{p+2},z) = \frac{\cosh k_{p+2,n}(h_{p+2}+z)}{\cosh k_{p+2,n} h_{p+2}}. \tag{5.8c}$$

Further, using the condition (5.3d), ϕ_{p+2} can be reduced to the following form:

$$\phi_{p+2} = \sum_{n=0}^{N} C_n \big\{ \exp[\mathrm{i}K_{p+2,n}(x-L)] + \exp[-\mathrm{i}K_{p+2,n}(x-L-2D)] \big\} Z_{p+2,n}(h_{p+2},z). \tag{5.9}$$

When the energy loss during the whole process of scattering is discussed, the following definition is to be used:

$$E_{\mathrm{loss}} = (1 - |R_0|^2 - |C_0|^2) \times 100\%. \tag{5.10}$$

Using the matching conditions (5.4a,b) along the boundary $x = x_1$, $-h_2 < z < 0$, we get

$$(1+R_0)Z_{1,0} + \sum_{n=1}^{N} R_n Z_{1,n} = \mathrm{i}R \sum_{n=0}^{N} [A_{2,n} + B_{2,n} \exp(\mathrm{i}K_{2,n}l) Z_{2,n}], \tag{5.11a}$$

$$K_{1,0}(1-R_0)Z_{1,0} - \sum_{n=1}^{N} K_{1,n} R_n Z_{1,n} = \gamma \sum_{n=0}^{N} [A_{2,n} - B_{2,n} \exp(\mathrm{i}K_{2,n}l) K_{2,n} Z_{2,n}]. \tag{5.11b}$$

Further, using the matching conditions (5.4c,d) along the boundary $x = x_j$, $-h_{j+1} \le z \le 0$ $(j = 2, 3, \ldots, p)$, it follows

$$\sum_{n=0}^{N} [A_{j,n} \exp(\mathrm{i}K_{j,n}l) + B_{j,n}] Z_{j,n} = \sum_{n=0}^{N} [A_{j+1,n} + B_{j+1,n} \exp(\mathrm{i}K_{j+1,n}l)] Z_{j+1,n}, \tag{5.11c}$$

$$\sum_{n=0}^{N}[A_{j,n}\exp(\mathrm{i}K_{j,n}l)-B_{j,n}]K_{j,n}Z_{j,n}=\sum_{n=0}^{N}[A_{j+1,n}-B_{j+1,n}\exp(\mathrm{i}K_{j+1,n}l)]K_{j+1,n}Z_{j+1,n}. \tag{5.11d}$$

Applying the matching conditions (5.4e,f) along the boundary $x = x_{p+1} = L$, $-h_{p+2} < z < 0$, we obtain

$$\mathrm{i}R\sum_{n=0}^{N}[A_{p+1,n}\exp(\mathrm{i}K_{p+1,n}l)+B_{p+1,n}]Z_{p+1,n}=\sum_{n=0}^{N}C_n\big[1+\exp(2\mathrm{i}K_{p+2,n}D)\big]Z_{p+2,n}, \tag{5.11e}$$

$$\gamma\sum_{n=0}^{N}[A_{p+1,n}\exp(\mathrm{i}K_{p+1,n}l)-B_{p+1,n}]K_{p+1,n}Z_{p+1,n}=\sum_{n=0}^{N}C_n\big[1-\exp(2\mathrm{i}K_{p+2,n}D)\big]K_{p+2,n}Z_{p+2,n}. \tag{5.11f}$$

Further, using the orthogonality property of $Z_{2,m}$, $Z_{j+1,m}$ $(j = 2, 3, \ldots, p)$ and $Z_{p+2,m}$, for each $m = 0, 1, \ldots, N$, in equations (5.11a,b), (5.11c,d) and (5.11e,f), respectively, we have

$$\sum_{n=0}^{N}\mathcal{B}_{1,n,m}R_n-\mathrm{i}Ra_{2,m}A_{2,m}-\mathrm{i}R\exp(\mathrm{i}K_{2,m}l)a_{2,m}B_{2,m}=-\mathcal{B}_{1,0,m}, \tag{5.12a}$$

$$\sum_{n=0}^{N}\mathcal{B}_{1,n,m}K_{1,n}R_n+\gamma K_{2,m}a_{2,m}A_{2,m}-\gamma K_{2,m}\exp(\mathrm{i}K_{2,m}l)a_{2,m}B_{2,m}=K_{1,0}\mathcal{B}_{1,0,m}, \tag{5.12b}$$

$$\sum_{n=0}^{N}\exp(\mathrm{i}K_{j,n}l)\mathcal{B}_{j,n,m}A_{j,n}+\sum_{n=0}^{N}\mathcal{B}_{j,n,m}B_{j,n}-a_{j+1,m}A_{j+1,m}-\exp(\mathrm{i}K_{j+1,n}l)a_{j+1,m}B_{j+1,m}=0, \tag{5.12c}$$

$$\sum_{n=0}^{N}K_{j,n}\exp(\mathrm{i}K_{j,n}l)\mathcal{B}_{j,n,m}A_{j,n}-\sum_{n=0}^{N}K_{j,n}\mathcal{B}_{j,n,m}B_{j,n}-K_{j+1,m}a_{j+1,m}A_{j+1,m}-K_{j+1,m}\exp(\mathrm{i}K_{j+1,m}l)a_{j+1,m}B_{j+1,m}=0, \tag{5.12d}$$

$$\mathrm{i}R\sum_{n=0}^{N}\exp(\mathrm{i}K_{p+1,n}l)\mathcal{B}_{p+1,n,m}A_{p+1,n}+\mathrm{i}R\sum_{n=0}^{N}\mathcal{B}_{p+1,n,m}B_{p+1,n}-\big[1+\exp(2\mathrm{i}K_{p+2,n}D)\big]a_{p+2,m}C_m=0, \tag{5.12e}$$

$$\gamma\sum_{n=0}^{N}K_{p+1,n}\exp\left(\mathrm{i}K_{p+1,n}l\right)\mathcal{B}_{p+1,n,m}A_{p+1,n}-\gamma\sum_{n=0}^{N}K_{p+1,n}\mathcal{B}_{p+1,n,m}B_{p+1,n}$$
$$-K_{p+2,m}\left[1-\exp\left(2\mathrm{i}K_{p+2,n}D\right)\right]a_{p+1,m}C_m=0, \qquad (5.12f)$$

where

$$\mathcal{B}_{q,n,m} = \int_{-h_{q+1}}^{0} Z_{q,n}Z_{q+1,m}dz$$
$$= \begin{cases} \dfrac{1}{K_{1,n}^2-K_{2,m}^2}\left[\nu(1-\mathrm{i}R)-\dfrac{K_{1,n}\sinh K_{1,n}(h_2-h_1)}{\cosh K_{1,n}h_1\cosh K_{2,m}h_2}\right] & \text{when } q=1,\\ \dfrac{1}{K_{q,n}^2-K_{q+1,m}^2}\left[-\dfrac{K_{q,n}\sinh K_{q,n}(h_{q+1}-h_q)}{\cosh K_{q,n}h_q\cosh K_{q+1,m}h_{q+1}}\right] & \text{when } q=2,3,\ldots,p,\\ \dfrac{1}{K_{p+1,n}^2-K_{p+2,m}^2}\left[\nu(\mathrm{i}R-1)-\dfrac{K_{p+1,n}\sinh K_{p+1,n}(h_{p+2}-h_{p+1})}{\cosh K_{p+1,n}h_{p+1}\cosh K_{p+2,m}h_{p+2}}\right] & \text{when } q=p+1. \end{cases}$$

Equations (5.12a–f) can now be written as the following system:

$$\boldsymbol{A}\boldsymbol{X}=\boldsymbol{c},$$

where $\boldsymbol{A}$ is a square matrix of size $2(p+1)(N+1)$,

$\boldsymbol{X}=[R_0,\ldots R_N,A_{2,0},B_{2,0}\ldots,A_{2,N},B_{2,N},\cdots\cdots,A_{p+1,0},B_{p+1,0},\ldots,A_{p+1,N},B_{p+1,n},$
$C_0,\ldots,C_N]^T$ is the unknown vector,

and $\boldsymbol{c}=[-\mathcal{B}_{1,0,0},\ldots,\mathcal{B}_{1,0,N},K_{1,0}\mathcal{B}_{1,0,0},\ldots,K_{1,0}\mathcal{B}_{1,0,N},\underbrace{0,\ldots\ldots\ldots,0}_{2\mathrm{p(N+1)\text{-}times}}]^T.$

By solving the above system of linear equations, $|R_0|$ and $|C_0|$ can be evaluated and subsequently the overall scattering phenomenon by the porous structure can be discussed.

5.3 Numerical results

Results are shown for variation in the reflection coefficient $|R_0|$ and the dimensionless amplitude $|C_0|$ of the transmitted wave against the dimensionless width of the porous structure L/h_1 as well as the angle of incidence θ for various parameters such as the number of evanescent modes

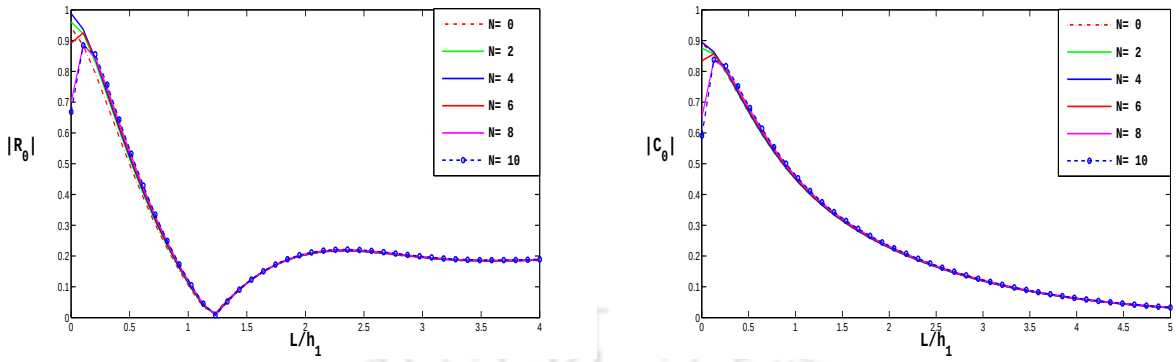

(a) Variation of $|R_0|$ (b) Variation of $|C_0|$

Figure 5.2: Effect of dimensionless width of the porous structure L/h_1 for different numbers of evanescent modes N with $\nu h_1 = 0.8$, $D/h_1 = 10$, $\theta = 0^0$, $\gamma = 0.9$, $f = 1$ and $p = 7$

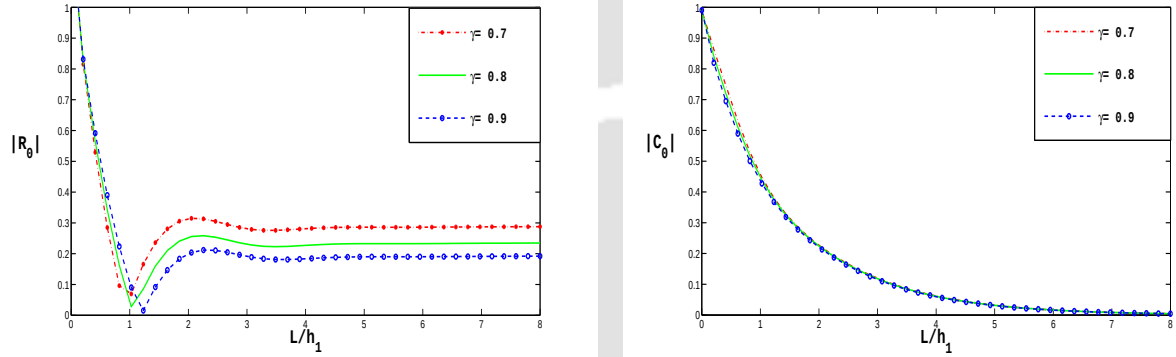

(a) Variation of $|R_0|$ (b) Variation of $|C_0|$

Figure 5.3: Effect of dimensionless width of the porous structure L/h_1 for different γ with $\nu h_1 = 0.8$, $D/h_1 = 10$, $\theta = 0^0$, $N = 10$, $f = 1$ and $p = 7$

N, porosity γ, friction factor f and number of steps p. Energy loss curves are also plotted against L/h_1 and θ. For computational purpose, some constant values for different parameters are considered: $L/h_1 = 3$, $\theta = 0^0$, $N = 10$, $\gamma = 0.9$, $f = 1$ and $p = 7$. Throughout the computation, the dimensionless wave number νh_1 is considered fixed at $\nu h_1 = 0.8$.

In order to study the effect of the number of evanescent modes on scattering characteristics, $|R_0|$ and $|C_0|$ are plotted against L/h_1 in figure 5.2 by keeping all other parameters fixed. Figure 5.2(a) shows large values of $|R_0|$ for relatively small values of L/h_1, suggesting that in order to get lower reflection, thin porous structure needs to be avoided. It is noticed that around $L/h_1 = 1.25$, the reflection coefficient attains the minimum value and then increases with an increase in the value of L/h_1 before stabilizing at a fixed value of $|R_0| \approx 0.2$. The

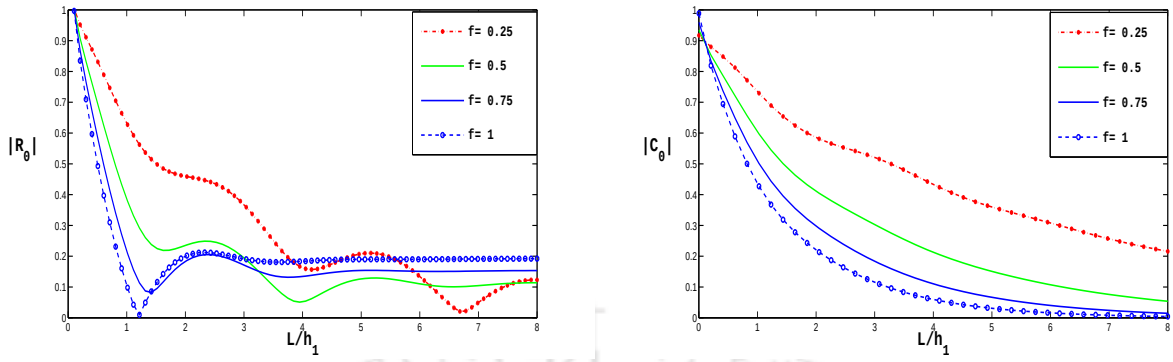

(a) Variation of $|R_0|$ (b) Variation of $|C_0|$

Figure 5.4: Effect of dimensionless width of the porous structure L/h_1 for different f with $\nu h_1 = 0.8$, $D/h_1 = 10$, $\theta = 0^0$, $N = 10$, $\gamma = 0.9$, and $p = 7$

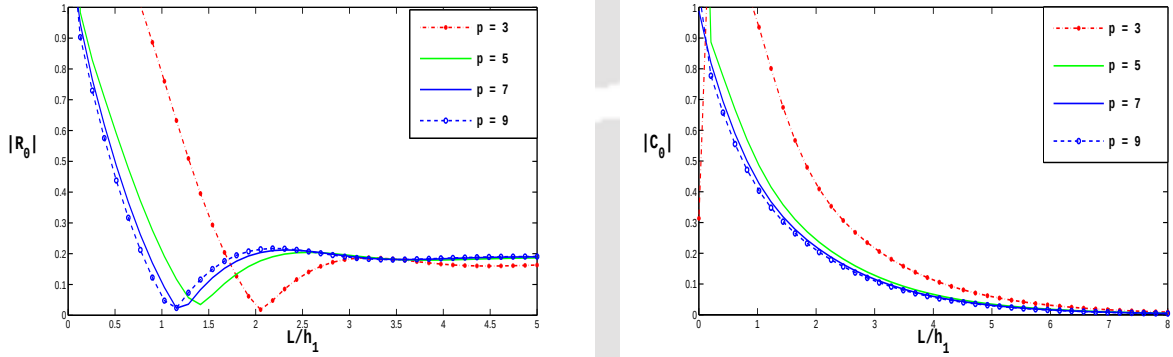

(a) Variation of $|R_0|$ (b) Variation of $|C_0|$

Figure 5.5: Effect of dimensionless width of the porous structure L/h_1 for different p with $\nu h_1 = 0.8$, $D/h_1 = 10$, $\theta = 0^0$, $N = 10$, $\gamma = 0.9$ and $f = 1$

minimum value may occur due to the cancelation of reflection from the step bottom as well as the rigid vertical wall and vertical front face of the porous structure (Straub *et al.* (1957)). It is also found that the reflection is independent of the number of evanescent modes. Now large transmission is found to take place corresponding to relatively lower values of L/h_1 (figure 5.2(b)). Further increase in L/h_1 results in decreasing values of $|C_0|$ and it ultimately approaches zero. The behaviour of $|C_0|$ is also independent of the number of evanescent modes.

The effect of different values of porosity on scattering phenomenon is studied by plotting $|R_0|$ and $|C_0|$ against L/h_1 (figure 5.3). From figure 5.3(a), it is observed that in each curve, as the dimensionless width of the structure is increased, $|R_0|$ initially decreases rapidly, attains a minimum value and again increases slightly before obtaining a constant value. It is observed

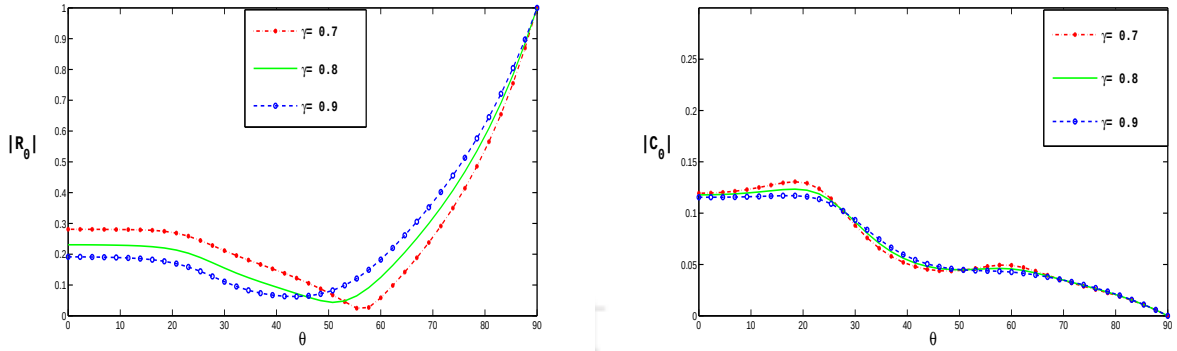

(a) Variation of $|R_0|$ (b) Variation of $|C_0|$

Figure 5.6: Effect of angle of incidence θ for different γ with $\nu h_1 = 0.8$, $D/h_1 = 10$, $L/h_1 = 3$, $N = 10$, $f = 1$ and $p = 7$

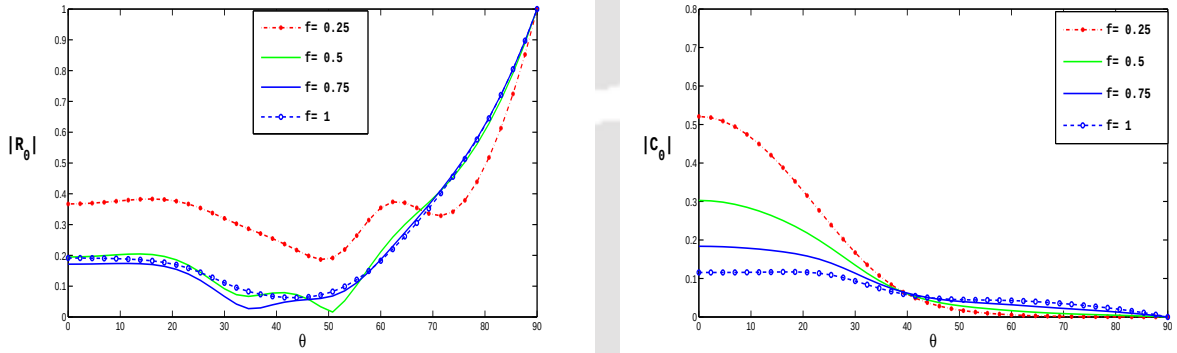

(a) Variation of $|R_0|$ (b) Variation of $|C_0|$

Figure 5.7: Effect of angle of incidence θ for different f with $\nu h_1 = 0.8$, $D/h_1 = 10$, $L/h_1 = 3$, $N = 10$, $\gamma = 0.9$, and $p = 7$

that higher value of porosity gives rise to lower $|R_0|$ which is as per expectation. Figure 5.3(b) suggests that $|C_0|$ is independent of the value of the porosity considered. It is observed that higher values of $|C_0|$ occur for a thin porous structure but with an increase in L/h_1, $|C_0|$ decreases rapidly before converging to zero.

In figure 5.4, $|R_0|$ and $|C_0|$ are plotted against different values of friction factor f in order to illustrate its effect on scattering characteristics. Values of both $|R_0|$ and $|C_0|$ are very high for small L/h_1 and a further increase in L/h_1 reduces the values of $|R_0|$ as well as those of $|C_0|$. Oscillation in $|R_0|$ is observed in figure 5.4(a) for lower value of the friction factor ($f = 0.25$). But the oscillation disappears if higher value of friction factor is considered ($f = 1$). Higher value of friction factor results in lower $|C_0|$ (figure 5.4(b)) and approaches zero for large values

of L/h_1.

Now variation in $|R_0|$ and $|C_0|$ against L/h_1 is studied for different numbers of steps p in figure 5.5. It is noticeable from figure 5.5(a) that for $p = 3$, a very steep portion of the curve exists in $0.8 < L/h_1 < 2$ which suggests the minimum admissible length of the porous structure. For higher number of steps, the nature of the curve remains the same but the minimum admissible length of the porous structure decreases. It is also observed that $|R_0|$ converges as the number of steps is increased. Similar kind of behaviour exists for $|C_0|$ also (figure 5.5(b)). Higher admissible length of the porous structure is required for $p = 3$. $|C_0|$ is very high for the initial portion of the curve but decreases with an increase in L/h_1 and finally converges to zero for all the values of the number of steps considered.

We observe in figures 5.2-5.5 that reflection and transmission are very high when the porous structure is very thin. When the width of the porous structure is almost zero, i.e., no porous structure is present, total transmission takes place and hence the amplitude of incoming wave is same as the amplitude of the transmitted wave. We also observe that the left propagating mode arising from the solid wall placed at $x = L + D$ has the same magnitude as that of the transmitted wave. This left propagating mode is responsible for reflection taking place (virtually) at $x = 0$. Therefore $|R_0| = 1$ in this case. This is the reason why both the reflection and transmission are very high when $L \to 0$.

Further $|R_0|$ and $|C_0|$ are plotted in figure 5.6 against the angle of incidence θ for different values of porosity. From figure 5.6(a) it is observed that, with an increase in θ, $|R_0|$ decreases slowly before reaching the minimum value and then increases rapidly until it reaches $|R_0| = 1$ at $\theta = 90^0$ which is justified as the wave passes tangentially with respect to the front surface of the porous structure causing no penetration in the structure. It is observed that in $0^0 < \theta < 44^0$ (approx), lower porosity results in higher reflection. But afterwards this characteristic starts reversing and from $\theta = 52^0$ (approx) onwards, higher porosity gives rise to higher reflection. Figure 5.6(b) shows that $|C_0|$ is independent of the values of porosity. It takes very small value for $\theta = 0$ and decreases to zero as θ is increased.

In figure 5.7 the effect of incident wave angle on scattering characteristics is studied for different values of friction factor. Figure 5.7(a) shows the variation of $|R_0|$ for different values of f. Oscillation is observed for lower values of friction factor ($f = 0.25$) and it disappears if higher value of friction factor ($f = 1$) is considered. Convergence of $|R_0|$ is observed for higher values of friction factor. Variation in $|C_0|$ for different values of f is shown in figure 5.7(b). For higher values of θ, $|C_0|$ takes lower values before converging to zero. It is found that up to $\theta = 40^0$ (approx), $|C_0|$ is higher for lower values of f considered. Afterwards the above

mentioned property reverses but the difference in their values is very small compared to that when $\theta = 0$.

5.4 Energy loss

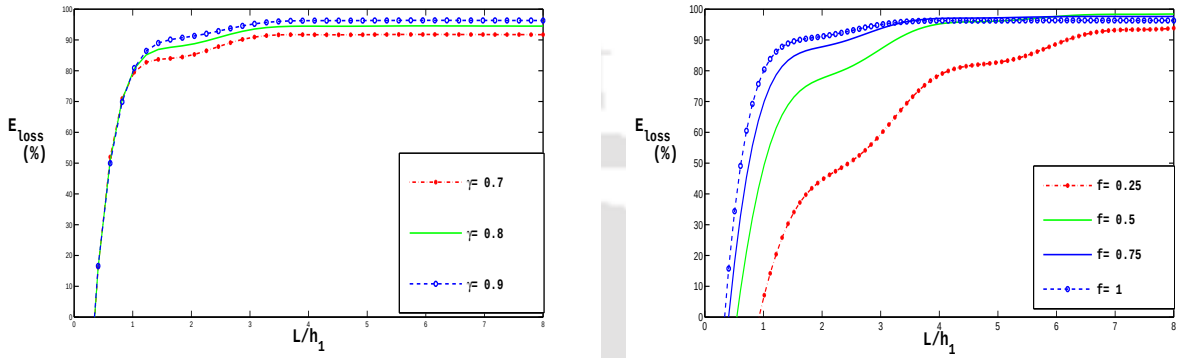

(a) for different γ (b) for different f

Figure 5.8: Energy loss (%) against dimensionless width of the porous structure L/h_1 with $\nu h_1 = 0.8$, $D/h_1 = 10$, $\theta = 0^0$, $N = 10$ and $p = 7$

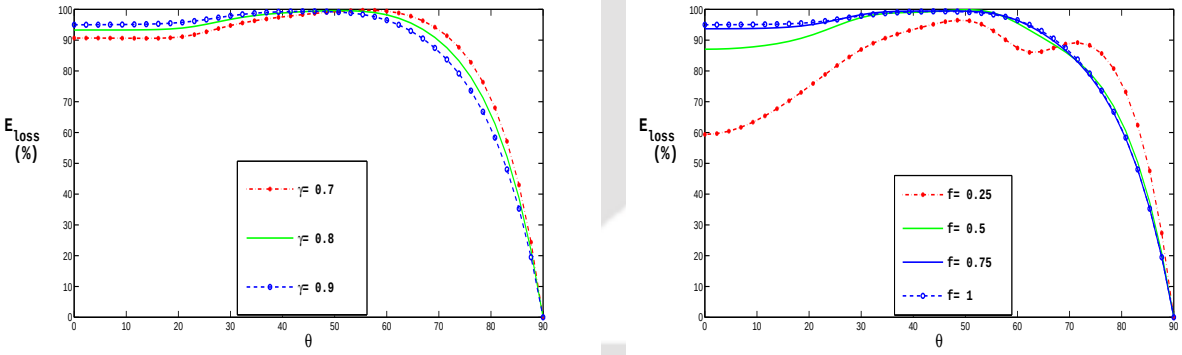

(a) for different γ (b) for different f

Figure 5.9: Energy loss (%) against angle of incidence θ with $\nu h_1 = 0.8$, $D/h_1 = 10$, $L/h_1 = 3$, $N = 10$ and $p = 7$

Now the energy loss of the wave, incident on the porous structure, is discussed graphically in figures 5.8–5.9.

Figure 5.8 depicts the energy loss (in %) against L/h_1 for different values of porosity and friction factor. Steep portion of the energy loss curve in figure 5.8(a) suggests the admissible width of the porous structure in order to be an effective wave absorber. Further increase in

L/h_1 results in obtaining a constant values of energy loss. This characteristic is observed for all the values of porosity taken. It is also found that higher porosity causes higher energy loss as compared to lower values of porosity. Minimum admissible width of the porous structure varies for different values of f (figure 5.8(b)). Larger width of the porous structure is required for lower values of f as compared to that corresponding to higher values of f. It is notable that higher f results in higher energy loss but converges to $E_{\text{loss}} = 96\%$ for larger width of the structure.

The effect of θ on scattering phenomenon for different values of porosity and friction factor is studied graphically from figure 5.9. Energy loss is very high for different values of porosity considered (figure 5.9(a)). But a steep descent in the energy loss curves is observed for large values of θ before converging to zero. It is observed that energy loss is higher for higher values of porosity when $\theta < 50^0$ (approx.). Beyond this range of θ, the curves cross each other and the characteristic reverses. Convergence in energy loss curves is found for higher values of friction factor taken (figure 5.9(b)). Maximum energy loss occurs in $40^0 < \theta < 50^0$, irrespective of the values of f. When $\theta = 0$, i.e., for normal incidence, energy loss is much higher for $f = 1$ than that for $f = 0.25$, but energy loss increases rapidly for $f = 0.25$ as θ increases. Oscillation in the energy loss curve is observed for $f = 0.25$ also.

5.5 Comparison with existing result

In order to ascertain that our model is effective, we compare our reflection coefficients plotted against the dimensionless porous structure width $k_{1,0}L$ with those in the work of Madsen (1983). This is accomplished by taking $h_1 = h_{p+1}$, i.e., by placing the porous structure on the horizontal ocean-bed instead of a p-step bottom. The excellent agreement between our result and Madsen's result can be observed from figure 4.25 in Chapter 4. This confirms that our model is valid and hence can be employed effectively to investigate various issues related to scattering of waves by a porous structure placed on a p-step bottom.

5.6 Special case: unbounded $(p+2)$-th region

5.6.1 Formulation

In this case, the formulation of the problem is same as that of the previous one except for the last region where no solid wall is placed, i.e., the last region is unbounded (figure 5.10).

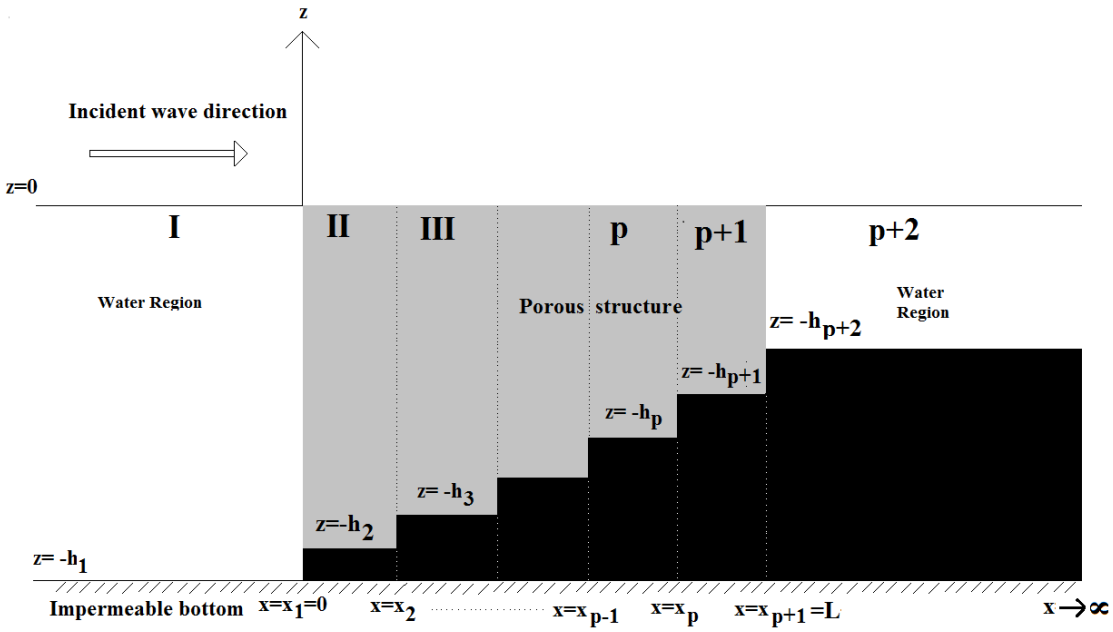

Figure 5.10: Schematic diagram of the problem of particular case

5.6.2 Solution

Potential functions ϕ_j, depth dependent function $Z_{j,n}$ $(n = 0, 1, \ldots, N)$ and $K_{j,n}$ in region j $(j = 1, 2, \ldots, p+1)$ satisfy the forms as described earlier. The only difference occurs in the potential function ϕ_{p+2} in region $p+2$ which, after truncating the infinite sum at $n = N$, can be written in the following form:

$$\phi_{p+2}(x,z) = \sum_{n=0}^{N} T_n \exp\left[\mathrm{i}K_{p+2,n}(x-L)\right] Z_{p+2,n}(h_{p+2}, z), \tag{5.13}$$

where T_0 is the complex transmission coefficient and T_n $(n = 1, 2, \ldots, N)$ define the decaying mode, $Z_{p+2,n}$ satisfies equation (5.8c) and $K_{p+2,n} = (k_{p+2,n}^2 - l^2)^{1/2}$ with $k_{p+2,n}$ satisfying equation (5.8b). It is to be noted that now complex transmission coefficient $|T_0|$ appears in $\phi_{p+2}(x,z)$ because of the consideration of an infinite fluid domain.

By applying the same technique adopted earlier, the following system of linear equations

is obtained:

$$\sum_{n=0}^{N}\mathcal{B}_{1,n,m}R_n - \mathrm{i}Ra_{2,m}A_{2,m} - \mathrm{i}R\exp(\mathrm{i}K_{2,m}l)a_{2,m}B_{2,m} = -\mathcal{B}_{1,0,m}, \tag{5.14a}$$

$$\sum_{n=0}^{N}\mathcal{B}_{1,n,m}K_{1,n}R_n + \gamma K_{2,m}a_{2,m}A_{2,m} - \gamma K_{2,m}\exp(\mathrm{i}K_{2,m}l)a_{2,m}B_{2,m} = K_{1,0}\mathcal{B}_{1,0,m}, \tag{5.14b}$$

$$\sum_{n=0}^{N}\exp(\mathrm{i}K_{j,n}l)\mathcal{B}_{j,n,m}A_{j,n} + \sum_{n=0}^{N}\mathcal{B}_{j,n,m}B_{j,n} - a_{i+1,m}A_{j+1,m} - \exp(\mathrm{i}K_{j+1,n}l)a_{j+1,m}B_{j+1,m} = 0, \tag{5.14c}$$

$$\sum_{n=0}^{N}K_{j,n}\exp(\mathrm{i}K_{j,n}l)\mathcal{B}_{j,n,m}A_{j,n} - \sum_{n=0}^{N}K_{j,n}\mathcal{B}_{j,n,m}B_{j,n} - K_{j+1,m}a_{i+1,m}A_{j+1,m} - K_{j+1,m}\exp(\mathrm{i}K_{j+1,n}l)a_{j+1,m}B_{j+1,m} = 0, \tag{5.14d}$$

$$\mathrm{i}R\sum_{n=0}^{N}\exp(\mathrm{i}K_{p+1,n}l)\mathcal{B}_{p+1,n,m}A_{p+1,n} + \mathrm{i}R\sum_{n=0}^{N}\mathcal{B}_{p+1,n,m}B_{p+1,n} - a_{p+2,m}T_m = 0, \tag{5.14e}$$

$$\gamma\sum_{n=0}^{N}K_{p+1,n}\exp(\mathrm{i}K_{p+1,n}l)\mathcal{B}_{p+1,n,m}A_{p+1,n} - \gamma\sum_{n=0}^{N}K_{p+1,n}\mathcal{B}_{p+1,n,m}B_{p+1,n} - K_{p+2,m}a_{p+1,m}T_m = 0. \tag{5.14f}$$

A matrix system can be constructed as per our earlier discussion and subsequently the scattering phenomenon can be discussed.

5.6.3 Numerical results

Here also the same study is carried out as was done for the previous case, with the same set of fixed parameter values.

Figure 5.11 depicts the variation of $|R_0|$ and $|T_0|$ against L/h_1 for different numbers of evanescent modes. Both $|R_0|$ and $|T_0|$ are independent of N and follow the same pattern observed in figure 5.2. But the difference occurs in $|R_0|$ (figure 5.11(a)) where, for thin porous structure, the value of $|R_0|$ is quite small and the minimum value occurs at a smaller value of L/h_1 compared to that in figure 5.2(a).

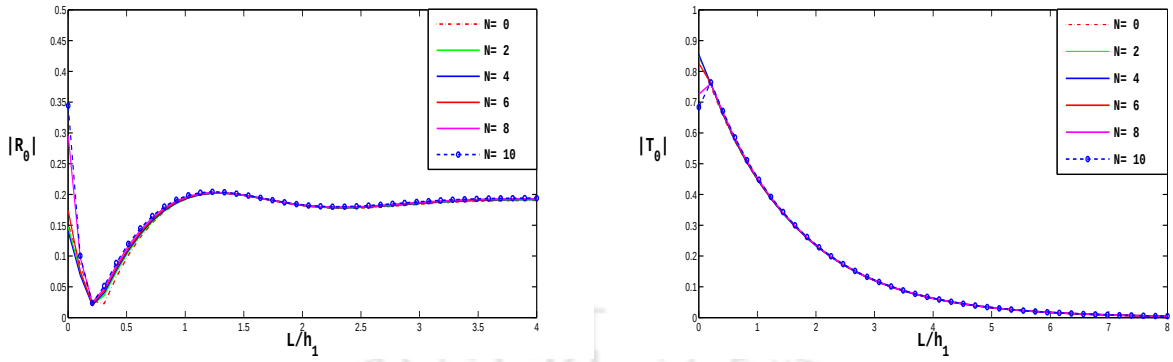

(a) Variation of $|R_0|$ (b) Variation of $|T_0|$

Figure 5.11: Effect of dimensionless width of the porous structure L/h_1 for different numbers of evanescent modes N with $\nu h_1 = 0.8$, $\theta = 0^0$, $\gamma = 0.9$, $f = 1$ and $p = 7$

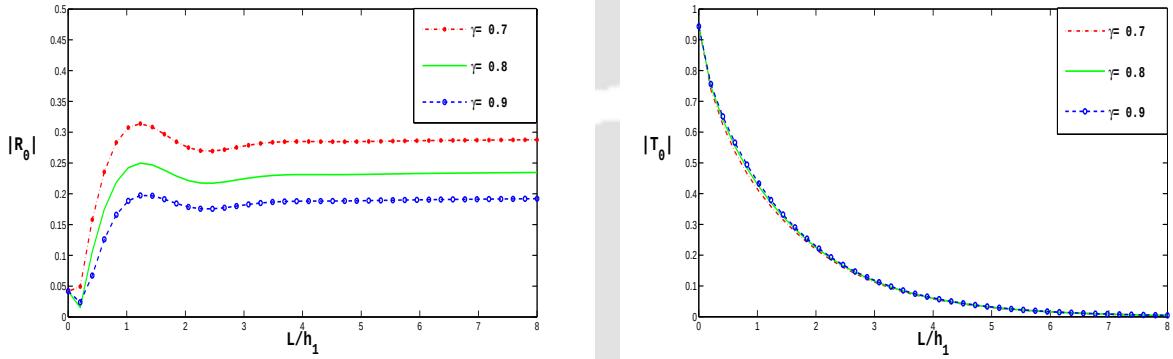

(a) Variation of $|R_0|$ (b) Variation of $|T_0|$

Figure 5.12: Effect of dimensionless width of the porous structure L/h_1 for different γ with $\nu h_1 = 0.8$, $\theta = 0^0$, $N = 10$, $f = 1$ and $p = 7$

The effect of porosity on scattering process is shown in figure 5.12. Reflection characteristic (figure 5.12(a)) is same as described in figure 5.3(a) except for the fact that the value of $|R_0|$ is small for small values of L/h_1 as compared to that in figure 5.3(a). Figure 5.12(b) describes the effect of L/h_1 on $|T_0|$ for different values of porosity. The nature of the curves is very similar to that in figure 5.3(b).

Further, figure 5.13 shows the variation of $|R_0|$ and $|T_0|$ against L/h_1 for different values of friction factor. Small value of friction factor ($f = 0.25$) results in oscillation in the values of $|R_0|$ which disappears with an increase in the value of friction factor (figure 5.13(a)). Moreover, higher friction factor gives rise to higher reflection except for a thin width of the porous structure. The nature of transmission (figure 5.13(b)) is same as described in figure 5.4(b).

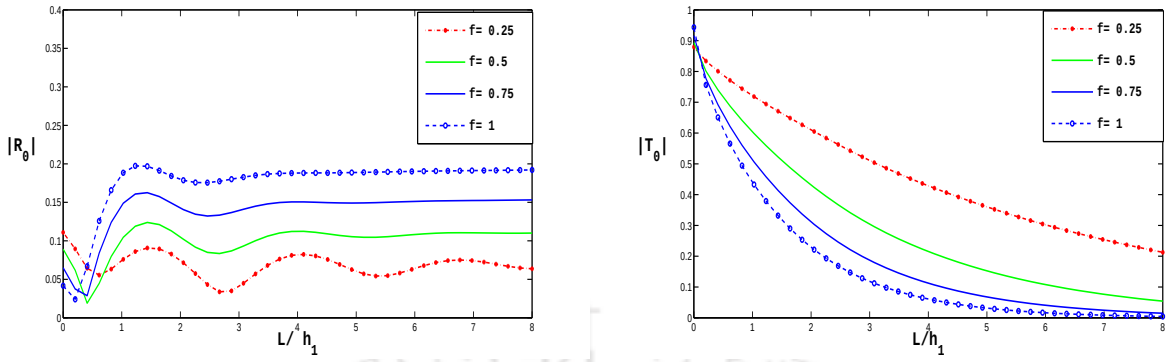

(a) Variation of $|R_0|$ (b) Variation of $|T_0|$

Figure 5.13: Effect of dimensionless width of the porous structure L/h_1 for different f with $\nu h_1 = 0.8$, $\theta = 0^0$, $N = 10$, $\gamma = 0.9$, and $p = 7$

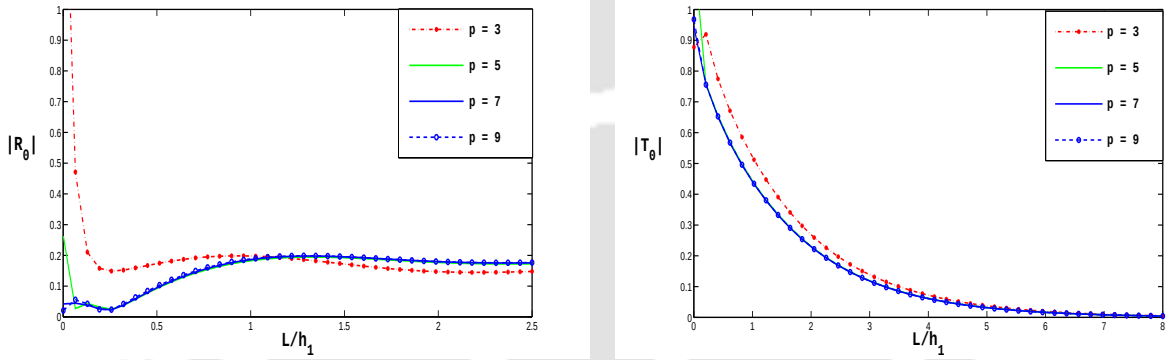

(a) Variation of $|R_0|$ (b) Variation of $|T_0|$

Figure 5.14: Effect of dimensionless width of the porous structure L/h_1 for different p with $\nu h_1 = 0.8$, $\theta = 0^0$, $N = 10$, $\gamma = 0.9$ and $f = 1$

The effect of number of steps on variation of $|R_0|$ and $|T_0|$ is shown in figure 5.14. In figure 5.14(a), the steep vertical portion of the curve for $p = 3$ defines the minimum admissible width of the porous structure. Convergence of the curves for higher values of p is observed from the graph. $|T_0|$ is very high for a thin porous structure (figure 5.14(b)) for all the values of p and decreases with an increase in the value of L/h_1 before vanishing for large values of L/h_1.

Figure 5.15 demonstrates scattering against the angle of incidence for different values of porosity. The nature of the curves is very similar to that discussed in figure 5.6.

Moreover, the study of scattering characteristics against θ for different values of friction factor is carried out (figure 5.16). Unlike the behaviour observed in figure 5.7(a), the oscillation in $|R_0|$ does not exist for $f = 0.25$ in figure 5.16(a). It is also noticeable that up to $\theta = 44^0$

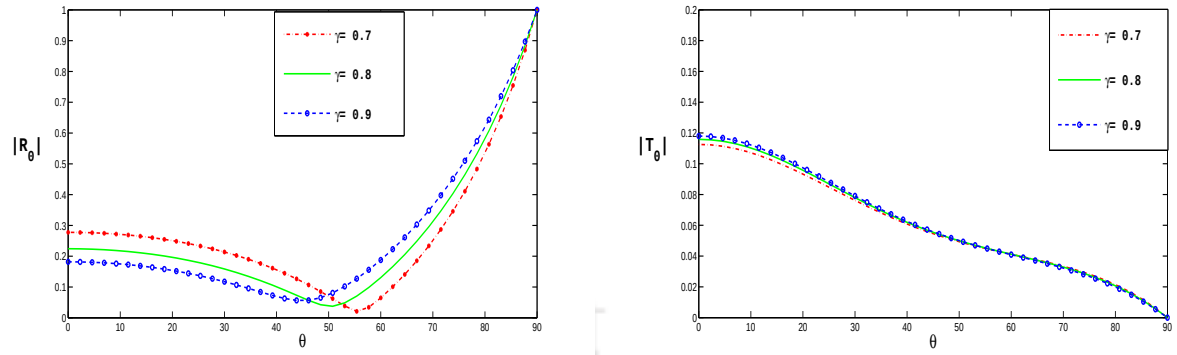

(a) Variation of $|R_0|$ (b) Variation of $|T_0|$

Figure 5.15: Effect of angle of incidence θ for different γ with $\nu h_1 = 0.8$, $L/h_1 = 3$, $N = 10$, $f = 1$ and $p = 7$

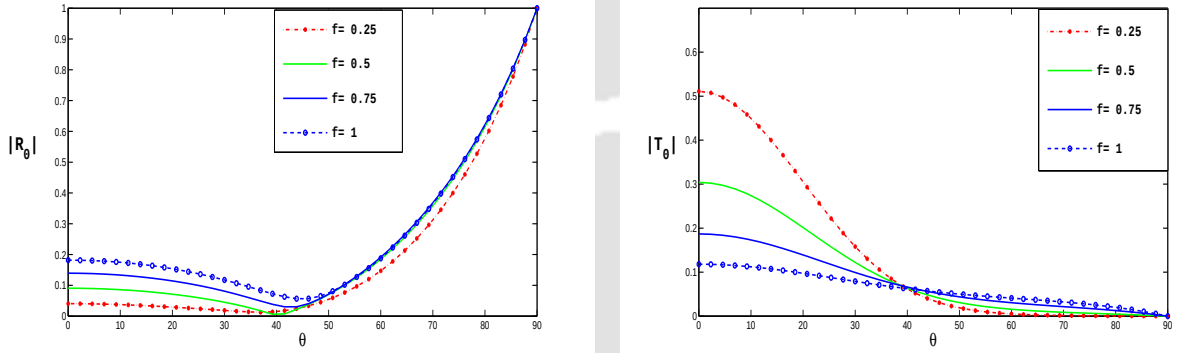

(a) Variation of $|R_0|$ (b) Variation of $|T_0|$

Figure 5.16: Effect of angle of incidence θ for different f with $\nu h_1 = 0.8$, $L/h_1 = 3$, $N = 10$, $\gamma = 0.9$, and $p = 7$

(approx.), higher values of friction factor result in relatively higher $|R_0|$ as against that of lower friction factor. Beyond the aforementioned value of θ, $|R_0|$ begins to increase with an increase in the value of θ. The nature of transmission characteristics (figure 5.16(b)) is very much similar as discussed in figure 5.7(b).

5.6.4 Energy loss

The associated energy loss is discussed in figures 5.17–5.18 due to the propagation of water wave through the porous structure.

In figure 5.17, energy loss against L/h_1 is discussed for different values of porosity and friction factor. Now when $L/h_1 \to 0$ (implying non-existence of porous structure), E_{loss}

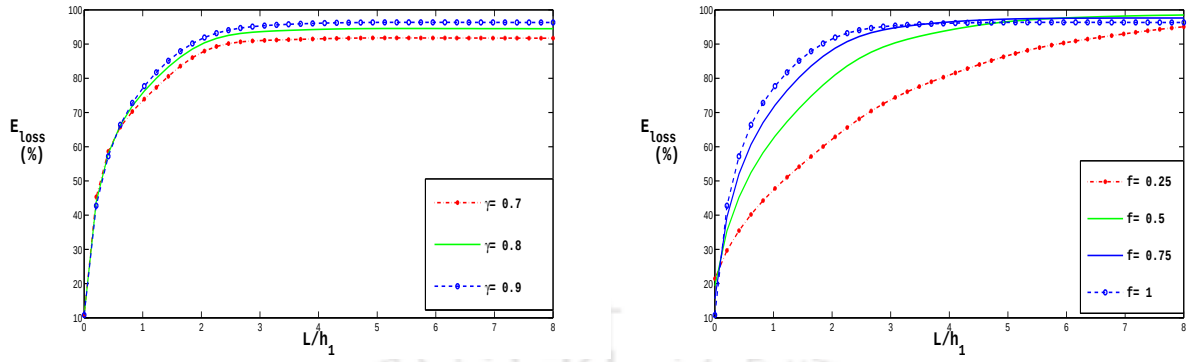

(a) for different γ (b) for different f

Figure 5.17: Energy loss (%) against dimensionless width of the porous structure L/h_1 with $\nu h_1 = 0.8$, $\theta = 0^0$, $N = 10$ and $p = 7$

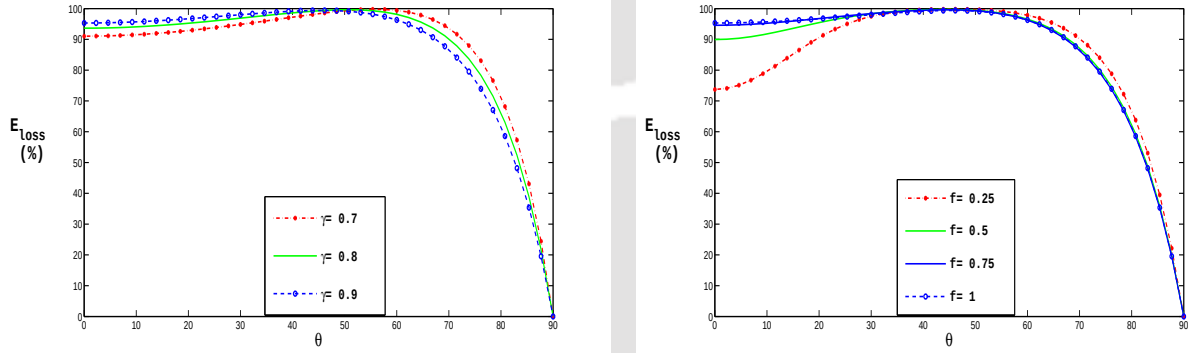

(a) for different γ (b) for different f

Figure 5.18: Energy loss (%) against angle of incidence θ with $\nu h_1 = 0.8$, $L/h_1 = 3$, $N = 10$ and $p = 7$

should be zero due to the absence of the porous structure, because incident wave coming from $x \to -\infty$ will transmit towards $x \to \infty$ without passing through any dissipative medium. It is noticeable that the curves do not exactly start from zero. This is due to the difference in height between region I and region $p + 2$ (Massel (1993)). Each of the energy loss curves increases rapidly with an increase in the value of L/h_1 and attains a constant value afterwards (figure 5.17(a)). For a thin porous structure, energy loss is independent of the values of porosity taken. Higher porosity gives rise to higher energy loss compared to the lower values of porosity. The analogous pattern exists for the energy loss for different values of friction factor. But the energy loss curves converge to each other at large values of L/h_1 unlike the curves for different porosity where they do not converge to each other for large values of L/h_1.

Figure 5.18 illustrates the nature of energy loss against θ for different values of porosity and friction factor. Energy loss for different values of porosity is shown in figure 5.18(a) which is very much similar to that of figure 5.9(a). It is noticeable that oscillation does not exist in the energy loss curve for $f = 0.25$ (figure 5.18(b)) unlike that in figure 5.9(b). Though energy loss for $f = 0.25$ is much less at $\theta = 0^0$ as compared to the other values of f considered, energy loss increases rapidly and attains the maximum value at other values of f.

5.7 Conclusion

Variation of the reflection coefficient and the dimensionless amplitude of the transmitted wave is studied against the dimensionless width of a porous structure for different values of number of evanescent modes, porosity, friction factor and steps, in the presence of a rigid vertical wall placed at a finite distance from the porous structure. It is observed that for a thin porous structure that, irrespective of the parameters considered, the reflection coefficient decreases rapidly from a very high value to attain a constant value which is observed for relatively higher dimensionless width of the porous structure. Reflection is independent of the number of evanescent modes considered whereas higher porosity gives rise to lower reflection. Lower values of friction factor leads to oscillation in reflection coefficient which disappears with an increase in the value of friction factor. That a minimum admissible length is required for the porous structure in order to be able to act as an effective wave absorber is observed from the very steep portion of the graphs. This admissible length of the porous structure decreases with an increase in number of steps. The dimensionless amplitude of the transmitted wave, irrespective of the different parameters considered, decreases from a very high value attained at lower values of the dimensionless width of the porous structure, to zero with an increase in the dimensionless width. The dimensionless amplitude of the transmitted wave is independent of the number of evanescent modes and porosity, but lower friction factor as well as lower number of steps result in higher transmission. The effect of the angle of incidence on scattering phenomena for different values of porosity and friction factor is also taken into account. Lower reflection is observed for higher values of porosity up to a fixed range of the angle of incidence beyond which the characteristic reverses and the reflection coefficients start assuming higher values after attaining the minimum reflection. Oscillation in the reflection coefficient for lower value of friction factor is observed. The dimensionless amplitude of the transmitted wave is independent of the values of porosity considered whereas lower friction factor results in higher amplitude which reduces with an increase in the angle of incidence. Further the energy loss

pattern is studied against dimensionless width of the porous structure and the angle of incidence for different values of porosity and friction factor. The requirement of minimum width of the porous structure is observed. Higher values of porosity and friction factor cause higher energy loss. Up to a fixed range of incident angle, higher porosity results in higher energy loss. Lower value of friction factor shows oscillation in energy loss. A convergence is observed for higher values of the friction factor. For the validity of our mathematical model, we compare our work with Madsen (1983) by plotting reflection coefficient against dimensionless width of the porous structure for different values of porosity and we find excellent agreement in this regard.

A special case of an unbounded $(p + 2)$-th region is considered and the same study is carried out corresponding to the same set of fixed parameter values. For this case also we observe similar reflection characteristics as in the earlier case except for when the structure is very thin in which case reflection is less. For lower values of friction factor, oscillation in the reflection coefficient and in the energy loss curves against dimensionless width as well as the angle of incidence do not exist.

Chapter 6

Wave damping by two thin vertical porous plates placed at finite distance from each other

In this chapter, the oblique water wave scattering problem due to the presence of two thin parallel vertical surface piercing porous plates of different heights and different porous effect parameters in an infinite channel of constant depth is solved with the help of linear water wave theory. Such structures can have useful applications such as continuation of water circulation below the penetration depth, usefulness of horizontal rigid plate connecting the tips of the vertical plates for pedestrians and vehicular traffic, control of wave reflection by changing the porosity of both the vertical plates, less adverse impact on the marine biology and ecosystem, etc. (Cox *et al.* (1998)). The effect of various relevant parameters on the reflection and transmission coefficients and hence on energy loss are investigated.

6.1 Mathematical formulation

It is fairly important to discuss some general features and equations which usually arise in wave propagation across a thin porous structure. Therefore, these are described separately in brief in the following subsection ahead of the formulation of the present problem. Some of the relevant equations are already discussed in Chapter 1.

6.1.1 General theory for flow across thin porous structure

Let us consider a vertical thin porous plate of width b placed at $x = 0$ where the x and z axes are defined along transverse and longitudinal directions, respectively, of the porous plate (figure 6.1). If L_0 is the length scale along the z-direction, it is assumed that

$$\frac{b}{L_0} \ll 1. \tag{6.1}$$

Small amplitude wave motion is considered within an undeformable porous medium. It is

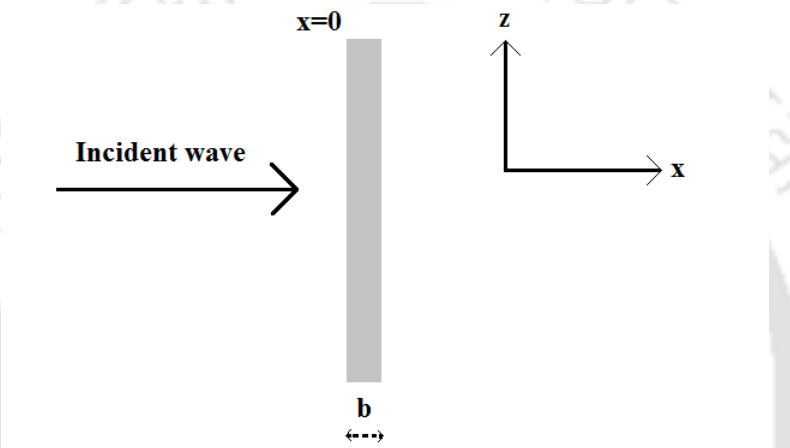

Figure 6.1: Schematic diagram for flow near porous boundary

assumed that the porous structure is homogeneous and isotropic. The fluid motion follows the continuity equation and the equation of motion as described in Section 1.3.

Now using the small thickness assumption (6.1) and the continuity of mass flux and pressure along the boundary $x = 0^{\pm}$, the following porous boundary condition can be obtained (Yu (1995))

$$\boldsymbol{u}|_{x=0^+} = \boldsymbol{u}|_{x=0^-} = \frac{k_0 G}{\rho\omega}\Big(p|_{x=0^-} - p|_{x=0^+}\Big) \quad \text{at} \quad x = 0^{\pm}, \tag{6.2}$$

where k_0 is the incident wave number and G is the dimensionless complex porous effect parameter defined by

$$G = \frac{\gamma}{k_0 b R} = G_r + \mathrm{i}G_i. \tag{6.3}$$

with $\mathrm{G_r}$ being the real part and $\mathrm{G_i}$ the imaginary part. It is noted that G = 0 when either $\gamma = 0$ or $R \to \infty$ (i.e., both the real and imaginary parts of R tend to ∞) or when the plate is solid. With an increase in either $\mathrm{G_r}$ or $\mathrm{G_i}$, the wall starts to behave like a permeable structure. In practice, G always possesses positive real and imaginary parts except when the resistance

effect against the flow dominates the inertial effect of the fluid inside the porous material, in which case G becomes real. Similarly, when the inertial effect dominates the resistance effect, G becomes purely imaginary.

When the velocity component is replaced by the gradient of its potential ,i.e.,

$$\mathbf{u}|_{x=0^+} = \frac{\partial \phi}{\partial x}|_{x=0^+} \qquad \text{and} \qquad \mathbf{u}|_{x=0^-} = \frac{\partial \phi}{\partial x}|_{x=0^-}, \tag{6.4}$$

and with the consideration of linearized Bernoulli's equation:

$$p|_{x=0^-} = \mathrm{i}\rho\omega\phi|_{x=0^-} \qquad \text{and} \qquad p|_{x=0^+} = \mathrm{i}\rho\omega\phi|_{x=0^+}, \tag{6.5}$$

Eq. (6.2) can be converted into the following equation:

$$\frac{\partial \phi}{\partial x}|_{x=0^-} = \frac{\partial \phi}{\partial x}|_{x=0^+} = \mathrm{i}k_0\mathrm{G}(\phi|_{x=0^-} - \phi|_{x=0^+}). \tag{6.6}$$

6.2 Boundary value problem

Let us consider two vertical thin porous plates of heights d_1 (first porous plate) and d_2 (second porous plate), respectively, a portion of each of which is above the free surface, placed at a distance L from each other in a water region of constant depth $z = -h$ from the mean free surface. The upper tips of the plates above the water region are connected by some rigid horizontal deck so as to make the structure stable and the deck used for some useful purpose. Such arrangements can be found in some earlier works, e.g., Cox *et al.* (1998). Using Cartesian coordinate system, the positive x-direction is defined as the direction of the normal on the sea-ward porous plate at $x = 0$ towards the second porous plate placed at $x = L$, the y-direction along the transverse direction of the porous plate, the positive z-direction vertically upwards and the mean free surface as $z = 0$. The semi-infinite regions, namely $-\infty < x < 0, -h < z < 0$ and $L < x < \infty, -h < z < 0$ are labeled as region I and region III, respectively, whereas the bounded region $0 < x < L, -h < z < 0$ is labeled as region II (figure 6.2). The fluid is assumed to be incompressible, homogeneous and inviscid, and the motion irrotational. We define three velocity potentials, namely $\Phi_1(x, y, z, t) = \phi_1(x, z)\exp(\mathrm{i}ly - \mathrm{i}\omega t)$, $\phi_2(x, y, z, t) = \phi_2(x, z)\exp(\mathrm{i}ly - \mathrm{i}\omega t)$ and $\phi_3(x, y, z, t) = \phi_3(x, z)\exp(\mathrm{i}ly - \mathrm{i}\omega t)$ in region I, region II and region III, respectively.

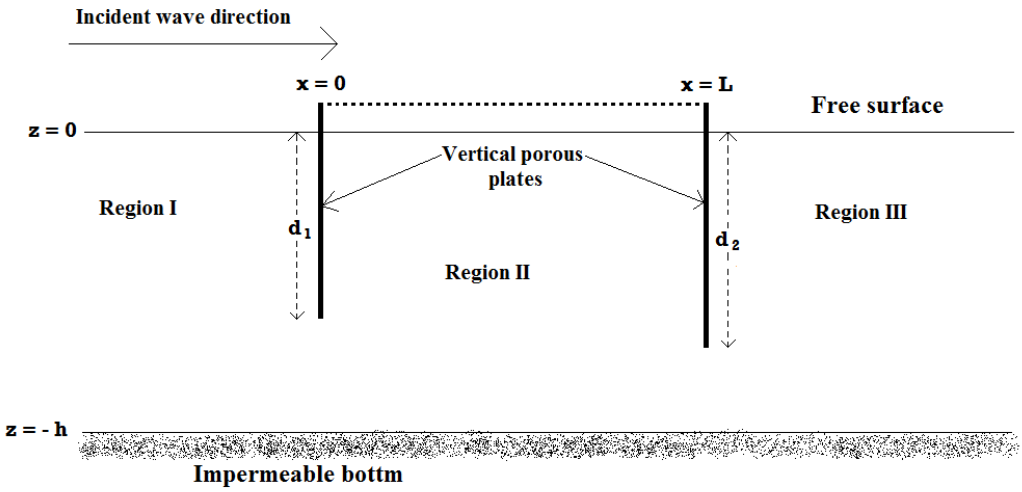

Figure 6.2: Schematic diagram of the problem

The governing equations and the boundary conditions in the three regions are

$$\nabla^2\phi_j - l^2\phi_j = 0; \qquad -h < z < 0, \tag{6.7a}$$

$$\frac{\partial\phi_j}{\partial z} - \nu\phi_j = 0; \qquad z = 0, \tag{6.7b}$$

$$\frac{\partial\phi_j}{\partial z} = 0; \qquad z = -h, \tag{6.7c}$$

where $j = 1, 2, 3$ refer to the regions I, II and III, respectively, each of which has different horizontal extent in the x-direction.

The matching conditions along the boundaries $x = 0$ and $x = L$ are given by

$$\frac{\partial\phi_1}{\partial x} = \frac{\partial\phi_2}{\partial x} = \mathrm{i}k_0 G_1(\phi_1 - \phi_2); \qquad x = 0, \quad -d_1 < z < 0, \tag{6.8a}$$

$$\frac{\partial\phi_1}{\partial x} = \frac{\partial\phi_2}{\partial x}; \qquad x = 0, \quad -h < z < -d_1, \tag{6.8b}$$

$$\phi_1 = \phi_2; \qquad x = 0, \quad -h < z < -d_1, \tag{6.8c}$$

$$\frac{\partial\phi_2}{\partial x} = \frac{\partial\phi_3}{\partial x} = \mathrm{i}k_0 G_2(\phi_1 - \phi_2); \qquad x = L, \quad -d_2 < z < 0, \tag{6.8d}$$

$$\frac{\partial\phi_2}{\partial x} = \frac{\partial\phi_3}{\partial x}; \qquad x = L, \quad -h < z < -d_2, \tag{6.8e}$$

$$\phi_2 = \phi_3; \qquad x = L, \quad -h < z < -d_2, \tag{6.8f}$$

where G_1 and G_2 are the dimensionless porous effect parameters of the perforated plates placed at $x = 0$ and $x = L$, respectively. It is to be noted that Eqs. (6.8a) and (6.8d) are direct consequence of Eq. (6.6) at $x = 0$ and $x = L$, respectively. Similarly, Eqs. (6.8c) and (6.8f) follow from Eq. (6.5) at $x = 0$ and $x = L$, respectively.

6.3 Reflection and transmission by the porous structure

The velocity potential $\phi_1(x, z)$ in region I can be written in the following form by using separation of variables method:

$$\phi_1(x,z) = [\exp(\mathrm{i}K_0 x) + R_0 \exp(-\mathrm{i}K_0 x)]Z_0(h,z) + \sum_{n=1}^{\infty} R_n \exp(-\mathrm{i}K_n x)Z_n(h,z), \tag{6.9}$$

where the depth-dependent function $Z_n(h, z)$ and K_n are, respectively, given by

$$Z_n(h,z) = \frac{\cosh k_n(h+z)}{\cosh k_n h}, \quad n = 0, 1, 2, \cdots, \tag{6.10a}$$

$$K_n = (k_n^2 - l^2)^{1/2}, \tag{6.10b}$$

where k_n satisfies the dispersion relation

$$\nu = k_n \tanh k_n h. \tag{6.10c}$$

We truncate the infinite sum at $n = N$ so as to consider a finite number of evanescent modes N only:

$$\phi_1(x,z) = [\exp(\mathrm{i}K_0 x) + R_0 \exp(-\mathrm{i}K_0 x)]Z_0(h,z) + \sum_{n=1}^{N} R_n \exp(-\mathrm{i}K_n x)Z_n(h,z). \tag{6.11}$$

Similarly, the velocity potentials $\phi_2(x, z)$ and $\phi_3(x, z)$, after truncating the infinite sums at $n = N$, can be written as

$$\phi_2(x,z) = \sum_{n=0}^{N} \{A_n \exp(\mathrm{i}K_n x) + B_n \exp[-\mathrm{i}K_n(x-L)]\} Z_n(h,z), \tag{6.12a}$$

$$\phi_3(x,z) = \sum_{n=0}^{N} \{T_n \exp[\mathrm{i}K_n(x-L)]\} Z_n(h,z), \tag{6.12b}$$

where A_n and B_n are arbitrary constants, T_0 is the complex transmission coefficient and T_n $(n = 1, 2, \ldots N)$ are related to the decaying modes of transmission. Energy loss due to the interaction of water waves with the porous plates is calculated by using the following result:

$$E_{\text{loss}} = (1 - |R_0|^2 - |T_0|^2) \times 100\%. \tag{6.13}$$

Now using the continuity of the horizontal velocity components $\frac{\partial \phi_1}{\partial x}$ and $\frac{\partial \phi_2}{\partial x}$ along $x = 0$, $-h < z < 0$ (using equations (6.8a) and (6.8b)), we obtain

$$R_0 = 1 - A_0 + B_0 \exp(\mathrm{i}k_0 L), \tag{6.14a}$$

$$R_n = B_n \exp(\mathrm{i}k_n L) - A_n. \tag{6.14b}$$

Further, using the second equality in equation (6.8a), we get

$$\sum_{n=0}^{N} (k_n + 2k_0 G_1) A_n Z_n - \sum_{n=0}^{N} k_n \exp(\mathrm{i}k_n L) B_n Z_n - 2k_0 G_1 Z_0 = 0, \qquad -d_1 < z < 0. \tag{6.15a}$$

Similarly, equation (6.8c) results in

$$2Z_0 - 2\sum_{n=0}^{N} A_n Z_n = 0, \qquad -h < z < d_1. \tag{6.15b}$$

We use the least square method, the usefulness of which is detailed in the next section, to find the unknown coefficients appearing in equations (6.15a,b). In order to do so, we define a new quantity $\mathcal{H}(z)$ in the following form:

$$\mathcal{H}(z) = \begin{cases} \displaystyle\sum_{n=0}^{N} (k_n + 2k_0 G_1) A_n Z_n - \sum_{n=0}^{N} k_n \exp(\mathrm{i}k_n L) B_n Z_n - 2k_0 G_1 Z_0, & -d_1 < z < 0, \\ \displaystyle 2Z_0 - 2\sum_{n=0}^{N} A_n Z_n, & -h < z < -d_1. \end{cases} \tag{6.16}$$

The requirement of the method is that the relation

$$\int_{-h}^{0} |\mathcal{H}(z)|^2 \mathrm{d}z = \text{ minimum} \tag{6.17}$$

holds in order to satisfy $\mathcal{H}(z) = 0$ in the region $-h < z < 0$.

Then minimizing the integral in equation (6.17) with respect to each of A_m $(m = 0, 1, \ldots N)$, the following integral equation is obtained:

$$\int_{-h}^{0} \mathcal{H}^*(z) \frac{\partial \mathcal{H}(z)}{\partial A_m} \mathrm{d}z = 0, \quad m = 0, 1, \ldots N, \tag{6.18}$$

where $\mathcal{H}^*(z)$ denotes the complex conjugate of $\mathcal{H}(z)$.

A system of linear equations is obtained from the above equation, after integrating with respect to z, as follows:

$$\sum_{n=0}^{N} p_{m,n}^{(1)} A_n^* + \sum_{n=0}^{N} q_{m,n}^{(1)} B_n^* = r_m^{(1)}, \quad m = 0, 1, \ldots N, \tag{6.19}$$

where

$$p_{m,n}^{(1)} = (k_n^* + 2k_0 G_1^*)(k_m + 2k_0 G_1) \int_{-d_1}^{0} Z_m Z_n \mathrm{d}z + 4 \int_{-h}^{-d_1} Z_m Z_n \mathrm{d}z, \tag{6.20a}$$

$$q_{m,n}^{(1)} = -(k_m + 2k_0 G_1) k_n^* \zeta_n^* \int_{-d_1}^{0} Z_m Z_n \mathrm{d}z, \tag{6.20b}$$

$$r_m^{(1)} = 2k_0 G_1^* (k_m + 2k_0 G_1) \int_{-d_1}^{0} Z_m Z_0 \mathrm{d}z + 4 \int_{-h}^{-d_1} Z_m Z_0 \mathrm{d}z, \tag{6.20c}$$

with $\zeta_n = \exp(\mathrm{i}k_n L)$ and * in the above equations and elsewhere in the manuscript denotes the complex conjugate of the corresponding quantity.

Further, making use of the continuity of $\dfrac{\partial \phi_2}{\partial x}$ and $\dfrac{\partial \phi_3}{\partial x}$ along $x = L$, $-h < z < 0$ (using equations (6.8d) and (6.8e)), we obtain

$$T_n = A_n \exp(\mathrm{i}k_n L) - B_n. \tag{6.21}$$

Using the second equality of equation (6.8d), the following equation is obtained:

$$\sum_{n=0}^{N} k_n \exp(\mathrm{i}k_n L) A_n Z_n - \sum_{n=0}^{N} (k_n + 2k_0 G_2) B_n Z_n = 0. \tag{6.22a}$$

Also, equation (6.8f) gives rise to the following equation

$$\sum_{n=0}^{N} 2B_n Z_n = 0. \tag{6.22b}$$

Now using the least square method, a system of linear equations is obtained as

$$\sum_{n=0}^{N} p^{(2)}_{m,n} A^*_n + \sum_{n=0}^{N} q^{(2)}_{m,n} B^*_n = 0, \quad m = 0, 1, \ldots N, \tag{6.23}$$

where

$$p^{(2)}_{m,n} = -k^*_n \zeta^*_n (k_m + 2k_0 G_2) \int_{-d_2}^{0} Z_m Z_n \mathrm{d}z, \tag{6.24a}$$

$$q^{(2)}_{m,n} = (k^*_n + 2k_0 G^*_2)(k_m + 2k_0 G_2) \int_{-d_2}^{0} Z_m Z_n \mathrm{d}z + 4 \int_{-h}^{-d_1} Z_m Z_0 \mathrm{d}z. \tag{6.24b}$$

From the system of equations given by equations (6.19) and (6.23), the following matrix system is constructed:

$$\begin{aligned} \boldsymbol{AX} &= \boldsymbol{c}, \\ \text{where } \boldsymbol{A} &\quad \text{is a square matrix of size } [2(N+1)], \\ \boldsymbol{X} &= [A^*_0, \ldots A^*_N, B^*_0, \ldots, B^*_N]^T \\ &\quad \text{is the unknown vector,} \\ \text{and } \quad \boldsymbol{c} &= [r_0, \ldots, r_{N+1}, \underbrace{0, \ldots\ldots\ldots 0}_{\text{(N+1)-times}}]^T. \end{aligned}$$

The above matrix system can be solved to get the unknown coefficients A^*_n and B^*_n, and consequently $|R_0|$, $|T_0|$ and E_{loss} can be calculated by using equations (6.14a), (6.21) and (6.13), respectively.

6.4 Numerical results

We would like to mention, at this point, about least square method which was developed by Kelman and Chester (1973) to solve dual series relation. The convergence of this method was discussed theoretically by Finerman and Kelman (1974) and this theory was found to be

applicable to square integrable functions. Hence, the square-root singularity at the tip of the porous plates can be treated efficiently by employing this method. Also this method is much faster than the matched eigenfunction expansion method and the advantage is in being able to obtain the solution completely with much faster convergence. This method has been adopted to solve water wave scattering and trapping problems by various researchers earlier.

N \ L/h	0.0001	0.4212	0.8422	1.2632	1.6842	2
0	0.252923373	0.285655784	0.228822633	0.125197866	0.071317032	0.136033049
5	0.360347281	0.408930381	0.312442937	0.125696654	0.096926336	0.221748634
10	0.374952355	0.432282485	0.326918511	0.120252508	0.108295308	0.242889554
15	0.381019453	0.442334148	0.333289337	0.117418024	0.114618384	0.253252107
20	0.38275353	0.446591999	0.336044037	0.116123678	0.11770863	0.258053857
25	0.383459699	0.448296535	0.337181847	0.115513265	0.119135701	0.260252026
30	0.383630865	0.448961454	0.337640719	0.115240305	0.119758849	0.261215415

Table 6.1: Convergence of $|R_0|$ at different values of L/h_1; $d_1 = 0$, $d_2 = h/2$ and $G_2 = 0$

Tables 6.1 and 6.2 show the convergence of $|R_0|$ and $|T_0|$, respectively, for the number of evanescent modes at different values of L/h_1. From the tables, it is evident that taking $N = 30$ gives a 2-digit accuracy on both $|R_0|$ and $|T_0|$, which are quite satisfactory for engineering purposes.

N \ L/h	0.0001	0.4212	0.8422	1.2632	1.6842	2
0	0.839374354	0.804248035	0.790777604	0.772174015	0.750227169	0.739215084
5	0.886911113	0.804854654	0.796073177	0.764099122	0.712913269	0.683069754
10	0.900080369	0.816151037	0.812879539	0.7800272	0.721512942	0.68630555
15	0.907892016	0.823440194	0.82348777	0.790902599	0.728909927	0.690915711
20	0.912831646	0.827281661	0.829032435	0.796802821	0.733259026	0.693929436
25	0.915208534	0.829411913	0.832056776	0.800156122	0.735951602	0.695974188
30	0.91645681	0.830483621	0.833559848	0.80186305	0.737386978	0.697111937

Table 6.2: Convergence of $|T_0|$ at different values of L/h_1; $d_1 = 0$, $d_2 = h/2$ and $G_2 = 0$

6.4.1 Comparison with existing result

In order to validate the current method, comparison is made with the corresponding cases available in the literature. Current configuration of the problem can be converted to one of

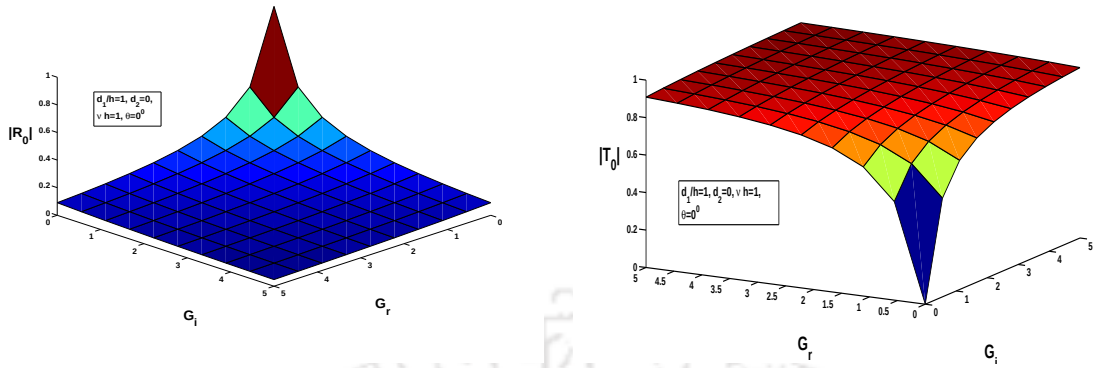

(a) Variation of $|R_0|$ (b) Variation of $|T_0|$

Figure 6.3: Effect of (G) with $\nu h = 1$, $\theta = 0^0$ and $N = 30$

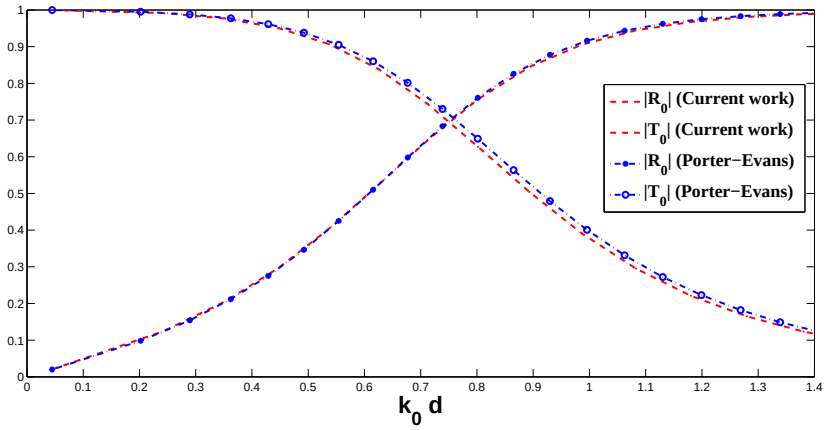

Figure 6.4: Comparison between Porter and Evans (1995) and the current work

the configurations considered by Yu (1995) by taking $d_1/h = 1$ and $d_2 = 0$. It is shown in Figs. 6.3 that as both the real and imaginary parts of G tend towards zero (i.e., $\mathrm{G_r} \to 0$ and $\mathrm{G_i} \to 0$), full reflection takes place whereas transmission vanishes at the same time. This same observation was justified by Yu (1995) and hence G = 0 can be considered as a rigid wall.

With $d_1 = 0$, $d_2 = h/2$ and $G_2 = 0$, the structure reduces to a single rigid vertical plate which was studied by Porter and Evans (1995). Comparison of the reflection and transmission coefficients obtained in the present problem with those of Porter and Evans (1995) is shown in figure 6.4.

By assuming $d_1 = d_2$ and $\mathrm{G}_2 = 0$, the current configuration matches with the problem considered by Liu and Li (2011a). Figure 6.8 shows the comparison where the parameter values are $d_1/h = 1, \nu h = 1.6, \mathrm{G}_1 = 0.5$.

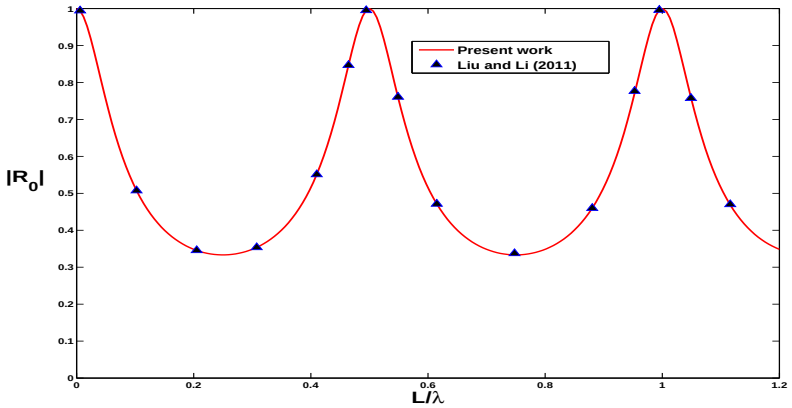

Figure 6.5: Comparison between Liu and Li (2011a) and the current work

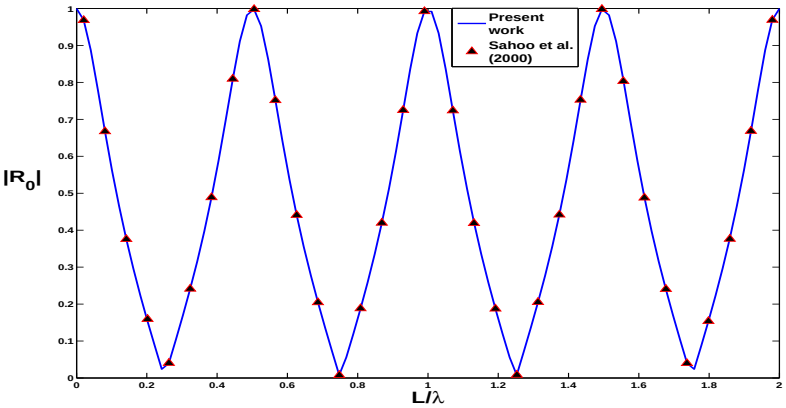

Figure 6.6: Comparison between Sahoo *et al.* (2000b) and the current work

Another comparison is made with the work of Sahoo *et al.* (2000b). With the consideration of $d_2/h = 1$ and $G_2 = 0$, the geometry of the problem exactly matches with one of the configurations considered by Sahoo *et al.* (2000b). The parameter values considered for the study are $d_1/h = 1, \nu h = 1$ and $G_1 = 1$ and Fig. 6.9 illustrates good agreement between the results.

Good agreement of the results shows the validation of the formulation of the current problem and it confirms that further study on scattering process for such porous plate problems for different parameters can be carried out.

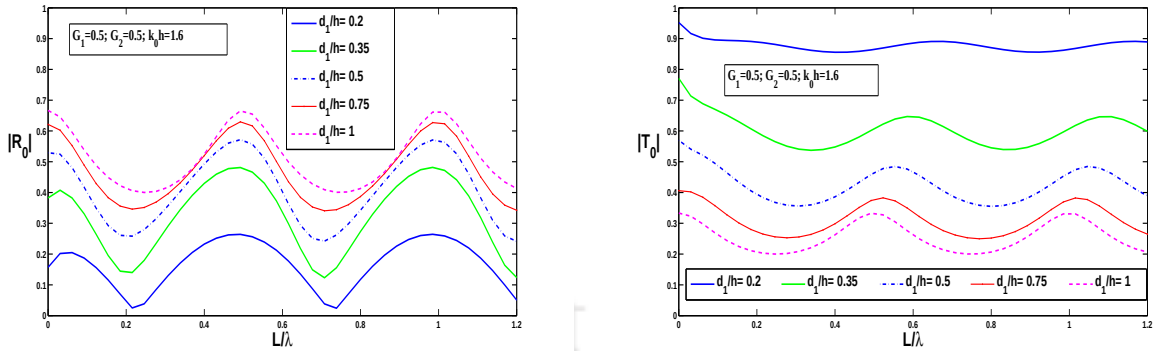

(a) Variation of $|R_0|$ (b) Variation of $|T_0|$

Figure 6.7: Effect of L/λ for different d_1/h with $G_1 = G_2 = 0.5$, $k_0h = 1.6$, $d_2 = d_1$, $\theta = 0^0$ and $N = 30$

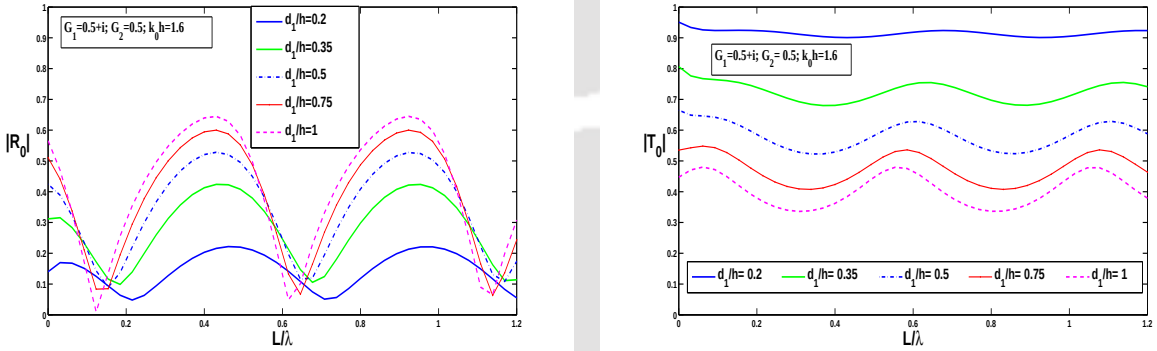

(a) Variation of $|R_0|$ (b) Variation of $|T_0|$

Figure 6.8: Effect of L/λ for different d_1/h with $G_1 = 0.5 + \mathrm{i}$, $G_2 = 0.5$, $k_0h = 1.6$, $d_2 = d_1$, $\theta = 0^0$ and $N = 30$

6.4.2 Results

In figure 6.7, the reflection and transmission coefficients are plotted against dimensionless distance L/λ (λ being the wavelength of incident wave) between the porous plates for different values of the dimensionless height d_1/h of the first plate. Some specific values of other parameters are taken, such as $G_1 = 0.5$, $G_2 = 0.5$, $k_0h = 1.6$ and $d_2 = d_1$. Oscillating natures of $|R_0|$ and $|T_0|$ are observed for these values of d_1/h. Both the minimum and maximum values of $|R_0|$ are obtained at specific values of L/λ corresponding to all values of d_1/h but on the other hand, optimum values of $|R_0|$ increase with an increase in the value of d_1/h. In the case of $|T_0|$, reverse characteristic is observed, i.e., with an increase in d_1/h, $|T_0|$ decreases with the addition of the fact that optimum values of $|T_0|$ show a leftward movement with an increase

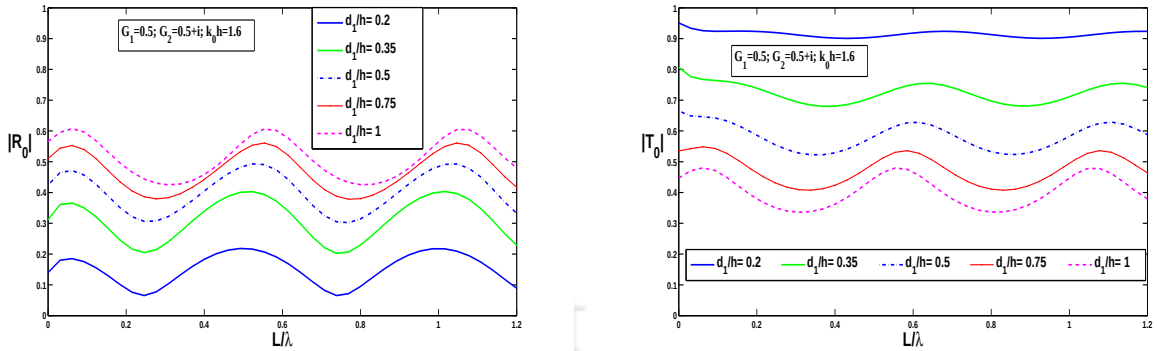

(a) Variation of $|R_0|$ (b) Variation of $|T_0|$

Figure 6.9: Effect of L/λ for different d_1/h with $G_1 = 0.5$, $G_2 = 0.5 + \mathrm{i}$, $k_0h = 1.6$, $d_2 = d_1$, $\theta = 0^0$ and $N = 30$

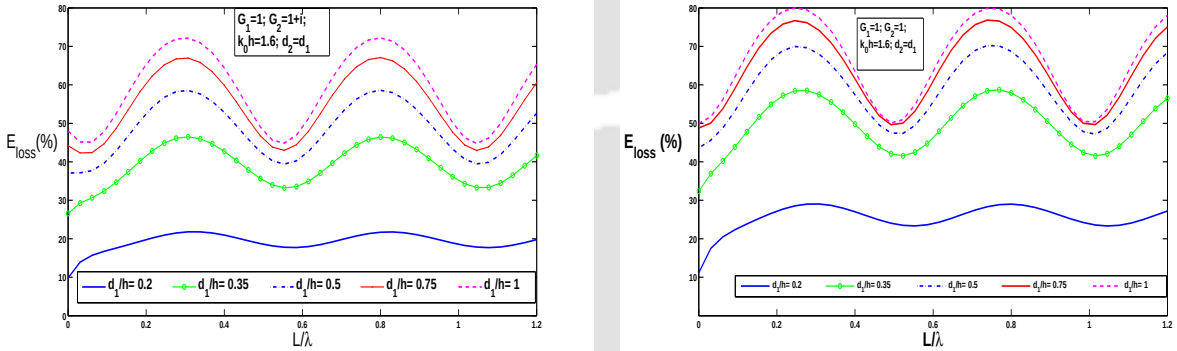

(a) $G_2 = 1 + \mathrm{i}$ (b) $G_2 = 1$

Figure 6.10: Energy loss (%) against L/λ for different values of d_1/h with $G_1 = 1$, $k_0h = 1.6$, $d_2 = d_1$, $\theta = 0^0$ and $N = 30$

in the value of d_1/h.

The same study is carried out by adding an imaginary quantity to G_1, i.e., $G_1 = 0.5 + \mathrm{i}$ and the results are shown in figure 6.8. By comparing figure 6.8(a) with figure 6.7(a), a significant amount of change in the minimum value of $|R_0|$ is observed for $d_1/h = 0.35, 0.5, 0.75, 1$. Hence it can be deduced that the imaginary part of G_1, which causes the inertial effect, plays a significant role in reducing reflection by the porous plate. But by comparing figure 6.8(b) with figure 6.7(b), it is found that the value of $|T_0|$ increases for those aforesaid values of d_1/h which, on the other hand, present significantly reduced values of $|R_0|$.

Further study is carried out for the coefficients $|R_0|$ and $|T_0|$ by plotting them against L/λ with $G_1 = 0.5$ and by adding an imaginary quantity to G_2: $G_2 = 0.5 + \mathrm{i}$ (figure 6.9). Comparing

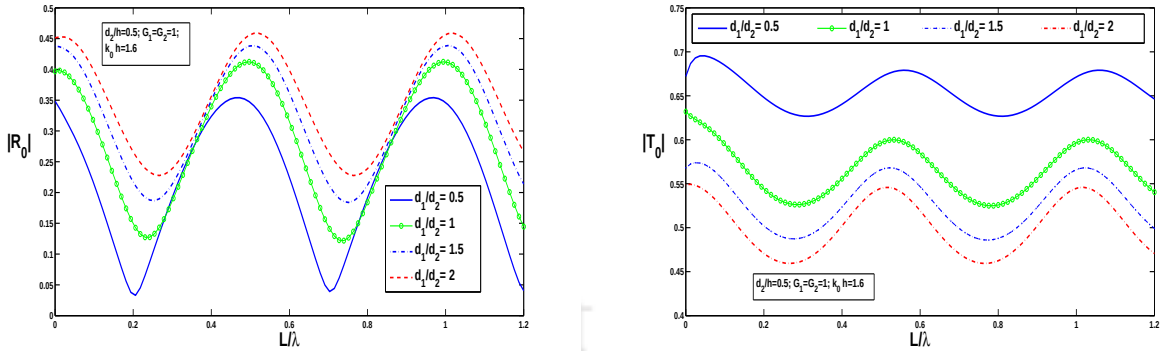

(a) Variation of $|R_0|$ (b) Variation of $|T_0|$

Figure 6.11: Effect of L/λ for different values of d_1/h with $d_2/h = 0.5$, $G_1 = G_2 = 1$, $k_0h = 1.6$, $\theta = 0^0$ and $N = 30$

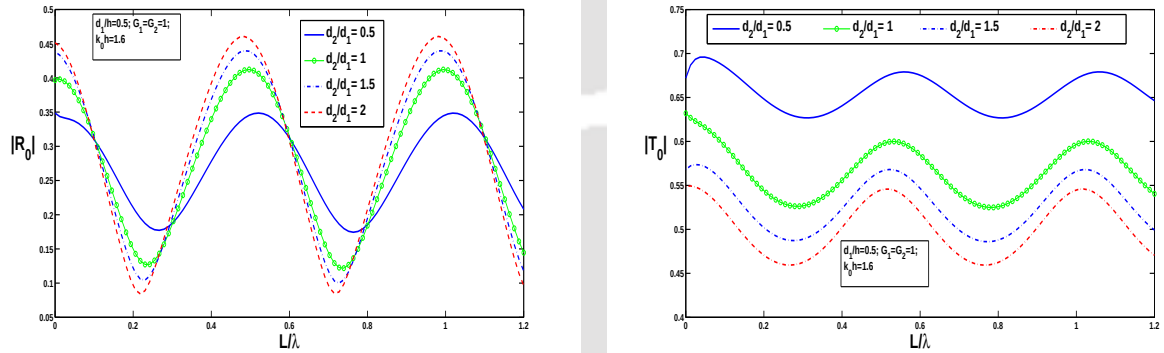

(a) Variation of $|R_0|$ (b) Variation of $|T_0|$

Figure 6.12: Effect of L/λ for different values of d_2/h with $d_1/h = 0.5$, $G_1 = G_2 = 1$, $k_0h = 1.6$, $\theta = 0^0$ and $N = 30$

figure 6.9 with figure 6.7, an increase and a decrease in the minimum and maximum values of $|R_0|$, respectively, are observed with the value of $|T_0|$ increasing significantly. One interesting observation made by comparing figures 6.8(b) and 6.9(b) is that interchanging the values of G_1 and G_2 does not lead to any change in $|T_0|$.

The energy loss is plotted against L/λ for different values of d_1/h in figure 6.10. It is observed that higher values of d_1/h result in higher energy loss. Also, more oscillation in the energy loss curve is found corresponding to higher values of d_1/h. But from comparison of these two curves, it is evident that, for a specific value of d_1/h, real values of G_2 show higher maximum value in energy loss as compared to that due to the complex values of G_2.

So far our investigation is limited to the consideration of porous plates of the same height

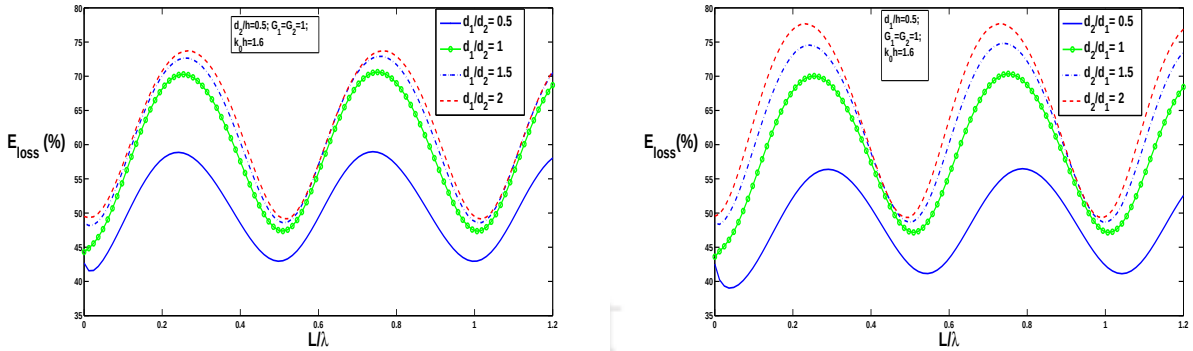

(a) Against various d_1/d_2 with $d_2/h = 0.5$ (b) Against various d_2/d_1 with $d_1/h = 0.5$

Figure 6.13: Energy loss (%) against L/λ with $G_1 = G_2 = 1$, $k_0h = 1.6$, $\theta = 0^0$ and $N = 30$

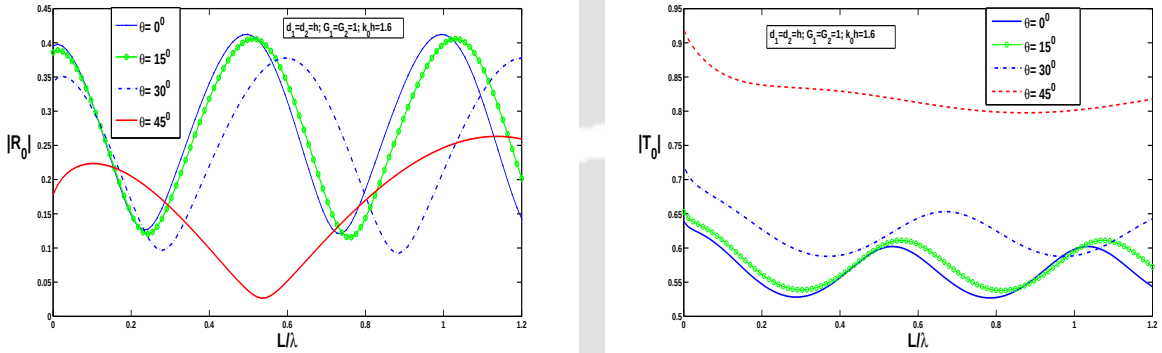

(a) Variation of $|R_0|$ (b) Variation of $|T_0|$

Figure 6.14: Effect of L/λ for different values of angle of incidence θ with $d_1 = d_2 = h/2$, $G_1 = G_2 = 1$, $k_0h = 1.6$ and $N = 30$

only. Hence a separate investigation is carried out by taking different heights of the porous plates ($d_1 \neq d_2$). Figure 6.11 shows the variation of $|R_0|$ and $|T_0|$ against L/λ for different values of d_1/d_2 with $d_2/h = 0.5$. It is observed from figure 6.11(a) that optimum values of the reflection coefficient are obtained periodically with respect to the values of L/λ irrespective of the values of d_1/d_2 but higher values of d_1/d_2 result in higher reflection and all the optimum values are less than 0.45. Moreover, the optimum values tend to shift rightward for higher values of d_1/d_2. The transmission coefficient follows the same oscillation pattern as in $|R_0|$, but higher values are obtained corresponding to lower values of d_1/d_2 (figure 6.11(b)).

Study on the reflection and transmission coefficients against L/λ for different values of d_2/d_1 is also carried out with the parameter d_1/h fixed at 0.5 (figure 6.12). Here both the minimum and maximum values of $|R_0|$ occur corresponding to the maximum value of d_2/d_1

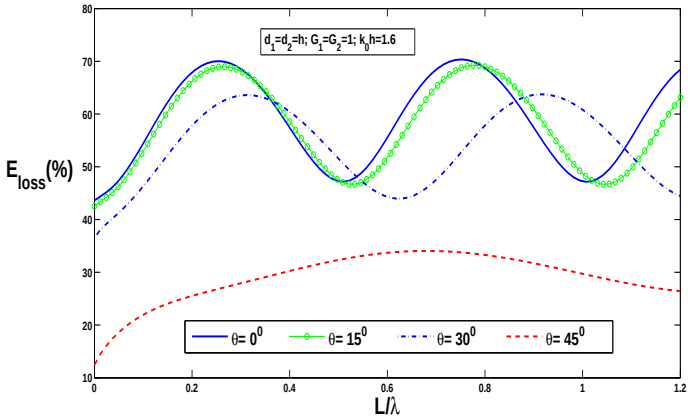

Figure 6.15: Energy loss (%) against L/λ with $d_1 = d_2 = h/2$, $G_1 = G_2 = 1$, $k_0h = 1.6$ and $N = 30$

considered and they are obtained periodically with respect to L/λ. By comparing figure 6.11(b) with figure 6.12(b), it is observed that $|T_0|$ is invariant under the interchange of the positions of the plates.

A study on energy loss (in %) against L/λ is carried out in figure 6.13. First, in figure 6.13(a), energy loss for different values of d_1/d_2 with $d_2/h = 0.5$ are plotted and periodic nature of the curves is observed. It is also observed that higher values of d_1/d_2 give rise to higher energy loss and the point of optimum values slightly shift towards right with an increase in the value of d_1/d_2. Figure 6.13(b) illustrates energy loss for different values of d_2/d_1 with $d_1/h = 0.5$. The same nature of the curves is observed as was the case in figure 6.13(a) with an exception that optimum values shift slightly towards left with an increase in the value of d_2/d_1. Moreover, by comparing figure 6.13(a) with figure 6.13(b), it is observed that greater height of second porous plate results in maximum energy loss in comparison with the energy loss caused by first porous plate with greater height.

An investigation on scattering process for various angles of incidence θ is also carried out in figure 6.14. It is observed that the reflection coefficient shows oscillation with respect to L/λ but with an increase in the value of θ, the period of oscillation increases. Moreover higher maximum reflection is found for lower angle of incidence (figure 6.14(a)). In the case of the transmission coefficient (figure 6.14(b)), the same nature of the curves is observed as in the case of the reflection coefficient with the exception that higher values of θ result in higher maximum transmission.

Energy loss is also plotted against L/λ for different values of θ in figure 6.15. Periodic

oscillation in the curves is observed with higher periodicity corresponding to higher value of θ. Moreover, higher energy loss is found for lower angles of incidence.

6.5 Conclusion

Based on linear water wave theory, oblique water wave scattering process by two thin parallel fixed vertical porous plates of different porosity and different porous effect parameters in an infinite channel of finite depth is investigated. Boundary value problems are set up in each region, and with the help of matching conditions across each porous plate as well as the virtual boundaries and the orthogonality of the depth dependent functions, a system of linear equations is obtained solving which the reflection and transmission coefficients and consequently energy loss (in %) are obtained. The effects of the porous effect parameters and the heights of both the porous plates, the angle of incidence on scattering process are studied graphically. Periodic oscillation is observed in all the graphs. Moreover, keeping the height of the porous plates fixed, it is found that by increasing the inertial effect of the porous plate, lower reflection is obtained but the corresponding transmission is high. But higher energy loss is obtained by reducing the inertial effect of the porous plates. For the second porous plate with its properties fixed, higher reflection occurs in the presence of the first porous plate of greater height and lower reflection for lesser height. But when the properties of the first porous plate are fixed, both the minimum and maximum values of reflection occur when the second porous plate is of greater height. One interesting observation is that interchanging the position of the plates does not affect the transmission coefficient. Maximum energy loss is achieved when the height of the second porous plate is greater and the angle of incidence is lower.

Chapter 7

Wave damping by two thin fully submerged vertical porous plates placed at finite distance from each other

In this chapter, the oblique water wave scattering problem due to the presence of two thin fully submerged parallel vertical porous plates of different heights and different porous effect parameters in an infinite channel of constant depth is solved with the help of linear water wave theory. The effect of various relevant parameters on the reflection and transmission coefficients and hence on energy loss are investigated. The problem considered in Chapter 6 can be considered a special case of this chapter when the upper tips of the porous plates touch the free surface.

7.1 Mathematical formulation

The mathematical theory for flow across the porous plates is described in Section 6.1.1.

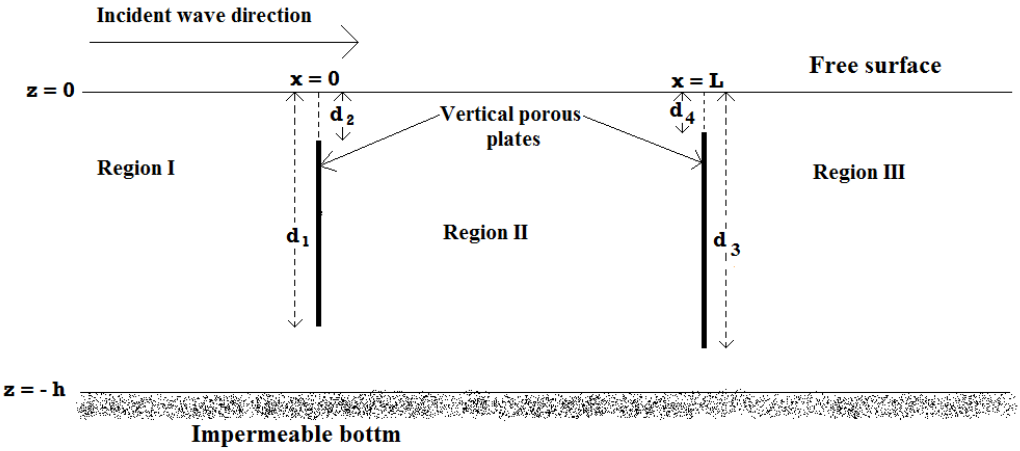

Figure 7.1: Schematic diagram of the problem

7.2 Boundary value problem

Let us consider two fully submerged thin vertical porous plates of different heights at $x = 0$ (first porous plate) and $x = L$ (second porous plate), respectively, in a water region of constant depth h from the mean free surface. Using Cartesian coordinate system, the positive x-direction is defined as the direction of the normal on the first porous plate towards the second porous plate, the y-direction along the transverse direction of the porous plate, the positive z-direction vertically upwards and the mean free surface as $z = 0$. Let us assume d_1 and d_3 to be the distances of the lower vertical tips of the first and second porous plates, respectively, from the free surface; d_2 and d_4 are the respective distances of the upper vertical tips. The semi-infinite regions, namely $-\infty < x < 0, -h < z < 0$ and $L < x < \infty, -h < z < 0$ are labeled as region I and region III, respectively, whereas the bounded region $0 < x < L, -h < z < 0$ is labeled as region II (figure 7.1). The fluid is assumed to be incompressible, homogeneous and inviscid, and the motion irrotational. We define three velocity potentials $\Phi_1(x, y, z, t) = \phi_1(x, z) \exp(\mathrm{i}ly - \mathrm{i}\omega t)$, $\Phi_2(x, y, z, t) = \phi_2(x, z) \exp(\mathrm{i}ly - \mathrm{i}\omega t)$ and $\Phi_3(x, y, z, t) = \phi_3(x, z) \exp(\mathrm{i}ly - \mathrm{i}\omega t)$ in region I, region II and region III, respectively.

The governing equations and boundary conditions in each of the regions are same as described in Chapter 6 (equations (6.7a–c)). The matching conditions along the vertical bound-

aries $x = 0$ and $x = L$ are given by

$$\frac{\partial \phi_1}{\partial x} = \frac{\partial \phi_2}{\partial x} = \mathrm{i}k_0 G_1(\phi_1 - \phi_2); \qquad x = 0, \qquad -d_1 < z < -d_2, \tag{7.1a}$$

$$\frac{\partial \phi_1}{\partial x} = \frac{\partial \phi_2}{\partial x}; \qquad x = 0, \qquad (-h < z < -d_1) \cup (-d_2 < z < 0), \tag{7.1b}$$

$$\phi_1 = \phi_2; \qquad x = 0, \qquad (-h < z < -d_1) \cup (-d_2 < z < 0), \tag{7.1c}$$

$$\frac{\partial \phi_2}{\partial x} = \frac{\partial \phi_3}{\partial x} = \mathrm{i}k_0 G_2(\phi_2 - \phi_3); \qquad x = L, \qquad -d_3 < z < -d_4, \tag{7.1d}$$

$$\frac{\partial \phi_2}{\partial x} = \frac{\partial \phi_3}{\partial x}; \qquad x = L, \qquad (-h < z < -d_3) \cup (-d_4 < z < 0), \tag{7.1e}$$

$$\phi_2 = \phi_3; \qquad x = L, \qquad (-h < z < -d_3) \cup (-d_4 < z < 0), \tag{7.1f}$$

where k_0 is the incident wave number; G_1 and G_2 are the dimensionless complex porous effect parameters of the porous plates placed at $x = 0$ and $x = L$, respectively.

7.3 Reflection and transmission by the porous structure

Velocity potentials $\phi_1(x, z)$, $\phi_2(x, z)$ and $\phi_3(x, z)$ have the same form as given by equations (6.11), (6.12a) and (6.12b), respectively, of Chapter 6. Also the depth dependent function $Z_n(h, z)$ and wave numbers k_n are same as described in Chapter 6. Now using the continuity of the horizontal velocity components $\frac{\partial \phi_1}{\partial x}$ and $\frac{\partial \phi_2}{\partial x}$ along $x = 0$, $-h < z < 0$ (using equations (7.1a) and (7.1b)), we obtain

$$R_0 = 1 - A_0 + B_0 \exp(\mathrm{i}k_0 L), \tag{7.2a}$$

$$R_n = B_n \exp(\mathrm{i}k_n L) - A_n. \tag{7.2b}$$

Further, using the second equality in equation (7.1a), we get

$$\sum_{n=0}^{N} (K_n + 2K_0 G_1) A_n Z_n - \sum_{n=0}^{N} K_n \exp(\mathrm{i}K_n L) B_n Z_n - 2K_0 G_1 Z_0 = 0, \qquad -d_2 < z < -d_1. \tag{7.3a}$$

Similarly, equation (7.1c) results in

$$2Z_0 - 2\sum_{n=0}^{N} A_n Z_n = 0, \qquad (-h < z < -d_1) \cup (-d_2 < z < 0). \tag{7.3b}$$

We use least square method to find the unknown coefficients in equations (7.3a,b). In order to do so, we define a new quantity $\mathcal{H}(z)$ in the following form:

$$\mathcal{H}(z) = \begin{cases} \sum_{n=0}^{N} (K_n + 2K_0G_1)A_nZ_n - \sum_{n=0}^{N} K_n \exp(\mathrm{i}K_nL)B_nZ_n - 2K_0G_1Z_0, & -d_1 < z < -d_2, \\ 2Z_0 - 2\sum_{n=0}^{N} A_nZ_n, & (-h < z < -d_1) \cup (-d_2 < z < 0). \end{cases} \tag{7.4}$$

The requirement of the method is that the relation

$$\int_{-h}^{0} |\mathcal{H}(z)|^2 \mathrm{d}z = \text{ minimum} \tag{7.5}$$

holds in order to satisfy $\mathcal{H}(z) = 0$ in the region $-h < z < 0$.

Then minimizing the integral in equation (7.5) with respect to each of A_m $(m = 0, 1, \ldots N)$, the following integral equation is obtained:

$$\int_{-h}^{0} \mathcal{H}^*(z) \frac{\partial \mathcal{H}(z)}{\partial A_m} \mathrm{d}z = 0, \quad m = 0, 1, \ldots N, \tag{7.6}$$

where $\mathcal{H}^*(z)$ denotes the complex conjugate of $\mathcal{H}(z)$.

A system of linear equations is obtained from the above equation, after integrating with respect to z, as follows:

$$\sum_{n=0}^{N} p_{m,n}^{(1)} A_n^* + \sum_{n=0}^{N} q_{m,n}^{(1)} B_n^* = r_m^{(1)}, \quad m = 0, 1, \ldots N, \tag{7.7}$$

where

$$p_{m,n}^{(1)} = (k_n^* + 2K_0G_1^*)(K_m + 2K_0G_1) \int_{-d_1}^{-d_2} Z_mZ_n \mathrm{d}z + 4\left[\int_{-h}^{-d_1} Z_mZ_n \mathrm{d}z + \int_{-d_2}^{0} Z_mZ_n \mathrm{d}z\right], \tag{7.8a}$$

$$q_{m,n}^{(1)} = -(K_m + 2K_0G_1)\zeta_n^* \int_{-d_1}^{-d_2} Z_mZ_n \mathrm{d}z, \tag{7.8b}$$

$$r_m^{(1)} = 2K_0G_1^*(K_m + 2K_0G_1) \int_{-d_1}^{0} Z_mZ_0 \mathrm{d}z + 4\left[\int_{-h}^{-d_1} Z_mZ_0 \mathrm{d}z + \int_{-d_1}^{0} Z_mZ_0 \mathrm{d}z\right], \tag{7.8c}$$

with $\zeta_n = \exp(\mathrm{i}k_nL)$.

Further, making use of the continuity of the horizontal velocity components $\frac{\partial \phi_2}{\partial x}$ and $\frac{\partial \phi_3}{\partial x}$ along $x = L$, $-h < z < 0$ (using equations (7.1d) and (7.1e)), we obtain

$$T_n = A_n \exp(\mathrm{i}k_n L) - B_n. \tag{7.9}$$

Using the second equality of equation (7.1d), the following equation is obtained:

$$\sum_{n=0}^{N} K_n \exp(\mathrm{i}K_n L) A_n Z_n - \sum_{n=0}^{N} (K_n + 2K_0 G_2) B_n Z_n = 0. \tag{7.10a}$$

Also, equation (6.8f) gives rise to the following equation:

$$\sum_{n=0}^{N} 2B_n Z_n = 0. \tag{7.10b}$$

Now using the least square method, a system of linear equations is obtained as

$$\sum_{n=0}^{N} p_{m,n}^{(2)} A_n^* + \sum_{n=0}^{N} q_{m,n}^{(2)} B_n^* = 0, \quad m = 0, 1, \ldots N, \tag{7.11}$$

where

$$p_{m,n}^{(2)} = -K_n^* \zeta_n^* (K_m + 2K_0 G_2) \int_{-d_3}^{-d_4} Z_m Z_n \mathrm{d}z, \tag{7.12a}$$

$$q_{m,n}^{(2)} = (K_n^* + 2K_0 G_2^*)(K_m + 2K_0 G_2) \int_{-d_3}^{-d_4} Z_m Z_n \mathrm{d}z + 4 \left[\int_{-h}^{-d_3} Z_m Z_0 \mathrm{d}z + \int_{-d_4}^{0} Z_m Z_0 \mathrm{d}z \right]. \tag{7.12b}$$

From the system of equations given by equations (7.7) and (7.11), the following matrix system is constructed:

$$\begin{aligned} \boldsymbol{AX} &= \boldsymbol{c}, \\ \text{where } \boldsymbol{A} &\quad \text{is a square matrix of size } [2(N+1)], \\ \boldsymbol{X} &= [A_0^*, \ldots A_N^*, B_0^*, \ldots, B_N^*]^T \\ &\quad \text{is the unknown vector,} \end{aligned}$$

$$\text{and} \quad \boldsymbol{c} = [r_0, \ldots, r_{N+1}, \underbrace{0, \ldots\ldots\ldots 0}_{\text{(N+1)-times}}]^T.$$

The above matrix system can be solved to get the unknown coefficients A_n^* and B_n^*, and consequently $|R_0|$, $|T_0|$ and E_{loss} can be calculated by using equations (7.2a), (7.9) and (6.13), respectively.

7.4 Numerical results

N \ L/h	0.0001	0.4212	0.8422	1.2632	1.6842	2
0	0.252923373	0.285655784	0.228822633	0.125197866	0.071317032	0.136033049
5	0.360347281	0.408930381	0.312442937	0.125696654	0.096926336	0.221748634
10	0.374952355	0.432282485	0.326918511	0.120252508	0.108295308	0.242889554
15	0.381019453	0.442334148	0.333289337	0.117418024	0.114618384	0.253252107
20	0.38275353	0.446591999	0.336044037	0.116123678	0.11770863	0.258053857
25	0.383459699	0.448296535	0.337181847	0.115513265	0.119135701	0.260252026
30	0.383630865	0.448961454	0.337640719	0.115240305	0.119758849	0.261215415

Table 7.1: Convergence of $|R_0|$ at different values of L/h_1; $d_1 = d_2 = 0$, $d_3 = h/2$, $d_4 = 0$, $G_1 = 0.5$, $G_2 = 0$ and $\nu h = 0.8$

Tables 7.1 and 7.2 show the convergence of $|R_0|$ and $|T_0|$, respectively, for the number of evanescent modes at different values of L/h_1. From the tables, it is evident that taking $N = 30$ gives a 2-digit accuracy on both $|R_0|$ and $|T_0|$, which are quite satisfactory for engineering purposes. Here λ is the wavelength of the incident wave. The following constant values are considered throughout for the study: $k_0 h = 1.6$, $\theta = 0^0$ and $N = 30$. It is to be noted that for numerical purpose, we consider only the normal incidence of waves, i.e., $\theta = 0$.

7.4.1 Comparison with existing result

In order to validate the current method, comparison is made with the corresponding cases available in the literature. With $d_1 = d_2 = d_4 = 0$, $d_3 = h/2$ and $G_2 = 0$, the structure reduces to a single rigid vertical plate which was studied by Porter and Evans (1995). Comparison of the reflection and transmission coefficients obtained in the present problem with those of Porter and Evans (1995) is shown in figure 6.4 of Chapter 6. Good agreement of the results shows the validation of the formulation of the current problem and it confirms that further

N \ L/h	0.0001	0.4212	0.8422	1.2632	1.6842	2
0	0.839374354	0.804248035	0.790777604	0.772174015	0.750227169	0.739215084
5	0.886911113	0.804854654	0.796073177	0.764099122	0.712913269	0.683069754
10	0.900080369	0.816151037	0.812879539	0.7800272	0.721512942	0.68630555
15	0.907892016	0.823440194	0.82348777	0.790902599	0.728909927	0.690915711
20	0.912831646	0.827281661	0.829032435	0.796802821	0.733259026	0.693929436
25	0.915208534	0.829411913	0.832056776	0.800156122	0.735951602	0.695974188
30	0.91645681	0.830483621	0.833559848	0.80186305	0.737386978	0.697111937

Table 7.2: Convergence of $|T_0|$ at different values of L/h_1; $d_1 = d_2 = 0$, $d_3 = h/2$, $d_4 = 0$, $G_1 = 0.5$, $G_2 = 0$ and $\nu h = 0.8$

study on scattering process for such porous plate problems for different parameters can be carried out.

7.4.2 Results

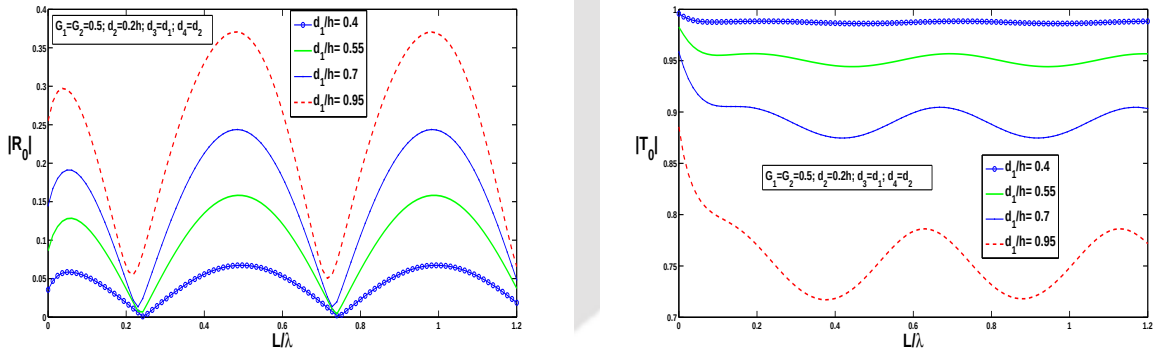

(a) Variation of $|R_0|$ (b) Variation of $|T_0|$

Figure 7.2: Effect of L/λ for different d_1/h with $G_1 = G_2 = 0.5$, $k_0h = 1.6$, $d_2 = 0.5h$, $d_3 = d_1$, $d_4 = d_2$, $\theta = 0^0$ and $N = 30$

In figure 7.2, the reflection and transmission coefficients are plotted against dimensionless distance L/λ between the porous plates for different values of d_1/h of the first plate. Some specific values of other parameters are considered as $d_2/h = 0.2$, $d_3 = d_1$, $d_4 = d_2$, $G_1 = 0.5$ and $G_2 = 0.5$. Oscillating nature of $|R_0|$ and $|T_0|$ is observed for these values of d_1/h. Both the minimum and maximum values of $|R_0|$ are obtained at specific values of L/λ corresponding to all values of d_1/h, but on the other hand optimum values of $|R_0|$ increase with an increase in the value of d_1/h. But with an increase in d_1/h, $|T_0|$ decreases and higher oscillation is

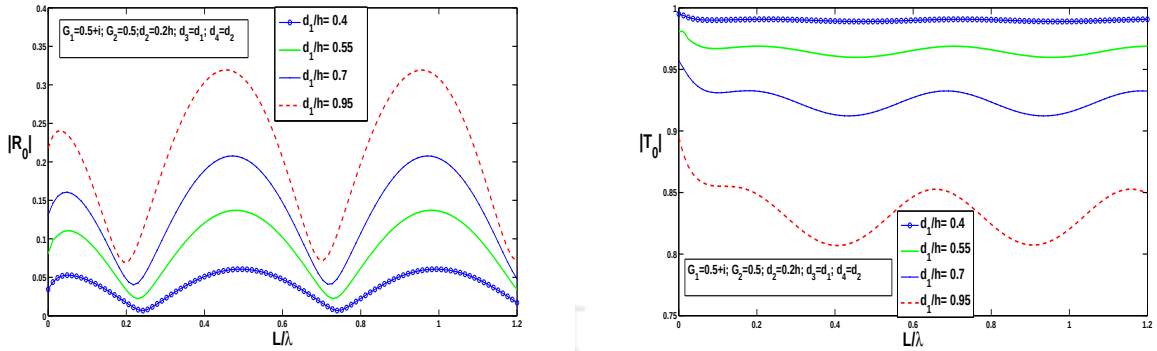

(a) Variation of $|R_0|$ (b) Variation of $|T_0|$

Figure 7.3: Effect of L/λ for different d_1/h with $G_1 = 0.5 + \mathrm{i}$, $G_2 = 0.5$, $k_0h = 1.6$, $d_2 = 0.5h$, $d_3 = d_1$, $d_4 = d_2$, $\theta = 0^0$ and $N = 30$

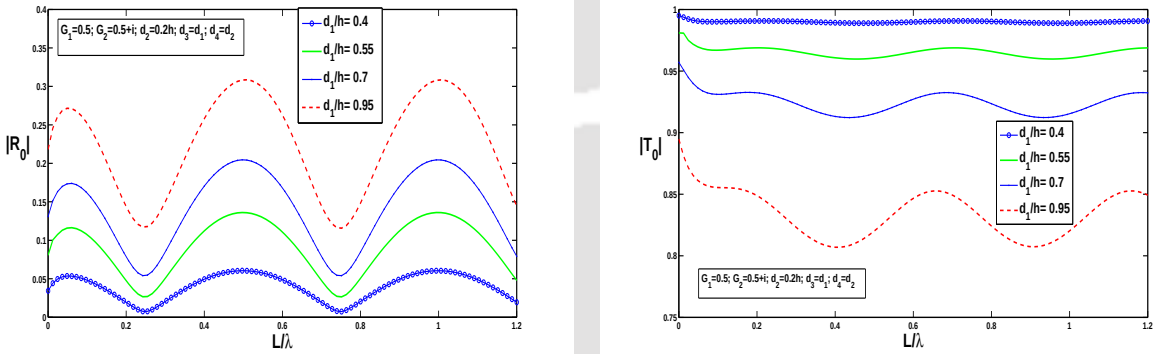

(a) Variation of $|R_0|$ (b) Variation of $|T_0|$

Figure 7.4: Effect of L/λ for different d_1/h with $G_1 = 0.5$, $G_2 = 0.5 + \mathrm{i}$, $k_0h = 1.6$, $d_2 = 0.5h$, $d_3 = d_1$, $d_4 = d_2$, $\theta = 0^0$ and $N = 30$

observed for higher values of d_1/h considered.

The same study is carried out by adding an imaginary quantity to G_1: $G_1 = 0.5 + \mathrm{i}$ (figure 7.3). By comparing figure 7.3(a) with figure 7.2(a), it is observed that maximum values of the reflection coefficient reduce for higher values of d_1/h taken. Hence it can be deduced that the imaginary part of G_1, which causes the inertial effect, plays a significant role in reducing reflection by the porous plate. But by comparing figure 7.3(b) with figure 7.2(b), it is found that the value of $|T_0|$ increases for higher values of d_1/h.

Further study is carried out (figure 7.4) with $G_1 = 0.5$ and by adding an imaginary quantity to G_2 (in this case $G_2 = 0.5 + \mathrm{i}$). By comparing figure 7.4(a) with figure 7.2(a), it is observed that the amplitude of the oscillation in the values of $|R_0|$ reduces. Comparison of figure 7.4(b)

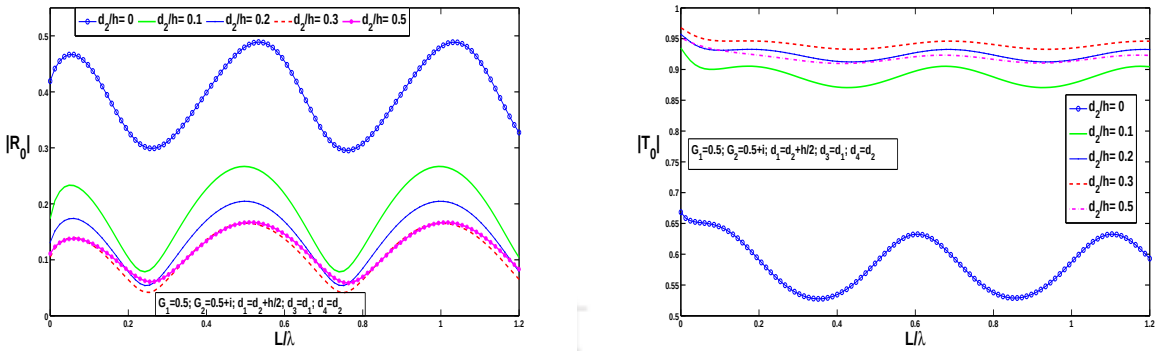

(a) Variation of $|R_0|$ (b) Variation of $|T_0|$

Figure 7.5: Effect of L/λ for different values of d_2/h with $G_1 = 0.5$, $G_2 = 0.5 + \mathrm{i}$, $k_0h = 1.6$, $d_1 = d_2 + h/2$, $d_3 = d_1$, $d_4 = d_2$, $\theta = 0^0$ and $N = 30$

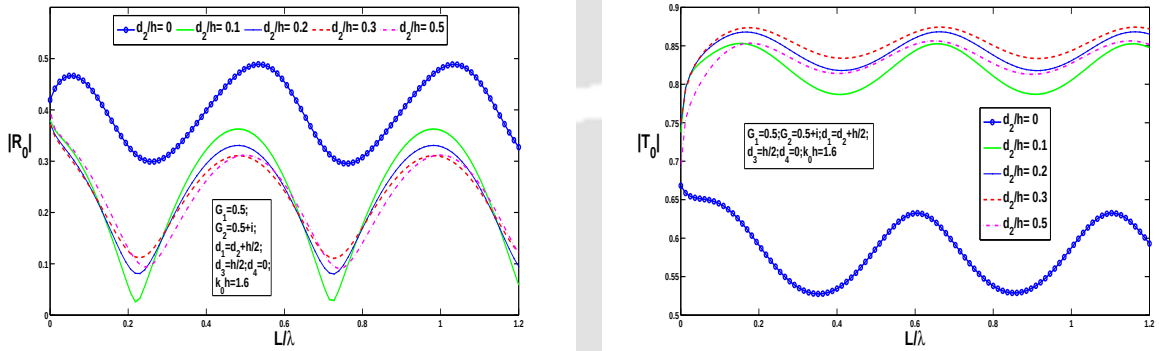

(a) Variation of $|R_0|$ (b) Variation of $|T_0|$

Figure 7.6: Effect of L/λ for different values of d_2/h with $G_1 = 0.5$, $G_2 = 0.5 + \mathrm{i}$, $k_0h = 1.6$, $d_1 = d_2 + h/2$, $d_3 = h/2$, $d_4 = 0$, $\theta = 0^0$ and $N = 30$

with figure 7.3(b) shows no change in the values of $|T_0|$ implying that interchanging the position of porous plates does not affect the transmission characteristics.

In figure 7.5, the reflection and transmission coefficients are plotted against L/λ for different values of d_2/h by taking a fixed length $h/2$ of the porous plates ($d_1 = d_2 + h/2$). Other fixed parameter values considered are $G_1 = 0.5$, $G_2 = 0.5 + \mathrm{i}$, $d_3 = d_1$ and $d_4 = d_2$. From figure 7.5(a), it is observed that the reflection is quite high when $d_2/h = 0$ (the case of porous plates touching the free surface) as compared against other values of d_2/h considered. Oscillation in $|R_0|$ is observed too. With an increase in the values of d_2/h, overall reflection minimizes. Completely reverse characteristics is observed for the case of transmission (figure 7.5(b)). The value of $|T_0|$ for $d_2/h = 0$ is much less in comparison to that for other values of d_2/h considered.

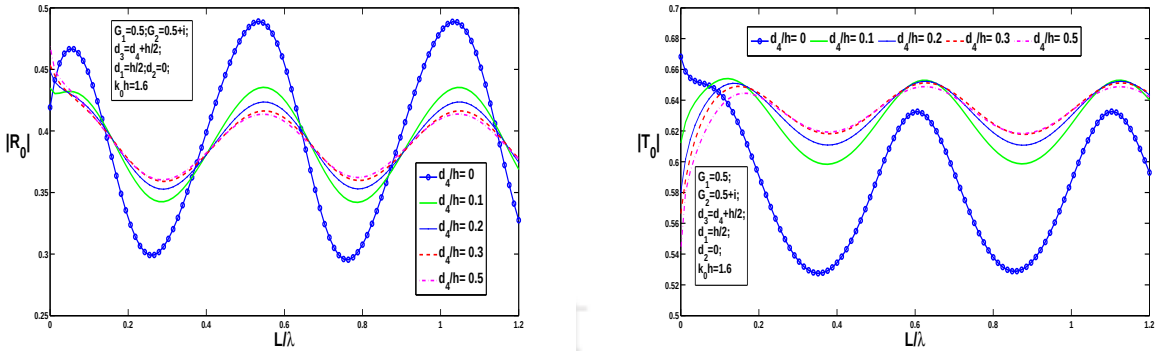

(a) Variation of $|R_0|$ (b) Variation of $|T_0|$

Figure 7.7: Effect of L/λ for different values of d_4/h with $G_1 = 0.5$, $G_2 = 0.5 + \mathrm{i}$, $k_0h = 1.6$, $d_3 = d_4 + h/2$, $d_1 = h/2$, $d_2 = 0$, $\theta = 0^0$ and $N = 30$

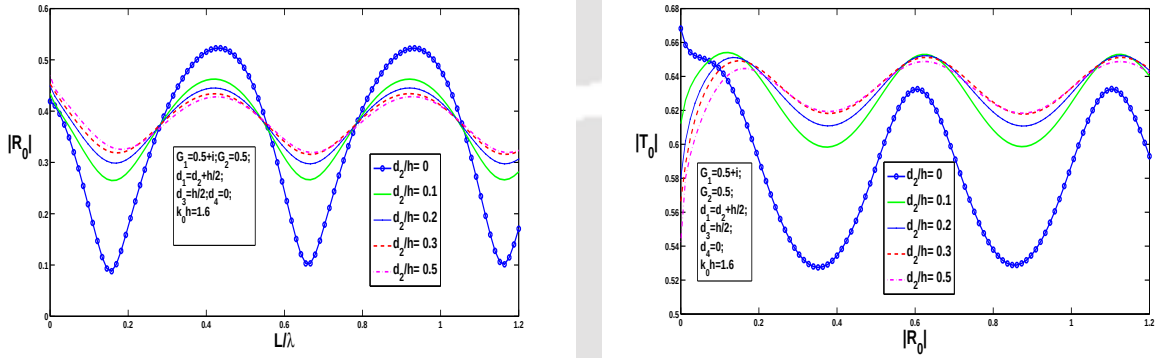

(a) Variation of $|R_0|$ (b) Variation of $|T_0|$

Figure 7.8: Effect of L/λ for different values of d_2/h with $G_1 = 0.5 + \mathrm{i}$, $G_2 = 0.5$, $k_0h = 1.6$, $d_1 = d_2 + h/2$, $d_3 = h/2$, $d_4 = 0$, $\theta = 0^0$ and $N = 30$

Now the behaviour of $|R_0|$ and $|T_0|$ are investigated by fixing the position of the second porous plate and changing the position of the first porous plate vertically inside the water region (figure 7.6). The fixed parameter values considered are $G_1 = 0.5$, $G_2 = 0.5 + \mathrm{i}$, $d_1 = d_2 + h/2$, $d_3 = h/2$ and $d_4 = 0$. It is observed from figure 7.6(a) that the maximum and minimum values of $|R_0|$ is much higher when $d_2/h = 0$ (the case of plates touching the free surface) in comparison to those for other values of d_2/h. But when the porous plate is fully submerged, the lowest value of d_2/h (here 0.1) gives rise to both the maximum and minimum reflection. Moreover, the amplitude of the oscillation reduces with an increase in the value of d_2/h. In figure 7.6(b), it is observed that when the first porous plate just touches the surface, the value of $|T_0|$ becomes significantly low in comparison to those corresponding to other values of d_2/h.

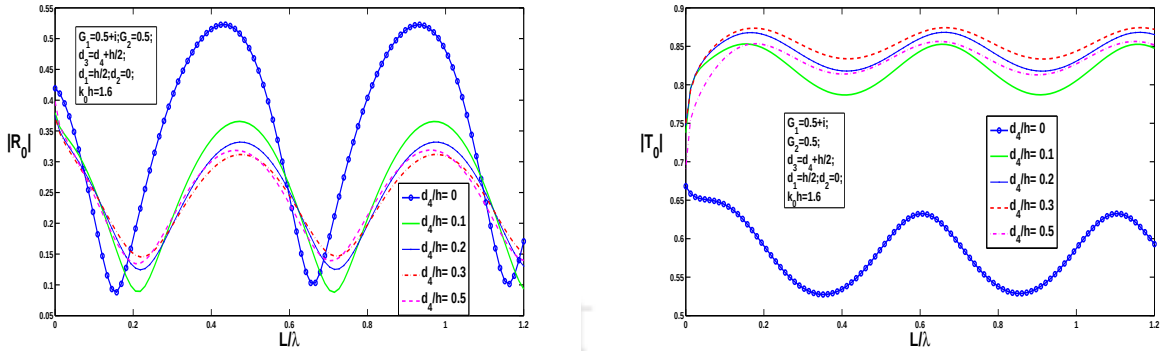

(a) Variation of $|R_0|$ (b) Variation of $|T_0|$

Figure 7.9: Effect of L/λ for different values of d_4/h with $G_1 = 0.5 + \mathrm{i}$, $G_2 = 0.5$, $k_0h = 1.6$, $d_3 = d_4 + h/2$, $d_1 = h/2$, $d_2 = 0$, $\theta = 0^0$ and $N = 30$

Another study on scattering process is carried out by fixing the position of the first porous plate and changing the position of the second porous plate vertically inside the water region (figure 7.7). The fixed parameter values are $G_1 = 0.5$, $G_2 = 0.5 + \mathrm{i}$, $d_3 = d_4 + h/2$, $d_1 = h/2$ and $d_2 = 0$. Both the maximum and minimum values of $|R_0|$ occur when $d_4/h = 0$ (touching the free surface) (figure 7.7(a)). With an increase in the values of d_4/h, the oscillation in the values of $|R_0|$ reduces. But minimum transmission occurs for $d_4/h = 0$ (figure 7.7(b)). With an increase in the values of d_4/h, oscillation in $|T_0|$ reduces. An observation is made when the distance between the porous plates are very small ($L/\lambda < 0.1$): maximum transmission occurs for $d_4/h = 0$.

Figure 7.8 deals with scattering by the same physical construction of the porous plates as considered in figure 7.6 except for the fact that now $G_1 = 0.5 + \mathrm{i}$ and $G_2 = 0.5$. By comparing figure 7.8(a) with figure 7.6(a), higher oscillation for the curve corresponding to $d_2/h = 0$ is observed, but for other curves, oscillation reduces. But comparing it with figure 7.7(a), the same nature is observed with increased optimum values of $|R_0|$. As far as the transmission is concerned, interchanging the positions of the porous plates does not affect it (Comparing figure 7.8(b) with figure 7.7(b)).

Using the same physical configuration of the porous plates considered in figure 7.7, except for the porous effect parameters which are taken as $G_1 = 0.5 + \mathrm{i}$ and $G_2 = 0.5$, the scattering phenomenon is investigated in figure 7.9. By comparing figure 7.9(a) with figure 7.7(a), it is observed that large oscillations occur for all the curves in this case. Here also interchanging the position of the porous plates does not affect transmission (Comparison of figure 7.9(b) with figure 7.6(b)).

7.4.3 Energy loss

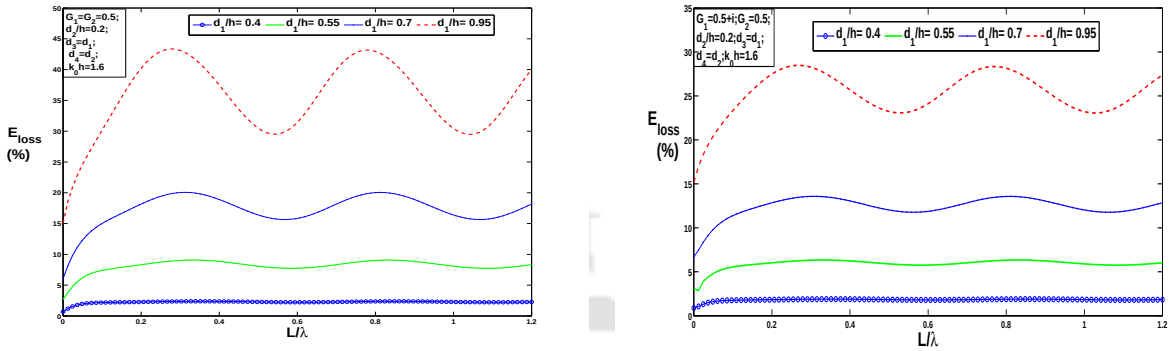

(a) $G_1 = G_2 = 0.5$ (b) $G_1 = 0.5 + i$ and $G_2 = 0.5$

Figure 7.10: Energy loss (%) against L/λ for different values of d_1/h with $k_0h = 1.6$, $d_2/h = 0.2$, $d_3 = d_1$, $d_4 = d_2$, $\theta = 0^0$ and $N = 30$

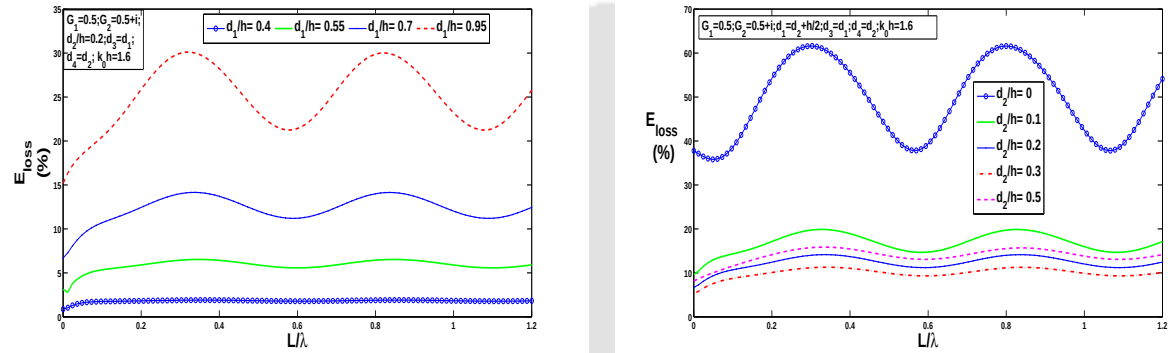

(a) Against various d_1/h with $d_2/h = 0.2$ (b) Against various d_2/h with $d_1 = d_2 + h/2$,

Figure 7.11: Energy loss (%) against L/λ with $G_1 = 0.5$, $G_2 = 0.5 + i$, $k_0h = 1.6$, $d_3 = d_1$, $d_4 = d_2$, $\theta = 0^0$ and $N = 30$

Now the energy loss is plotted against L/λ for different values of d_1/h in figure 7.10. All other constant parameter values are $d_2/h = 0.2$, $d_3 = d_1$ and $d_4 = d_2$. It is observed that higher values of d_1/h result in higher energy loss. Also, more oscillation in the energy loss curve is found for higher values of d_1/h. But from the comparison of these two curves, it is evident that, for a specific value of d_1/h, real values of G_1 show higher maximum value in energy loss as compared to the complex values of G_1.

In figure 7.11(a), energy loss is investigated for different values of d_1/h with $G_1 = 0.5$ and $G_2 = 0.5 + \mathrm{i}$. Comparing it with figure 7.10(b), it is observed that interchanging the porous

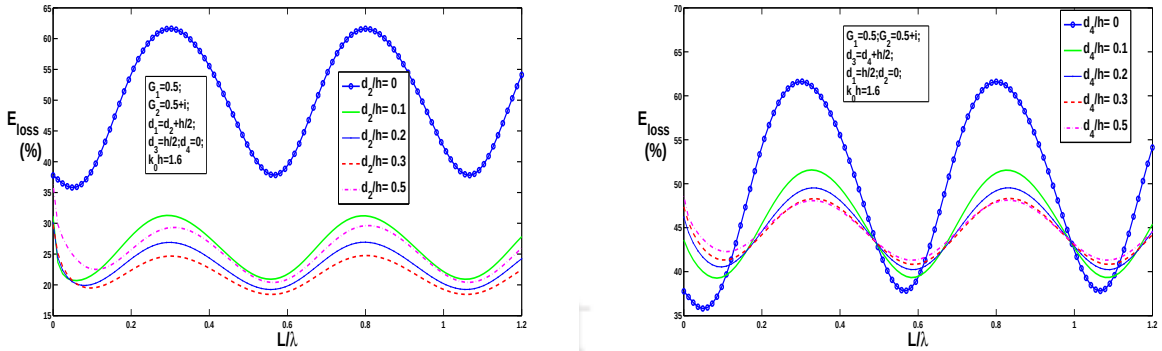

(a) Against various d_2/h with $d_1 = d_2 + h/2$, $d_3 = h/2$, $d_4 = 0$ (b) Against various d_4/h with $d_3 = d_4 + h/2$, $d_1 = h/2$, $d_2 = 0$

Figure 7.12: Energy loss (%) against L/λ with $G_1 = 0.5$, $G_2 = 0.5 + i$, $k_0h = 1.6$, $\theta = 0^0$ and $N = 30$

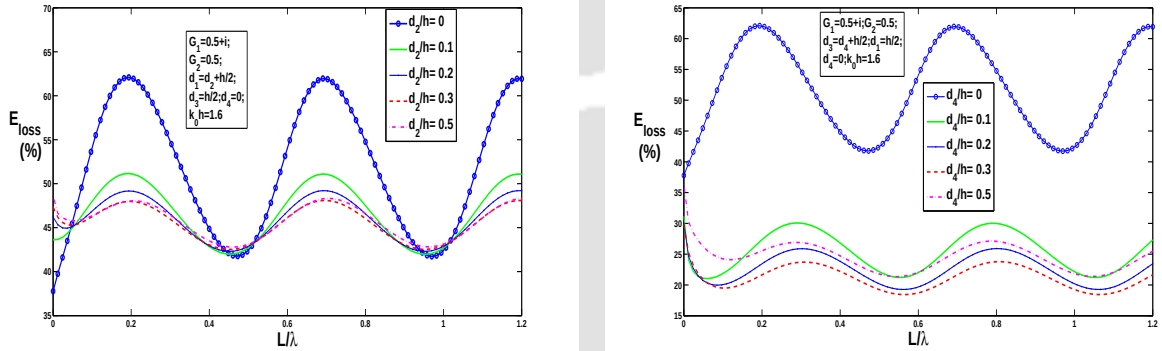

(a) Against various d_2/h (b) Against various d_4/h

Figure 7.13: Energy loss (%) against L/λ with $G_1 = 0.5+i$, $G_2 = 0.5$, $k_0h = 1.6$, $d_3 = d_4+h/2$, $d_1 = h/2$, $d_2 = 0$, $\theta = 0^0$ and $N = 30$

effect parameters of the porous plates does not affect much in energy loss. Figure 7.11(b) shows the energy loss pattern for various positions of the porous plates of same height. Maximum energy loss is observed when the porous plates touch the free surface. When the plates are fully submerged in the water region, oscillation reduces but the energy loss falls significantly.

Figure 7.12(a) deals with the energy loss due to the configuration when the second porous plate is fixed ($d_3 = h/2$, $d_4 = 0$) and the first porous plate moves vertically inside the water region. Length of the porous plates is considered as $h/2$. Maximum energy loss is observed when the first porous plate just touches the free surface and large oscillation in the curve is observed. But when the first porous plate is fully submerged in the water region, oscillation reduces significantly. The energy loss pattern due to the configuration when the first porous

plate is fixed ($d_1 = h/2$, $d_2 = 0$) and the second porous plate moves vertically in the water region is shown in figure 7.12(b). Here, both the maximum and minimum energy loss are observed for $d_4/h = 0$. Moreover, by comparing figure 7.12(b) with figure 7.12(a), it is observed that the second configuration causes more energy loss as compared to the first configuration. The fixed values considered here are $G_1 = 0.5$ and $G_2 = 0.5 + \mathrm{i}$.

Now, we study energy loss patterns for the same types of configurations as considered in figure 7.13 with a change in the values of porous effect parameters, namely, $G_1 = 0.5 + \mathrm{i}$ and $G_2 = 0.5$. It is observed that oscillation in the curves exists and the maximum oscillation occurs when both the porous plates touch the free surface (figure 7.13(a)). By comparing figure 7.13(a) with figure 7.12(a), it is observed that a significant increment in energy loss occurs by adding an imaginary part to the porous effect parameter of first porous plate when it is fully submerged in the water region. Comparison of figure 7.13(b) with figure 7.12(b) shows reverse effect, i.e., when an imaginary part is added to G_1 and the second porous plate is fully submerged, energy loss is less.

7.5 Conclusion

Based on linear water wave theory, oblique water wave scattering process by two thin parallel fixed vertical porous plates of different porosity and porous effect parameters in an infinite channel of finite depth is studied. Boundary value problems in each region are set up and with the help of matching conditions across the porous barrier as well as the virtual boundaries and the orthogonality of the depth dependent functions, a system of linear equations is obtained solving which the reflection and transmission coefficients, and consequently, energy loss (in %) are obtained. The effects of the porous effect parameter, height and positioning of both the porous plates on scattering process are studied graphically. Periodic oscillation is observed in all the graphs. Moreover, keeping the height of the porous plates fixed, it is found that by increasing the inertial effect of the porous plate, lower reflection is obtained but the corresponding transmission is higher. But higher energy loss is obtained by reducing the inertial effect of the porous plates. It is observed that when the porous plates touch the free surface, changing the porous effect parameters minimum reflection as well as transmission can be achieved which, in turn, results in maximum energy loss. One interesting observation is that interchanging the position of the plates does not affect the transmission coefficient.

Chapter 8

Summary and future work

8.1 Summary

In this thesis, oblique wave scattering/damping by a vertical porous structure and also by a pair of porous plates is investigated. Most part of the thesis is devoted to the wave scattering within a vertical porous structure placed on different types of bottoms and for different types of other conditions. The objective is to analyze the reflection/damping behaviour in all cases. Throughout this thesis, linear water wave theory is employed.

In Chapter 2, a study on reflection of oblique ocean water waves by a vertical rectangular porous structure placed on an elevated horizontal bottom is carried out. It is observed that up to a certain wave number, reflection can be described by the propagating mode alone. It is noticeable that the values of the reflection coefficient decrease as the porosity increases. Some more observations are made with respect to the depth, height of the elevated bottom and the width of the porous structure. We also study reflection due to oblique incidence by considering different angles of incidence and observe the effect due to the change in angles. The same investigation is carried out with the porous structure placed directly on the horizontal ocean bottom (without any elevation). The results of this particular case are compared with the elevated bottom case in order to examine the effect of presence of the elevated bottom. Comparison of our result with that of Madsen (1983) shows good agreement.

Chapter 3 is devoted to wave damping by a vertical porous structure placed near and far away from a rigid vertical wall. It is observed that, except for the case when the porous structure is thin, the reflection coefficient and the dimensionless amplitude of the progressive transmitted wave give rise to values as expected. In the case when the rigid wall is nearer

to the structure, the reflection coefficient decreases rapidly for a thin structure and converges afterwards for all numbers of evanescent modes. The dimensionless amplitude of the progressive transmitted wave also decreases as the width increases, ultimately converging and vanishing for a wide structure. When the wall is at a large distance away from the structure, the behaviour of both the reflection and the dimensionless amplitude of the progressive transmitted wave remain almost the same. For both cases of the wall being nearer to and far away from the structure, higher porosity gives rise to lower reflection coefficients and higher dimensionless amplitude of the progressive transmitted wave. However, the dimensionless amplitudes of the progressive transmitted wave converge and vanish when the porous structure is very wide. We also discuss the energy loss against the width of the porous structure for different number of modes and porosity. Irrespective of the positioning of the rigid wall, we observe that for higher values of porosity, energy loss is more pronounced when the structure is not thin whereas energy loss is same for all numbers of modes.

Chapter 4 deals with the reflection characteristics of oblique ocean water waves by a vertical porous structure placed on a multi-step impermeable bottom. It is observed that when the porous structure is considered above a 2-step bottom, the number of evanescent modes, porosity and the angle of incidence do not affect the reflection coefficient for relatively long waves. Lower values of the friction factor result in oscillation in the reflection coefficient which vanishes with an increase in the values of the friction factor. Up to a certain range of angles of incidence, reflection coefficient is independent of the values of porosity. When a p-step bottom is considered, certain observations remain the same except that the behaviour of reflection coefficient against the angle of incidence is different. At the end, both cases are compared by considering the same set of parameters.

Damping of oblique ocean waves by a porous structure placed on a multi-step bottom is studied in Chapter 5. It is observed that except for a thin porous structure, the reflection is low for various parameters. Number of evanescent modes merely affects the scattering phenomena. But higher value of porosity shows relatively lower reflection than that observed for lower porosity. Oscillation in the reflection coefficient is observed for lower values of friction factor which vanishes with an increase in the value of friction factor. Up to a certain range of the angle of incidence, higher value of porosity and lower value of friction factor give low and high reflection, respectively. Transmission is independent of the porosity of the structure. But lower value of friction factor causes higher transmission. Significant energy loss occurs when the width of the structure is increased and maximum energy loss occurs in a fixed range of the angle of incidence. A minimum admissible length of the porous structure is always required

in order that it is an effective wave absorber. The significant difference between the two cases considered here lies on the observation that reflection due to a thin porous structure is very high when the solid wall exists as compared to the case when no wall is present.

In Chapter 6, the oblique water wave scattering problem due to the presence of two thin parallel vertical surface piercing porous plates of different heights and porous effect parameters in an infinite channel of constant depth is investigated. The effects of the porous effect parameters and the heights of the porous plates, the angle of incidence, on scattering process is studied graphically. Periodic oscillation is observed in all the graphs. Moreover, keeping the heights of the porous plates fixed, it is found that lower reflection is obtained by increasing the inertial effect of the porous plate but the corresponding transmission is higher. But higher energy loss is obtained by reducing the inertial effect of the porous plates. For the second porous wall with its properties fixed, higher reflection occurs in the presence of the first porous plate for greater height and lower reflection for lesser height. But by fixing the properties of the first porous plate, both the minimum and maximum reflection occur when the second porous plate is of greater height. One interesting observation is that interchanging the position of the plates does not affect the transmission coefficient. Maximum energy loss is achieved when the height of the second porous plate is greater as well as the angle of incidence is lower.

Chapter 7 deals with the oblique water wave scattering problem due to the presence of two thin fully submerged vertical porous plates of different physical properties in an infinite channel of constant depth. The effect of various parameters such as the porous effect parameters, height of the porous plates, distance from the free surface on scattering phenomenon is studied graphically. Nature of the curves for the reflection, transmission as well as energy loss is very much same as the ones found in Chapter 6. One interesting observation is that when the porous plates touch the free surface, maximum energy loss occurs as compared to the case when the porous plates are fully submerged.

8.2 Future work

We now present some informal observations pertaining to the possible extensions of our results to different problems. We briefly outline some interesting problems which may be taken up in future.

Usually the ocean bottom is of uneven shape. The problems considered in Chapters 4 and 5 with multi-step bottoms can be revisited by taking any arbitrarily shaped bottom. We expect the same analysis as adopted in this thesis to be valid under some additional constraints.

Further, it is very likely that a physical situation with a two-layer fluid will depict a more realistic problem. The problems carried out here may be extended for a two-layer fluid.

In some cases of wave scattering problems, effect of surface tension is negligible while it is not for some other cases. The present problems may be reformulated and solved by considering surface tension at the free surface. It is to be noted that surface tension was neglected for all the problems in this thesis.

In practical applications, a set of porous cylinders may also be used as breakwater to solve the erosion of beaches, harbours etc. It is probably feasible to formulate and solve scattering/damping problem for this configuration.

Bibliography

Anglin, E. J., Cheng, L., Freeman, W. R., and Sailora, M. J. (2008). Porous silicon in drug delivery devices and materials. *Adv. Drug Deliv. Rev.*, 60(11):1266–1277.

Biot, M. A. (1956). Theory of propagation of elastic waves in a fluid-saturated porous solid. *J. Acoust. Soc. Am.*, 28(2):168–178.

Blunt, M. J. (1998). Physically-based network modeling of multiphase flow in intermediate-wet porous media. *J. Petro. Sc. Eng.*, 20(3–4):117–125.

Chamberlain, P. G. and Porter, D. (1995). The modified mild-slope equation. *J. Fluid Mech.*, 291:393–407.

Chamberlain, P. G. and Porter, D. (1999). On the solution of dispersion relation for water waves. *Appl. Ocean Res.*, 21(4):161–166.

Chen, H. B., Tsai, C. P., and Chiu, J. R. (2006). Wave reflection from vertical breakwater with porous structure. *Ocean Eng.*, 33(13):1705–1717.

Cho, I. H. and Kim, M. H. (2013). Transmission of oblique incident waves by a submerged horizontal porous plate. *Ocean Eng.*, 61:56–65.

Cho, I. H., Koh, H. J., Kim, J. R., and Kim, M. H. (2013). Wave scattering by dual submerged horizontal porous plates. *Ocean Eng.*, 73:149–158.

Chwang, A. T. (1983). A porous wavemaker theory. *J. Fluid Mech.*, 132:395–406.

Clement, T. P., Hooker, B. S., and Skeen, R. S. (1996). Macroscopic models for predicting changes in saturated porous media properties caused by microbial growth. *Groundwater*, 34:934–942.

Cox, R. J., Horton, P. R., and Bettington, S. H. (1998). Double walled, low reflection wave barriers. *Proc. 26th Coast. Eng. Conf. Am. Soc. Civ. Eng.*, pages 2221–2234.

Craik, A. D. D. (2004). The origins of water wave theory. *Annu. Rev. Fluid Mech*, 36:1–28.

Dalrymple, R. A., Losada, M. A., and Martin, P. A. (1991). Reflection and transmission from porous structures under oblique wave attack. *J. Fluid Mech.*, 224:625–644.

Dalrymple, R. A. and Martin, P. A. (1990). Wave diffraction through offshore breakwater. *J. Waterw. Port Coast. Ocean Eng.*, 116(10):727–741.

Darwiche, M. K. M., Williams, A. N., and Wang, K. H. (1994). Wave interaction with semi-porous cyllindrical breakwater. *J. Waterw. Port Coast. Ocean Eng.*, 120(4):382–403.

Das, P., Dolai, D. P., and Mandal, B. N. (1997). Oblique wave diffraction by parallel thin vertical barriers with gaps. *J. Waterw. Port Coast. Ocean Eng.*, 123:163–171.

Fienerman, R. P. and Kelman, R. B. (1974). The convergence of least square approximations for dual orthogonal series. *Glasgow Math. J.*, 15:82–84.

Gu, Z. and Wang, H. (1991). Gravity waves over porous bottom. *Coast. Eng.*, 15(5–6):497–524.

Hsu, H. J. and Huang, L. H. (2011). Oblique water waves impacting on a thin porous wall with a partial-slipping boundary condition. *J. Hydrodyn. Ser. B*, 23(3):361–371.

Kelman, R. B. and Chester, A. K., J. (1973). Least square approximations for dual trigonometric series. *Glasgow Math. J.*, 14:111–119.

Kirby, J. T. and Dalrymple, R. A. (1983). Propagation of obliquely incident water waves over a trench. *J. Fluid Mech.*, 133:47–63.

Lee, J. F. and Cheng, Y. (2007). A theory for waves interacting with porous structures with multiple regions. *Ocean Eng.*, 34(11-12):1690–1700.

Lee, T., Tsai, C., and Jeng, D. (2002). Ocean waves propagating over a porous sea-bed of finite thickness. *Ocean Eng.*, 29(12):1577–1601.

Li, J. and Jeng, D. (2008). Response of a porous sea-bed around breakwater heads. *Ocean Eng.*, 35(8–9):864–886.

Liu, Y. and Li, Y. C. (2011a). An alternative analytical solution for water-wave motion over a submerged horizontal porous plate. *J. Eng. Math.*, 69(4):385–400.

Liu, Y. and Li, Y. C. (2011b). Wave interaction with a wave absorbing double curtain-wall breakwater. *Ocean Eng.*, 38(10):1237–1245.

Liu, Y., Li, Y. C., Teng, B., and Dong, S. (2008). Wave motion over a submerged breakwater with an upper horizontal porous plate and a lower horizontal solid plate. *Ocean Eng.*, 35(16):1588–1596.

Losada, I. J., Dalrymple, R. A., and Martin, O. A. (1993). Water waves on crown breakwaters. *J. Waterw. Port Coast. Eng.*, 119(4):367–380.

Losada, I. J., Silva, R., and Losada, M. A. (1996a). 3-D non-breaking regular wave interaction with submerged breakwaters. *Coast. Eng.*, 28(1–4):229–248.

Losada, I. J., Silva, R., and Losada, M. A. (1996b). Interaction of non-breaking directional random waves with submerged breakwaters. *Coast. Eng.*, 28(1–4):249–266.

Madsen, O. S. (1974). Wave transmission through porous structure. *J. Waterw. Harbours Coast. Eng.*, 100(3):169–188.

Madsen, P. A. (1983). Wave reflection from a vertical permeable wave absorber. *Coast. Eng.*, 7:381–396.

Mallayachari, V. and Sundar, V. (1994). Reflection characteristics of permeable seawalls. *Coast. Eng.*, 23(1–2):135–150.

Martha, S. C., Bora, S. N., and Chakrabarti, A. (2007). Oblique water wave scattering by small undulation on a porous sea-bed. *Appl. Ocean Res.*, 29(1–2):86–90.

Massel, S. R. (1993). Extended refraction-diffraction equation for surface waves. *Coast. Eng.*, 19(1–2):97–126.

Massel, S. R. and Mei, C. C. (1977). Transmission of random wind waves through perforated or porous breakwaters. *Coast. Eng.*, 1:63–78.

Mendez, F. J. and Losada, I. J. (2004). A perturbation method to solve dispersion equations for water waves over dissipative media. *Coast. Eng.*, 51(1):81–89.

Porter, D. and Staziker, D. J. (1995). Extension of the mild-slope equation. *J. Fluid Mech.*, 300:367–382.

Porter, R. and Evans, D. V. (1995). Complementary approximations to wave scattering by vertical barriers. *J. Fluid Mech.*, 294:155–180.

Rojanakamthorn, S., Isobe, M., and Watanabe, A. (1989). A mathematical model of wave transformation over a submerged breakwater. *Coastal Eng. in Japan*, 32(2):209–234.

Sahoo, T., Chan, A. T., and Chwang, A. T. (2000a). Scattering of oblique surface waves by permeable barriers. *J. Waterw. Port Coast. Ocean Eng.*, 126(4):196–205.

Sahoo, T., Lee, M. M., and Chwang, A. T. (2000b). Trapping and generation of waves by vertical porous structures. *J. Eng. Mech.*, 126(10):1074–1082.

Sankarbabu, K., Sannasiraj, S. A., and Sundar, V. (2007). Interaction of regular waves with a group of dual porous circular cylinders. *Appl. Ocean Res.*, 29(4):180–190.

Silva, R., Salles, P., and Palacio, A. (2002). Linear waves propagating over a rapidly varying finite porous bed. *Coast. Eng.*, 44(3):239–260.

Sollitt, C. K. and Cross, R. H. (1972). Wave transmissions through permeable breakwaters. *Proc. 13th Coast. Eng. Conf.*, pages 1827–1846. Am. Soc. Civ. Eng.; Vancouver, Canada.

Straub, L. G., Bowers, C. E., and Herbich, J. B. (1957). Laboratory studies of permeable wave absorber. *Proc. 6th Coast. Eng. Conf.*, pages 729–742. Am. Soc. Civ. Eng.; Gainesville, Florida, USA.

Sulisz, W. (1985). Wave reflection and transmission at permeable breakwaters of arbitrary cross section. *Coast. Eng.*, 9(4):371–386.

Twu, S. W. and Liu, C. C. (1994). The elimination of re-reflected waves by a porous medium of finite thickness. *Ocean Eng.*, 21(2):179–194.

Twu, S. W., Liu, C. C., and Twu, C. W. (2002). Wave damping characteristics of vertically stratified porous structures under oblique wave action. *Ocean. Eng.*, 29(11):1295–1311.

Wang, K. H. and Ren, X. (1994). Wave interaction with a concentric porous cylinder system. *Ocean Eng.*, 21(4):343–360.

Ward, J. C. (1964). Turbulent flow in porous media. *Proc. J. Hyd. Div.*, 90(HY5):1–12.

Williams, A. N. and Li, W. (2000). Waterwave interaction with an array of bottom-mounted surface-piercing porous cylinder. *Ocean Eng.*, 27(8):841–866.

Wu, J., Zhuopei, W., and Ying, F. (1998). Wave reflection by a vertical wall with a horizontal submerged porous plate. *Ocean. Eng.*, 25(9):767–779.

Xi, D., Xu, S., Du, Y., and Yi, L. (2011). Wave propagation analysis of porous rocks with thermal activated relaxation mechanism. *J. Appl. Geophys.*, 73(3):289–303.

Yu, X. (1995). Diffraction of water waves by porous breakwaters. *J. Waterw. Port Coast. Ocean Eng.*, 121(6):275–282.

Zhao, F., Bao, W., Kinoshita, T., and Itakura, H. (2010). Interaction of waves and porous cylinder with an inner horizontal porous plate. *Appl. Ocean Res.*, 32(2):252–259.

Zhu, S. (2001). Water waves within a porous medium on an undulating bed. *Coast. Eng.*, 42(1):87–101.

Zhu, S. and Chwang, A. T. (2001). Analytical study of porous wave absorber. *J. Eng. Mech.*, 127(4):326–332.

Appendix A

Derivation of equation of motion inside the porous medium

Principle of conservation of mass inside a fluid region leads to the following equation known as the equation of continuity:

$$\frac{\partial \rho}{\partial t} + \boldsymbol{\nabla} \cdot (\rho \boldsymbol{U}) = 0. \tag{A.1}$$

Now for the steady state flow of fluid having constant density, equation (A.1) reduces to

$$\boldsymbol{\nabla} \cdot \boldsymbol{U} = 0. \tag{A.2}$$

For a potential flow, i.e., when $\boldsymbol{U} = \boldsymbol{\nabla}\phi$, the equation of continuity reduces to Laplace's equation

$$\boldsymbol{\nabla}^2 \phi = 0.$$

The incompressible equations of motion inside the porous structure can be written in the following form:

$$\boldsymbol{\nabla} \cdot \boldsymbol{U} = 0\,, \tag{A.3a}$$

$$\frac{\partial \boldsymbol{U}}{\partial t} = -\frac{\boldsymbol{\nabla} P}{\rho} + \text{resistance forces}. \tag{A.3b}$$

The resistance forces in equation (A.3b) are evaluated by combining known steady and unsteady stress relationships. Under steady state flow conditions, the pressure drop through the

porous medium is specified by Ward (1964) as

$$-\frac{\boldsymbol{\nabla} P}{\rho} = \frac{v_k}{K_p}\gamma \boldsymbol{U} + \frac{C_f}{\sqrt{K_p}}\gamma^2 \boldsymbol{U}|\boldsymbol{U}|, \tag{A.4}$$

where v_k is the kinematic viscosity, K_p is the intrinsic permeability and C_f is a dimensionless turbulent resistance coefficient of the medium.

It is hypothesized by Sollitt and Cross (1972) that unsteadiness may be accounted for by introducing an additional term which evaluates the added resistance caused by the virtual mass of discrete grains within the medium. The resistance force due to the virtual mass is equal to the product of the displaced fluid mass, the virtual mass coefficient and the acceleration in the approach velocity. The resulting force is distributed over the fluid mass within the pore so that the force per unit mass of fluid is simply

$$\frac{1-\gamma}{\gamma} C_M \frac{\partial \boldsymbol{U}}{\partial t}. \tag{A.5}$$

Combining equations (A.4) and (A.5), and replacing the resistance force in equation (A.3b) with them we get

$$\begin{aligned} \frac{\partial \boldsymbol{U}}{\partial t} &= -\frac{\boldsymbol{\nabla} P}{\rho} - \frac{v_k}{K_p}\gamma \boldsymbol{U} - \frac{C_f}{\sqrt{K_p}}\gamma^2 \boldsymbol{U}|\boldsymbol{U}| - \frac{1-\gamma}{\gamma} C_m \frac{\partial \boldsymbol{U}}{\partial t}, \\ \Rightarrow \quad S\frac{\partial \boldsymbol{U}}{\partial t} &= -\frac{\boldsymbol{\nabla} P}{\rho} - \frac{v_k}{K_p}\gamma \boldsymbol{U} - \frac{C_f}{\sqrt{K_p}}\gamma^2 \boldsymbol{U}|\boldsymbol{U}|, \end{aligned} \tag{A.6}$$

where

$$S = 1 + C_M \frac{1-\gamma}{\gamma}.$$

It is worth mentioning that $S = 1$ accounts for two different cases, namely, $\gamma = 1$, i.e., the absence of any structure and $C_M = 0$, i.e., the presence of an inviscid fluid.

Now, linearization of equation (A.6) is necessary in order to find an analytical solution and hence, the dissipative stress term is replaced by a linear stress term in $\boldsymbol{U}$ by the following form:

$$\frac{v_k}{K_p}\gamma \boldsymbol{U} + \frac{C_f}{\sqrt{K_p}}\gamma^2 \boldsymbol{U}|\boldsymbol{U}| \rightarrow f\omega \boldsymbol{U}. \tag{A.7}$$

Combination of equations (A.6)and (A.7) leads to equation (1.20b).

In order to evaluate f, Lorentz's principle of equivalent work is applied which states that the average rate of energy dissipation should be identical whether evaluated using the true

non-linear resistance law or its linearized equivalent. Since the resistance terms of the above relation represent friction force per unit mass acting at a point in the flow field, the following equality (energy dissipation) holds:

$$\int_V \gamma dV \int_t^{t+T} f\omega \boldsymbol{U} \cdot \rho \boldsymbol{U} dt = \int_V \gamma dV \int_t^{t+T} \left(\frac{v_k}{K_p} \gamma \boldsymbol{U} + \frac{C_f}{\sqrt{K_p}} \gamma^2 \boldsymbol{U} |\boldsymbol{U}| \right) \cdot \rho \boldsymbol{U} dt, \tag{A.8}$$

where V is the volume of the flow field and T is the wave period. Now assuming f to be constant throughout the flow field, the following expression for f can be written

$$f = \frac{1}{\omega} \frac{\int_V dV \int_t^{t+T} \gamma^2 \left(\frac{v_k \boldsymbol{U}^2}{K_p} + \frac{C_f \gamma}{K_p} |\boldsymbol{U}|^3 \right) dt}{\int_V dV \int_t^{t+T} \gamma \boldsymbol{U}^2 dt}. \tag{A.9}$$

Appendix B

Derivation of matching conditions between any two successive media

Let us consider $\boldsymbol{U}_1$ and $\boldsymbol{U}_2$, respectively, to be the velocities of a fluid at any point inside the water and porous regions attached to each other. Then the following relation holds true:

$$\boldsymbol{U}_i = \boldsymbol{\nabla}\Phi_i \quad i = 1, 2. \tag{B.1}$$

Now, inside the porous region

$$\begin{aligned}
& S\frac{\partial \boldsymbol{U}_2}{\partial t} && = -\frac{\boldsymbol{\nabla} P_2}{\rho} - f\omega \boldsymbol{U}_2, \\
\Rightarrow \quad & S\frac{\partial \Phi_2}{\partial t} && = -\frac{P_2}{\rho} - f\omega\Phi_2, \\
\Rightarrow \quad & -\mathrm{i}\omega S\phi_2 && = -\frac{P_2}{\rho} - f\omega\phi_2, \\
\Rightarrow \quad & \omega(f - \mathrm{i}S)\phi_2 && = -\frac{P_2}{\rho}, \\
\Rightarrow \quad & \omega R\phi_2 && = -\frac{P_2}{\rho},
\end{aligned} \tag{B.2}$$

where P_1 and P_2 are the dynamic pressures of the water and porous regions, respectively. In the water region, Bernoulli's equation gives

$$\frac{\partial \boldsymbol{U}_1}{\partial t} = -\frac{\boldsymbol{\nabla} P_1}{\rho},$$

$$\begin{aligned} \Rightarrow \quad \frac{\partial \Phi_1}{\partial t} &= -\frac{P_1}{\rho}, \\ \Rightarrow \quad -\mathrm{i}\omega\phi_1 &= -\frac{P_1}{\rho}. \end{aligned} \tag{B.3}$$

Now, along the vertical boundary between the water and porous regions, continuity of pressure ($P_1 = P_2$) results in (from equations (B.2) and (B.3)) the following matching condition:

$$\phi_1 = \mathrm{i}R\phi_2. \tag{B.4}$$

Mass flux per unit volume and unit time inside the porous region is $\rho \boldsymbol{U}\gamma$ and the same inside the water region is $\rho \boldsymbol{U}$. Along the vertical boundary, the continuity of mass flux implies

$$\begin{aligned} \rho \boldsymbol{U}_1 &= \rho \boldsymbol{U}_2 \gamma, \\ \Rightarrow \quad \frac{\partial \phi_1}{\partial x} &= \gamma \frac{\partial \phi_2}{\partial x} \quad \text{along } x\text{-direction.} \end{aligned} \tag{B.5}$$

Moreover, if both the regions consist of the same medium, then equations (B.4) and (B.5) reduce to

$$\phi_1 = \phi_2, \tag{B.6a}$$

$$\frac{\partial \phi_1}{\partial x} = \frac{\partial \phi_2}{\partial x} \quad \text{along } x\text{-direction.} \tag{B.6b}$$

It is obvious that these matching conditions are valid along the vertical boundary separating any two regions next to each other.

List of published and communicated papers

Based on the work in this thesis, the following published and communicated papers have resulted:

1. S. Das and S.N. Bora, "Reflection of oblique ocean water waves by a vertical rectangular porous structure placed on an elevated horizontal bottom", *Ocean Engineering*, (2014), 82 : 135 – 143, (DOI:10.1016/j.oceaneng.2014.02.035).

2. S. Das and S.N. Bora, "Wave damping by a vertical porous structure placed near and away from a rigid vertical wall", *Geophysical and Astrophysical Fluid Dynamics*, (2014), 108(2) : 147 – 167, (DOI:10.1080/03091929.2013.834051).

3. S. Das and S.N. Bora, "Reflection of oblique ocean water waves by a vertical porous structure placed on a multi-step impermeable bottom", *Applied Ocean Research* (2014), 47 : 373 – 385, (DOI:10.1016/j.apor.2014.07.001).

4. S. Das and S.N. Bora, "Damping of oblique ocean waves by a vertical porous structure placed on a multi-step bottom", *accepted for publication in Journal of Marine Science and Application*, (DOI:10.1007/s11804-009-7078-4).

5. S. Das and S.N. Bora, "Oblique ocean wave damping by two thin vertical parallel porous plates of different heights", *Revised version submitted to Journal of Engineering Mechanics, ASCE.*

6. S. Das and S.N. Bora, "Oblique water wave damping by two fully submerged thin vertical porous plates of different heights", *Submitted to IMA Journal of Applied Mathematics.*